Star Formation in the Milky Way and Nearby Galaxies

Robert C. Kennicutt, Jr.,[1] and Neal J. Evans II[2]

[1]Institute of Astronomy, University of Cambridge, Cambridge, CB3 0HA, United Kingdom; email: robk@ast.cam.ac.uk

[2]University of Texas at Austin, Texas 78712 and European Southern Observatory, Santiago 19, Chile; email: nje@astro.as.utexas.edu

Annu. Rev. Astron. Astrophys. 2012. 50:531–608

The *Annual Review of Astronomy and Astrophysics* is online at astro.annualreviews.org

This article's doi:
10.1146/annurev-astro-081811-125610

0066-4146/12/0922-0531$20.00

Keywords

clouds, evolution, interstellar medium (ISM), molecules

Abstract

We review progress over the past decade in observations of large-scale star formation, with a focus on the interface between extragalactic and Galactic studies. Methods of measuring gas contents and star-formation rates are discussed, and updated prescriptions for calculating star-formation rates are provided. We review relations between star formation and gas on scales ranging from entire galaxies to individual molecular clouds.

1. OVERVIEW

1.1. Introduction

Star formation encompasses the origins of stars and planetary systems. As a principal agent of galaxy formation and evolution, however, it is also a subject at the root of astrophysics on its largest scales.

The past decade has witnessed an unprecedented stream of new observational information on star formation on all scales, thanks in no small part to new facilities such as the *Galaxy Evolution Explorer* (GALEX), the *Spitzer Space Telescope*, and the *Herschel Space Observatory*; the introduction of powerful new instruments on the *Hubble Space Telescope* (HST); and a host of ground-based optical, infrared (IR), submillimeter, and radio telescopes. These new observations are providing a detailed reconstruction of the key evolutionary phases and physical processes that lead to the formation of individual stars in interstellar clouds, while extending the reach of integrated measurements of star-formation rates (SFRs) to the most distant galaxies known. The new data have also stimulated a parallel renaissance in theoretical investigation and numerical modeling of the star-formation process, on scales ranging from individual protostellar and protoplanetary systems to molecular clouds and star clusters, to entire galaxies and ensembles of galaxies, and even to the first objects, which are thought to have reionized the Universe and seeded today's stellar populations and Hubble sequence of galaxies.

The immense expansion of this subject, in terms of both the volume of results and the range of physical scales explored, may help to explain one of its idiosyncrasies, namely the relative isolation between the community studying individual star-forming regions and stars in the Milky Way (MW; also sometimes referred to as the Galaxy) and the largely extragalactic community that attempts to characterize the star-formation process on galactic and cosmological scales. Some aspects of this separation have been understandable. The key physical processes that determine how molecular clouds contract and fragment into clumps and cores and finally clusters and individual stars can be probed up close only in the Galaxy, and much of the progress in this subject has come from in-depth case studies of individual star-forming regions. Such detailed observations have been impossible to obtain for even relatively nearby galaxies. Instead, the extragalactic branch of the subject has focused on the collective effects of star formation, integrated over entire star-forming regions or, often, over entire galaxies. This collective conversion of baryons from interstellar gas to stars and the emergent radiation and mechanical energy from the stellar populations is most relevant to the formation and evolution of galaxies. As a result, much of our empirical knowledge of star formation on these scales consists of scaling laws and other parametric descriptions, in place of a rigorous, physically based characterization. Improving our knowledge of large-scale star formation and its attendant feedback processes is essential to understanding the birth and evolution of galaxies.

Over the past several years, it has become increasingly clear that many of the key processes influencing star formation lie at the interface between the scales within individual molecular clouds and those of galactic disks. It is now clear that the large-scale SFR is determined by a hierarchy of physical processes spanning a vast range of physical scales: the accretion of gas onto disks from satellite objects and the intergalactic medium (megaparsecs), the cooling of this gas to form a cool neutral phase (kiloparsecs), the formation of molecular clouds (~10–100 pc), the fragmentation and accretion of this molecular gas to form progressively denser structures such as clumps (~1 pc) and cores (~0.1 pc), and the subsequent contraction of the cores to form stars (solar radius) and planets (~astronomical units). The first and last of these processes operate on galactic (or extragalactic) and local cloud scales, respectively. However, the other processes occur at the boundaries between these scales, and the coupling between processes is not yet well understood. Indeed, different physical processes may provide the "critical path" to star formation in different interstellar and

galactic environments. Whatever the answer to these challenging questions, Nature is strongly signaling that we need a unified approach to understanding star formation, one that incorporates observational and astrophysical constraints on star-formation efficiencies, mass functions, etc., from small-scale studies along with a much deeper understanding of the processes that trigger and regulate the formation of star-forming clouds on galactic scales, which, in turn, set the boundary conditions for star formation within clouds.

This review makes a modest attempt to present a consolidated view of large-scale star formation, one that incorporates our new understanding of star formation within clouds and the ensemble properties of star formation in our own MW into our more limited but broader understanding of star formation in external galaxies. As will become clear, the subject is growing and transforming rapidly, so our goal is to present a progress report on what remains an exciting but relatively immature field. Nevertheless, a number of factors make this a timely occasion for such a review. The advent of powerful multiwavelength observations has transformed this subject in fundamental ways since the last large observational review of the galaxy-scale aspects (Kennicutt 1998a). Other reviews have covered various observational aspects of star formation within the MW (Evans 1999, Bergin & Tafalla 2007, Zinnecker & Yorke 2007), but the most comprehensive reviews have been theoretically based (Shu, Adams & Lizano 1987; McKee & Ostriker 2007). We here take an observational perspective, with emphasis on the interface between local and galactic scales. We focus on nearby galaxies and the MW, bringing in results from more distant galaxies only as they bear on the issues under discussion.

The remainder of this review is organized as follows. We show in the sidebar, Questions, a list of key questions in the field. Some have been or will be addressed by other reviews. Some are best answered by observations of other galaxies; some can be addressed only by observations of local star-forming regions in the MW. For each question, we list sections in this review where we review the progress to date in answering them, but many remain largely unanswered, and readers are referred to the last section of this review on future prospects. In Section 1.2, we list some definitions and conventions that are used throughout the paper.

All observations on this subject rest on quantitative diagnostics of gas properties and SFRs on various physical scales, so we review the current state of these diagnostics in Sections 2 and 3. In Section 4, we review the properties of Galactic star-forming regions that are most relevant for comparison to other galaxy-wide studies. In Section 5, we review the star-forming properties of galaxies on the large scale, including the MW; much of this section is effectively an update of the more extended review presented by Kennicutt (1998a). Section 6 updates our knowledge of relations between star formation and gas (e.g., the Schmidt law) and local tests of these relations. The review concludes in Section 7 with our attempted synthesis of what has been learned from the confluence of local and global studies and a look ahead to future prospects. Space limitations prevent us from citing even a fair fraction of the important papers in this subject, so instead we cite useful examples and refer the reader to richer lists of papers that are cited there.

1.2. Definitions and Conventions

The term cloud refers to a structure in the interstellar medium (ISM) separated from its surroundings by the rapid change of some property, such as pressure, surface density, or chemical state. Clouds have a complex structure, but theorists have identified two relevant structures: Clumps are the birthplaces of clusters; cores are the birthplaces of individual or binary stars (e.g., McKee & Ostriker 2007). The observational equivalents have been discussed (e.g., table 1 in Bergin & Tafalla 2007), and cores reviewed (di Francesco et al. 2007, Ward-Thompson et al. 2007a); we discuss them further in Section 2.2.

QUESTIONS

1. How should we interpret observations of the main molecular diagnostic lines (e.g., CO, HCN) and millimeter-wave dust emission? How does this interpretation change as a function of metallicity, surface density, location within a galaxy, and star-formation environment (Sections 2.4, 5.1, and 7.3)?
2. How does the structure of the ISM, the structure of star-forming clouds, and the star formation change as a function of metallicity, surface density, location within a galaxy, and star-formation environment (Sections 2.4, 5, and 7.3)?
3. How do the mass spectra of molecular clouds and dense clumps in clouds vary between galaxies and within a galaxy (Sections 2.5, 5.1, and 7.3)?
4. How constant is the IMF, and how are SFR measurements affected by possible changes in the IMF or by incomplete sampling of the IMF (Sections 2.5, 3.3, 4.2, and 6.4)?
5. What are the limits of applicability of current SFR tracers? How are current measurements biased by dust attenuation or the absence of dust, and how accurately can the effects of dust be removed? How do different tracers depend on metallicity, and what stellar-mass ranges and timescales do they probe (Section 3)?
6. How long do molecular clouds live, and how can we best measure lifetimes? Do these lifetimes change systematically as functions of cloud mass, location in a galaxy, or some other parameter (Sections 4.3 and 7.3)?
7. Do local observations provide any evidence for bimodality in modes of star formation, such as, for example, distributed versus clustered and low-mass versus high-mass star formation (Sections 4 and 7.3)?
8. On the scale of molecular clouds, what are the star-formation efficiencies [$\epsilon = M_\star/(M_\star + M_{\rm cloud})$], and SFRs per unit mass ($\epsilon' = \dot{M}_*/M_{\rm cloud}$), and do these efficiencies vary systematically as functions of cloud mass or other parameters (Sections 4 and 7.3)?
9. How do spatial sampling and averaging affect the observed form of the star-formation relations expressed in terms of total-, molecular-, or dense-gas surface densities? How well do $\dot{M}_*$ diagnostics used in extragalactic studies work on finer scales within a galaxy (Sections 3.9, 6, 6.4, and 7.3)?
10. Are there break points or thresholds where either tracers or star formation change their character (Sections 2, 3, and 7)?

In general, we explicitly use "surface density" or "volume density," but for clarity, symbols with Σ refer to surface density, N refers to column density, and symbols with n or ρ refer to number or mass volume density, respectively. The surface density of HI gas is represented by $\Sigma_{\rm HI}$ if He is not included and by Σ(atomic) if He is included. The surface density of molecular gas is symbolized by $\Sigma_{\rm H_2}$, which generally does not include He, or $\Sigma_{\rm mol}$, which generally does include He. For MW observations, He is almost always included in mass and density estimates, and $\Sigma_{\rm mol}$ may be determined by extinction or emission by dust (Section 2.3) or by observations of carbon monoxide (CO) isotopologues (Section 2.4). When applied to an individual cloud or clump, we refer to it as Σ (cloud) or Σ (clump). For extragalactic work, $\Sigma_{\rm H_2}$ and $\Sigma_{\rm mol}$ are almost always derived from CO observations, and inclusion of He is less universal. In the extragalactic context, $\Sigma_{\rm mol}$ is best interpreted as related to a filling factor of molecular clouds until $\Sigma_{\rm mol} \sim 100\ {\rm M}_\odot\ {\rm pc}^{-2}$, where the area filling factor of molecular gas may become unity (Section 2.4). Above this point, the meaning may change substantially. The total gas surface density, with He, is $\Sigma_{\rm gas} = \Sigma_{\rm mol} + \mu\Sigma_{\rm HI}$, where μ is the mean molecular weight per H atom; $\mu = 1.41$ for MW abundances (Kauffmann et al. 2008), though a value of 1.36 is commonly used. The conversion from CO intensity (usually in the $J = 1 \rightarrow 0$ rotational transition) to column density of H_2, not including He, is denoted X(CO), and the conversion from CO luminosity to mass, which usually includes the mass of He, is denoted $\alpha_{\rm CO}$.

The term dense gas refers generally to gas above some threshold of surface density, as determined by extinction or dust-continuum emission, or of volume density, as indicated by emission from molecular lines that trace densities higher than does CO. Although not precisely defined, suggestions include criteria of a threshold surface density, such as $\Sigma_{\rm mol} > 125\ M_\odot\ {\rm pc}^{-2}$ (Goldsmith et al. 2008; Heiderman et al. 2010; Lada, Lombardi & Alves 2010), a volume-density criterion (typically $n > 10^4\ {\rm cm}^{-3}$) (e.g., Lada 1992), and detection of a line from certain molecules, such as HCN. The surface- and volume-density criteria roughly agree in nearby clouds (Lada et al. 2012), but they may not in other environments.

The SFR is symbolized by SFR or $\dot{M}_*$, often with units of solar mass per year or solar mass per million years, and its meaning depends on how much averaging over time and space is involved. The surface density of SFR, Σ(SFR), has the same averaging issues. The efficiency of star formation is symbolized by ϵ when it means $M_*/(M_* + M_{\rm cloud})$, as it usually does in Galactic studies. For extragalactic studies, one usually means $\dot{M}_*/M_{\rm gas}$, which we symbolize by ϵ'. The depletion time is indicated by $t_{\rm dep} = 1/\epsilon'$. Another time often used is the dynamical time, $t_{\rm dyn}$, which can refer to the free-fall time ($t_{\rm ff}$), the crossing time ($t_{\rm cross}$), or the galaxy orbital time ($t_{\rm orb}$). In recent years, it also has become common to compare galaxies in terms of their SFR per unit galaxy mass, or specific SFR (SSFR). The SSFR scales directly with the stellar birthrate parameter b, the ratio of the SFR today to the average past SFR over the age of the galaxy, and thus provides a useful means for characterizing the star-formation history of a galaxy.

The far-IR luminosity has a number of definitions, and consistency is important in converting them to $\dot{M}_*$. A commonly used definition integrates the dust emission over the wavelength range 3–1,100 μm (Dale & Helou 2002), and following those researchers, we refer to this as the total-infrared (TIR) luminosity. Note, however, that other definitions based on a narrower wavelength band or even single-band IR measurements are often used in the literature.

We refer to mass functions with the following conventions. Mass functions are often approximated by power laws in log M:

$$dN/d\log\ M \propto M^{-\gamma}. \tag{1}$$

In particular, the initial mass function (IMF) of stars is often expressed by Equation 1 with a subscript to indicate stars (e.g., M_*).

Structures in gas are usually characterized by distributions versus mass, rather than logarithmic mass:

$$dN/dM \propto M^{-\alpha}, \tag{2}$$

for which $\alpha = \gamma + 1$. Terminology in this area is wildly inconsistent. To add to the confusion, some references use cumulative distributions, which decrease the index in a power law by 1.

The luminosities and masses of galaxies are well represented by an exponentially truncated power-law function (Schechter 1976):

$$\Phi(L) = (\Phi^*/L^*)(L/L^*)^\alpha e^{(-L/L^*)}. \tag{3}$$

The parameter α denotes the slope of the power-law function at low luminosities, and L^* represents the luminosity above which the number of galaxies declines sharply. For the relatively shallow slopes (α) that are typical of present-day galaxies, L^* also coincides roughly with the peak contribution to the total light of the galaxy population. As discussed in Section 5.2, the Schechter function also provides a good fit to the distribution function of total SFRs of galaxies, with the characteristic SFR in the exponential designated as SFR*, in analogy to L^* above.

The term starburst galaxy was introduced by Weedman et al. (1981), but nowadays the term is applied to a diverse array of galaxy populations. A common property of present-day populations of starbursts is an SFR out of equilibrium, much higher than the long-term average SFR of

the system. No universally accepted quantitative definition exists, however. Some of the more commonly applied criteria are SFRs that cannot be sustained for longer than a small fraction (e.g., ≤10%) of the Hubble time, i.e., with gas-consumption timescales of less than 1 Gyr, or galaxies with disk-averaged SFR surface densities $\Sigma(\mathrm{SFR}) \geq 0.1\ M_\odot\ \mathrm{year}^{-1}\ \mathrm{kpc}^{-2}$ (Section 5.2). Throughout this review, we use the term quiescent star-forming galaxies to characterize the nonstarbursting galaxy population. Note that these local criteria for identifying starbursts are not particularly useful for high-redshift galaxies; a young galaxy forming stars at a constant SFR may resemble a present-day starburst galaxy more than a normal galaxy.

2. INTERSTELLAR-MEDIUM DIAGNOSTICS: GAS AND DUST

2.1. Basics of the Interstellar Medium

The ISM is a complex environment encompassing a very wide range of properties (e.g., McKee & Ostriker 1977, Cox 2005). In the MW, approximately half the volume is filled by a hot ionized medium with $n < 0.01\ \mathrm{cm}^{-3}$ and $T_K > 10^5$ K, and half is filled by some combination of warm ionized medium (WIM) and warm neutral medium (WNM) with $n \sim 0.1$–$1\ \mathrm{cm}^{-3}$ and T_K of several thousand K (Cox 2005). The neutral gas is subject to a thermal instability that predicts segregation into the warm neutral and cold neutral media (CNM), the latter with $n > 10\ \mathrm{cm}^{-3}$ and $T_K < 100$ K (Field, Goldsmith & Habing 1969). The existence of the CNM is clearly revealed by emission in the hyperfine transition of HI, with median temperature of approximately 70 K, determined by comparison of emission to absorption spectra (Heiles & Troland 2003). However, the strict segregation into cold and warm stable phases is not supported by observations suggesting that approximately 48% of the WNM may lie in the thermally unstable phase (Heiles & Troland 2003). Finally, the molecular clouds represent the coldest ($T_K \sim 10$ K in the absence of star formation), densest ($n > 30\ \mathrm{cm}^{-3}$) part of the ISM. We focus on the cold ($T_K < 100$ K) phases here, as they are the only plausible sites of star formation. The warmer phases provide the raw material for the cold phases, perhaps through "cold" flows from the intergalactic medium (Dekel & Birnboim 2006). In the language of this review, such flows would be "warm."

In the next section, we introduce some terminology used for the molecular gas as a precursor to the following discussion of the methods for tracing it. We then discuss the use of dust as a tracer (Section 2.3) before discussing the gas tracers (Section 2.4).

2.2. Clouds and Their Structures

The CNM defined in the preceding section presents a wide array of structures, with a rich nomenclature, but we focus here on the objects referred to as clouds, invoking a kind of condensation process. This name is perhaps even more appropriate to the molecular gas, which corresponds to a change in chemical state. The molecular cloud boundary is usually defined by detection, above some threshold, of emission from the lower rotational transitions of CO. Alternatively, a certain level of extinction of background stars is often used. In confused regions, velocity coherence can be used to separate clouds at different distances along the line of sight. However, molecular clouds are surrounded by atomic envelopes and a transition region in which the hydrogen is primarily molecular, but the carbon is mostly atomic (van Dishoeck & Black 1988). These regions are known as PDRs (photodissociation regions or photon-dominated regions) (Hollenbach & Tielens 1997). More recently, they have been referred to as dark gas.

The structure of molecular clouds is complex, leading to considerable nomenclatural chaos. The boundaries of clouds, projected on the sky, defined by either dust or CO emission or extinction, can be characterized by a fractal dimension around 1.5 (Scalo 1990; Falgarone, Phillips & Walker 1991;

Stutzki et al. 1998), suggesting an intrinsic 3D dimension of 2.4. When mapped with sufficient sensitivity and dynamic range, clouds are highly structured, and filaments provide the dominant morphological theme; denser, rounder cores are often found within the filaments (e.g., André et al. 2010, Men'shchikov et al. 2010, Molinari et al. 2010).

The probability distribution function of surface densities, as mapped by extinction, can be fitted to a lognormal function for low extinctions, $A_V \leq 2$–5 mag (Lombardi, Lada & Alves 2010), with a power-law tail to higher extinctions, at least in some clouds. In fact, only the clouds with power-law tails have active star formation (Kainulainen et al. 2009). Further studies indicate that the power-law tail begins at $\Sigma_{mol} \sim 40$–$80\ M_\odot\ pc^{-2}$ and that the material in the power-law tail lies in unbound clumps with mean density of approximately $10^3\ cm^{-3}$ (Kainulainen et al. 2011).

Within large clouds, and especially within the filaments, there may be small cores, which are much less massive but much denser. Theoretically, these are the sites of formation of individual stars, either single or binary (Williams, Blitz & McKee 2000). Their properties have been reviewed by di Francesco et al. (2007) and Ward-Thompson et al. (2007a). Those cores without evidence of ongoing star formation are called starless cores, and the subset of those that are gravitationally bound are called prestellar cores. Distinguishing these two requires a good mass estimate, independent of the virial theorem, and observations of lines that trace the kinematics. A sharp decrease in turbulence may provide an alternative way to distinguish a prestellar core from its surroundings (Pineda et al. 2010a).

Although clouds and cores are reasonably well defined, intermediate structures are more problematic. Theoretically, one needs to name the entity that forms a cluster. Because large clouds can form multiple (or no) clusters, another term is needed. Williams, Blitz & McKee (2000) established the term clump for this structure. The premise was that this region should also be gravitationally bound, at least until the stars dissipate the remaining gas. Finding an observable correlative has been a problem (Section 2.5).

Finally, one must note that this hierarchy of structure is based on relatively large clouds. There are also many small clouds (Clemens & Barvainis 1988), some of which are their own clumps and/or cores. The suggestion by Bok & Reilly (1947) that these could be the sites of star formation was seminal.

2.3. Dust as an Interstellar-Medium Tracer

In the MW, roughly 1% of the ISM is found in solid form, primarily silicates and carbonaceous material (Draine 2003) (see also a very useful Web site: **http://www.astro.princeton.edu/~draine/dust/dust.html**). Dust grain sizes range from 0.35 nm to approximately 1 μm, with evidence for grain growth in molecular clouds. The column density of dust can be measured by studying either the reddening (using colors) or the extinction of starlight, using star counts referenced to an unobscured field. The relation between extinction (e.g., A_V) and reddening [e.g., $E(B-V)$] is generally parameterized by $R_V = A_V/E(B-V)$. In the diffuse medium, the reddening has been calibrated against atomic and molecular gas to obtain $N(\mathrm{HI}) + 2N(H_2) = 5.8 \times 10^{21}\ cm^{-2}\ E(B-V)$ (mag), not including helium (Bohlin, Savage & Drake 1978). For $R_V = 3.1$, this relation translates to $N(\mathrm{HI}) + 2N(H_2) = 1.87 \times 10^{21}\ cm^{-2}\ A_V$ (mag). This relation depends on metallicity, with coefficients larger by factors of approximately 4 for the Large Magellanic Cloud (LMC) and 9 for the Small Magellanic Cloud (SMC) (Weingartner & Draine 2001).

The relation derived for diffuse gas is often applied in molecular clouds, but grain growth flattens the extinction curve, leading to larger values of R_V and a much flatter curve in the IR

(Flaherty et al. 2007, Chapman et al. 2009). More appropriate conversions can be found in the curves for $R_V = 5.5$ in the Web site referenced above. There is evidence of continued grain growth in denser regions, which particularly affects the opacity at longer wavelengths, such as the millimeter/submillimeter regions (Shirley et al. 2011).

Reddening and extinction of starlight provided early evidence of the existence of interstellar clouds (Barnard 1908). Lynds (1962) provided the mostly widely used catalog of dark clouds based on star counts, up to $A_V \sim 6$ mag, at which point the clouds were effectively opaque at visible wavelengths. The availability of IR photometry for large numbers of background stars from 2MASS, ISO, and *Spitzer* toward nearby clouds has allowed extinction measurements up to $A_V \sim 40$ mag. These have proved very useful in characterizing cloud structure and in checking the gas tracers discussed in Section 2.4. Extinction mapping with sufficiently high spatial resolution can identify cores (e.g., Alves, Lombardi & Lada 2007), but many are not gravitationally bound (Lada et al. 2008) and are likely to dissipate.

At wavelengths with strong, diffuse Galactic background emission, such as the mid-IR, dust absorption against the continuum can be used in a way parallel to extinction maps (e.g., Bacmann et al. 2000, Stutz et al. 2007). The main uncertainties in deriving the gas column density are the dust opacity in the mid-IR and the fraction of foreground emission.

The energy absorbed by dust at short wavelengths is emitted at longer wavelengths, from IR to millimeter, with a spectrum determined by the grain temperature and the opacity as a function of wavelength. At ~1-mm wavelengths, the emission is almost always optically thin and close to the Rayleigh-Jeans limit for modest temperatures. (For $T_d = 20$ K, masses, densities, etc., derived in the Rayleigh-Jeans limit at $\lambda = 1$ mm must be multiplied by 1.5.) Thus, the millimeter-wave continuum emission provides a good tracer of dust (and gas, with knowledge of the dust opacity) column density and mass.

As a by-product of studies of the cosmic microwave background, COBE, WMAP, and *Planck* produce large-scale maps of millimeter/submillimeter emission from the MW. With *Planck*, the angular resolution reaches $\theta = 4.7$ arcmin at 1.4 mm in an all-sky map of dust temperature and optical depth (Planck Collaboration et al. 2011b). Mean dust temperature increases from $T_d = 14$–15 K in the outer Galaxy to 19 K around the Galactic center. A catalog of cold clumps with $T_d = 7$–17 K, mostly within 2 kpc of the Sun, many with surprisingly low column densities, also resulted from analysis of *Planck* data (Planck Collaboration et al. 2011c). *Herschel* surveys will be providing higher-resolution [25 arcsec at 350 μm (Griffin et al. 2010) and 6 arcsec at 70 μm (Poglitsch et al. 2010)] images of the nearby clouds (André et al. 2010), the Galactic plane (Molinari et al. 2010), and many other galaxies (e.g., Skibba et al. 2011, Wuyts et al. 2011). Still higher resolution is available at $\lambda \geq 350$ μm from ground-based telescopes at dry sites. Galactic-plane surveys at wavelengths near 1 mm have been carried out in both hemispheres (Schuller et al. 2009, Aguirre et al. 2011). Once these are put on a common footing, we should have maps of the Galactic plane with resolution of 20 arcsec to 30 arcsec. Deeper surveys of nearby clouds (Ward-Thompson et al. 2007b), the Galactic plane, and extragalactic fields are planned with SCUBA-2.

Although studies from ground-based telescopes offer higher resolution, the need to remove atmospheric fluctuations leads to loss of sensitivity to structures larger than typically approximately half the array footprint on the sky (Aguirre et al. 2011). Although the large-scale emission is lost, the combination of sensitivity to a minimum column density and a maximum size makes these surveys effectively select structures of a certain mean volume density. In nearby clouds, these correspond to dense cores (Enoch et al. 2009). For Galactic-plane surveys, sources mainly correspond to clumps, but they can be whole clouds at the largest distances (Dunham et al. 2011b).

2.4. Gas Tracers

One troublesome aspect of extragalactic studies has been the determination of the amount and properties of the gas. We discuss first the atomic phase, then the molecular phase, and finally tracers of dense gas.

2.4.1. The cold atomic phase. The cold, neutral atomic phase is traced by the hyperfine transition of hydrogen, occurring at 21 cm in the rest frame. This transition reaches optical depth of unity at

$$N(\mathrm{HI}) = 4.57 \times 10^{20}\ \mathrm{cm}^{-2}(T_{\mathrm{spin}}/100\ \mathrm{K})(\sigma_{\upsilon}/1\ \mathrm{km\ s}^{-1}), \quad (4)$$

where T_{spin} is the excitation temperature, usually equal to the kinetic temperature, T_K, and σ_{υ} is the velocity dispersion (equation 8.11 in Draine 2011). For dust in the diffuse ISM of the MW, this column density corresponds to $A_V = 0.24$ mag, and optical depth effects can be quite important. The warm, neutral phase is difficult to study, as lines become broad and weak, but it has been detected (Kulkarni & Heiles 1988). A detailed analysis of both CNM and WNM can be found in Heiles & Troland (2003).

With $I(\mathrm{HI}) = \int S_{\upsilon} d\upsilon$ (Jy km s^{-1}),

$$M(\mathrm{HI})/\mathrm{M}_{\odot} = 2.343 \times 10^{5}(1+z)^{-1}(D_L/\mathrm{Mpc})^2 I(\mathrm{HI}), \quad (5)$$

not including helium (equation 8.21 in Draine 2011). A coefficient of 2.536×10^5 is in common use among HI observers, usually traced to Roberts (1975). The difference is caused by an updated value for the Einstein A coefficient used by Draine (2011).

2.4.2. Molecular gas. The most abundant molecule is H_2, but its spectrum is not a good tracer of the mass in molecular clouds. The primary reason is not, as often stated, the fact that it lacks a dipole moment, but instead the low mass of the molecule. The effect of low mass is that the rotational transitions require quite high temperatures to excite, making the bulk of the H_2 in typical clouds invisible. Continuum optical depth at the mid-IR wavelengths of these lines is also an impediment. The observed rotational H_2 lines originate in surfaces of clouds, probing 1% to 30% of the gas in a survey of galaxies (e.g., Roussel et al. 2007).

CO is the most commonly used tracer of molecular gas because its lines are the strongest and therefore easiest to observe. These advantages are accompanied by various drawbacks, which MW observations may help to illuminate. Essentially, CO emission traces column density of molecular gas only over a very limited dynamic range. At the low end, CO requires protection from photodissociation and some minimum density to excite it, so it does not trace all the molecular (in the sense that hydrogen is in H_2) gas, especially if metallicity is low. At the high end, emission from CO saturates at modest column densities. A more complete review by A. Bolatto of the use of CO to trace molecular gas is scheduled for a future volume of the *Annual Review of Astronomy and Astrophysics*, so we briefly highlight the issues here.

CO becomes optically thick at very low total column densities. Using CO intensity to estimate the column density of a cloud is akin to using the presence of a brick wall to estimate the depth of the building behind it. The isotopologues of CO (^{13}CO and C^{18}O) provide lower optical depths, but at the cost of weaker lines. To use these, one needs to know the isotope ratios; these are fairly well known in the MW (Wilson & Rood 1994), but they may differ substantially in other galaxies. In addition, the commonly observed lower transitions of CO are very easily thermalized ($T_{\mathrm{ex}} = T_K$) making them insensitive to the presence of dense gas.

The common practice in studies of MW clouds is to use a combination of CO and ^{13}CO to estimate optical depth and, hence, CO column density N(CO). One can then correlate N(CO) or its isotopes against extinction to determine a conversion factor (Dickman 1978; Frerking, Langer & Wilson 1982). A recent, careful study of CO and ^{13}CO toward the Taurus molecular cloud shows that N(CO) traces A_V up to 10 mag in some regions but only up to 4 mag in other regions, and other issues cause problems below $A_V = 3$ mag (Pineda et al. 2010b). Freeze-out of CO and conversion to CO_2 ice causes further complications in cold regions of high column density (Lee et al. 2003, Whittet et al. 2007, Pontoppidan et al. 2008), but other issues likely dominate the interpretational uncertainties for most extragalactic CO observations.

Because studies of other galaxies generally have only CO observations available, the common practice has been to relate H_2 column density $N(H_2)$ to the integrated intensity of CO [$I(CO) = \int Tdv$ (K km s^{-1})] via the infamous X-factor: $N(H_2) = X(CO)I(CO)$. For example, Kennicutt (1998b) used $X(CO) = 2.8 \times 10^{20}$ cm^{-2} (K km s^{-1})$^{-1}$.

Pineda et al. (2010b) found $X(CO) = 2.0 \times 10^{20}$ cm^{-2} (K km s^{-1})$^{-1}$ in the parts of the cloud where both CO and ^{13}CO are detected along individual sight lines. CO does emit beyond the area where ^{13}CO is detectable and even, at a low level, beyond the usual detection threshold for CO. Stacking analysis of positions beyond the usual boundary of the Taurus cloud suggests a factor of 2 additional mass in this transition region (Goldsmith et al. 2008). Such low-intensity, but large-area, emission could contribute substantially to observations of distant regions in our Galaxy and in other galaxies. For the outer parts of clouds, where only CO is detected, and only by stacking analysis, X(CO) is six times higher (Pineda et al. 2010b). Even though approximately one-quarter of the total mass is in this outer region, Pineda et al. (2010b) argue that the best single value to use is $X(CO) = 2.3 \times 10^{20}$ cm^{-2} (K km s^{-1})$^{-1}$, similar to values commonly adopted in extragalactic studies. When possible, we use $X(CO) = 2.3 \times 10^{20}$ cm^{-2} (K km s^{-1})$^{-1}$ for this review. In contrast, Liszt, Pety & Lucas (2010) argued that X(CO) stays the same even in diffuse gas. If they are right, much of the integrated CO emission from some parts of galaxies could arise in diffuse, unbound gas.

Comparing to extinction measures in two nearby clouds extending up to $A_V = 40$ mag, Heiderman et al. (2010) found considerable variations from region to region, with I(CO) totally insensitive to increased extinction in many regions. Nonetheless, when averaged over the whole cloud, the standard X(CO) would cause errors in mass estimates of $\pm 50\%$, systematically overestimating the mass for $\Sigma_{mol} < 150$ M$_\odot$ pc^{-2} and underestimating for $\Sigma_{mol} > 200$ M$_\odot$ pc^{-2}. Simulations of turbulent gas with molecule formation also suggest that I(CO) can be a very poor tracer of A_V (Glover et al. 2010). Overall, the picture at this point is that measuring the extent of the brick wall will not tell you anything about particularly deep or dense extensions of the building, but if the buildings are similar, the extent of the wall is a rough guide to the total mass of the building (cf. Shetty et al. 2011b).

Following that thought, the luminosity of CO $J = 1 \rightarrow 0$ is often used as a measure of cloud mass, with the line width reflecting the virial theorem in a crude sense. In most extragalactic studies, individual clouds are not resolved, and the luminosity of CO is essentially a cloud-counting technique (Dickman, Snell & Schloerb 1986). Again, this idea works only if the objects being counted have rather uniform properties. In this approach, $M = \alpha_{CO} L(CO)$. For the standard value for X(CO) discussed above [$X(CO) = 2.3 \times 10^{20}$ cm^{-2} (K km s^{-1})$^{-1}$], $\alpha_{CO} = 3.6$ M$_\odot$ (K km s^{-1} pc^2)$^{-1}$ without helium, and $\alpha_{CO} = 4.6$ M$_\odot$ (K km s^{-1} pc^2)$^{-1}$ with correction for helium.

The effects of cloud temperature, density, metallicity, etc., on mass estimation from CO were discussed by Maloney & Black (1988), who concluded that large variations in the conversion factor are likely. Ignoring metallicity effects, they predicted $X(CO) \propto n^{0.5} T_K^{-1}$, where n is the mean

density in the cloud. Shetty et al. (2011b) found a weaker dependence on T_K, $X(\mathrm{CO}) \propto T_K^{-0.5}$. These scalings rest on some arguments that may not apply to other galaxies. Further modeling with different metallicities (Feldmann, Gnedin & Kravtsov 2011; Shetty et al. 2011a) has begun to provide some perspective on the range of behaviors likely in other galaxies.

There is observational evidence for changes in α_{CO} in centers of galaxies. For the MW central region, Oka et al. (1998) suggested a value for X(CO) a factor of 10 lower than in the MW disk. The value of α_{CO} appears to decrease by factors of 2–5 in nearby galaxy nuclei (e.g., Meier & Turner 2004; Meier, Turner & Hurt 2008), by a factor of approximately 5–6 in local ultraluminous infrared galaxies (ULIRGs) (Downes, Solomon & Radford 1993; Downes & Solomon 1998) and probably by a similar factor in high-redshift, molecule-rich galaxies (Solomon & Vanden Bout 2005).

A compilation of measurements indicates that α_{CO} decreases from the usually assumed value with increasing surface density of gas once $\Sigma_{\mathrm{mol}} > 100\ \mathrm{M}_\odot\ \mathrm{pc}^{-2}$ (**Figure 1**) (Tacconi et al. 2008). This Σ_{mol} corresponds to $A_{\mathrm{V}} \sim 10$ mag, approximately the point where CO fails to trace column density in Galactic clouds and the point where the beam on another galaxy may be filled with CO-emitting gas. Variation in α_{CO} has a direct bearing on interpretation of starbursts (Section 6), and it is highly unlikely that α_{CO} is simply bimodal over the full range of star-forming environments. Indeed, Narayanan et al. (2011) used a grid of model galaxies to infer a smooth function of I(CO): $\alpha_{\mathrm{CO}} = \min[6.3,\ 10.7 \times I(\mathrm{CO})^{-0.32}]Z'^{-0.65}$, where Z' is the metallicity divided by the solar value.

Other methods have been used to trace gas indirectly, including gamma-ray emission and dust emission. Gamma rays from decay of pions produced from high-energy cosmic rays interacting with baryons in the ISM directly trace all the matter if one knows the cosmic-ray flux (e.g., Bloemen 1989). Recent analysis of gamma-ray data from *Fermi* have inferred a low value for X(CO) of $(0.87 \pm 0.05) \times 10^{20}\ \mathrm{cm}^{-2}\ (\mathrm{K\ km\ s}^{-1})^{-1}$ in the Solar Neighborhood (Abdo et al. 2010). This value is a factor of 3 lower than other estimates and early results from dust emission using *Planck* that found $X(\mathrm{CO}) = (2.54 \pm 0.13) \times 10^{20}\ \mathrm{cm}^{-2}\ (\mathrm{K\ km\ s}^{-1})^{-1}$ for the Solar Neighborhood (Planck Collaboration et al. 2011b).

Abdo et al. (2010) also inferred the existence of dark gas, which is not traced by either HI or CO, surrounding the CO-emitting region in the nearby Gould Belt clouds, with mass of approximately half of that traced by CO. Planck Collaboration et al. (2011b) have also indicated the existence of dark gas with mass 28% of the atomic gas and 118% of the CO-emitting gas in the Solar Neighborhood. The dark gas appears around $A_{\mathrm{V}} = 0.4$ mag and is presumably the CO-poor, but H_2-containing, outer parts of clouds (e.g., Wolfire, Hollenbach & McKee 2010), which can be seen in [CII] emission at 158 μm and in fluorescent H_2 emission at 2 μm (e.g., Pak et al. 1998). It is dark only if one restricts attention to HI and CO emission. At low metallicities, the layer of C^+ grows, and a given CO luminosity implies a larger overall cloud (see figure 14 in Pak et al. 1998). However, Planck Collaboration et al. (2011b) also suggested that the dark gas may include some gas that is primarily atomic, but not traced by HI emission, owing to optical depth effects.

Dust emission is now being used as a tracer of gas for other galaxies. Maps of HI gas are used to break the degeneracy between the gas to dust ratio δ_{gdr} and α'_{CO} in the following equation:

$$\delta_{\mathrm{gdr}}\Sigma_{\mathrm{dust}} = \alpha'_{\mathrm{CO}} I(\mathrm{CO}) + \Sigma_{\mathrm{HI}}. \quad (6)$$

Leroy et al. (2011) minimized the variation in δ_{gdr} to find the best fit to α'_{CO} in several nearby galaxies. They determined Σ_{dust} from *Spitzer* images of 160-μm emission, with the dust temperature (or equivalently the external radiation field) constrained by shorter-wavelength far-IR emission. This method should measure everything with substantial dust that is not HI, and so includes the

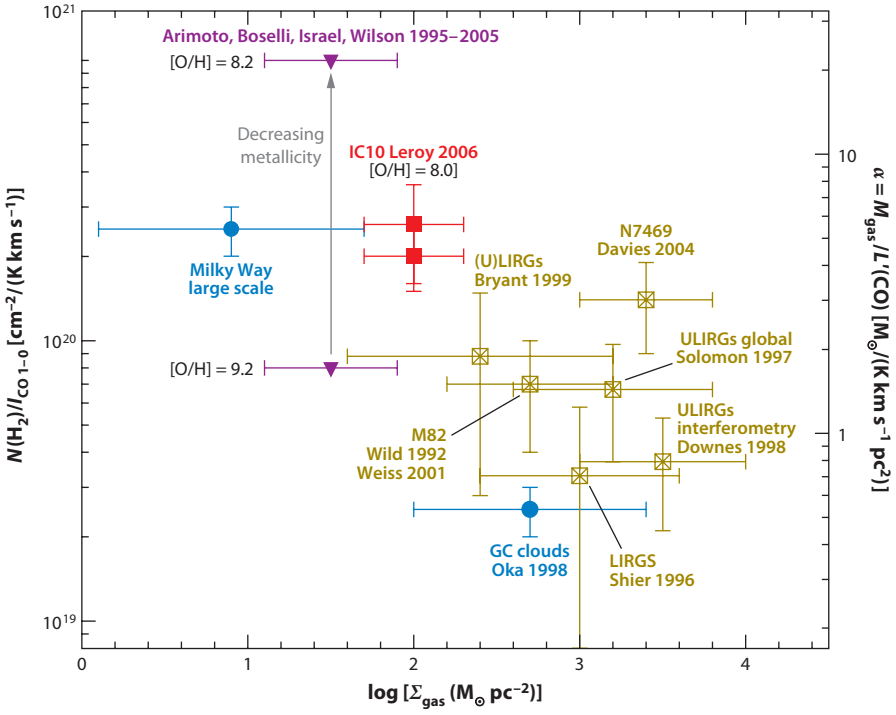

Figure 1

Compilation of the conversion factor X(CO) from the carbon monoxide (CO) $J = 1 \rightarrow 0$ integrated intensity [I_{CO} (K km s^{-1})] or luminosity [L'_{CO} (K km s^{-1} pc^2)] to H_2 column density (*left vertical scale*) and total (H_2 and He) gas mass (*right vertical scale*), derived in various Galactic and extragalactic targets. Blue circles denote measurements in the disk and center of the Milky Way, based on various virial, extinction, and isotopomeric analyses. Crossed dark yellow squares denote measurements in starbursts and (ultra)luminous infrared galaxies [(U)LIRGs], mainly based on dynamical constraints. Filled purple triangles denote conversion factors as a function of decreasing metallicity (*vertical gray arrow*) from [O/H] = 9.2 (*bottom*) to 8.2 (*top*), derived by several groups using mainly global (large-scale) dust mass measurements in nearby galaxies and dwarfs. In contrast, red-filled squares mark X-factor measurements toward individual clouds, over the same range in metallicity. Taken from Tacconi et al. (2008); references to the original work are given there. Reproduced by permission of the AAS.

so-called dark molecular gas. They found that $\alpha'_{CO} = 3$–9 $M_\odot$ pc^{-2} (K km s^{-1})$^{-1}$, similar to values based on MW studies, for galaxies with metallicities down to $12 + [O/H] \sim 8.4$ below which α'_{CO} increases sharply to values of approximately 70. Their method does not address the column density within clouds, but only the average surface density on scales larger than clouds. For galaxies not too different from the MW, the standard α'_{CO} will roughly give molecular gas masses, but in galaxies with lower metallicity, the effects can be large. An extreme is the SMC, where $\alpha'_{CO} \sim 220$ $M_\odot$ pc^{-2} (K km s^{-1})$^{-1}$ (Bolatto et al. 2011). Maps of dust emission at longer wavelengths should decrease the sensitivity to dust temperature.

2.4.3. Dense-gas tracers. Lines other than CO $J = 1 \rightarrow 0$ generally trace warmer (e.g., higher J CO lines) and/or denser (e.g., HCN, CS, etc.) gas. Wu et al. (2010a) showed that the line luminosities of commonly used tracers (CS $J = 2 \rightarrow 1$, $J = 5 \rightarrow 4$, and $J = 7 \rightarrow 6$; HCN

$J = 1 \rightarrow 0$, $J = 3 \rightarrow 2$) correlate well with the virial mass of dense gas; indeed, most follow relations that are close to linear. Because these lines are optically thick, the linear correlation is somewhat surprising, but it presumably has an explanation similar to the cloud-counting argument offered above for CO. Collectively, we refer to these lines as dense-gas tracers, but the effective densities increase with J and vary among species (for definitions and tables of effective and critical densities, see Evans 1999, Reiter et al. 2011b). As an example for HCN $J = 1 \rightarrow 0$,

$$\log(L'_{\mathrm{HCN1-0}}) = 1.04 \times \log[M_{\mathrm{Vir}}(R_{\mathrm{HCN1-0}})] - 1.35 \quad (7)$$

from a robust estimation fit to data on dense clumps in the MW (Wu et al. 2010a). The line luminosities of other dense-gas tracers also show strong correlations with both virial mass (Wu et al. 2010a) and the mass derived from dust-continuum observations (Reiter et al. 2011b).

These tracers of dense gas are subject to the same caveats about sensitivity to physical conditions, such as metallicity, volume density, turbulence, etc., as discussed above for CO. In fact, the other molecules are more sensitive to photodissociation than is CO, so they will be even more dependent on metallicity (e.g., Rosolowsky, Pineda & Gao 2011). Dense-gas tracers should become much more widely used in the Atacama Large Millimeter/submillimeter Array (ALMA) era, but caution is needed to avoid the kind of oversimplification that has tarnished the reputation of CO. Observations of multiple transitions and rare isotopes, along with realistic models, will help (e.g., Garcia-Burillo et al. 2011).

2.4.4. Summary. What do extragalactic observations of molecular tracers measure? None are tracing the surface density of a smooth medium, with the possible exception of the most extreme starbursts. The luminosity of CO is a measure of the number of emitting structures times the mean luminosity per structure. Dense-gas tracers work in a similar way, but compared with CO, they select gas above a higher density threshold. For CO $J = 1 \rightarrow 0$, the structure is the CO-emitting part of a cloud, which shrinks as metallicity decreases. For dense-gas tracers, the structure is the part of a cloud dense enough to produce significant emission, something like a clump if conditions are similar to those of the MW, but even more sensitive to metallicity. Using a conversion factor, one gets a "mass" in those structures.

Estimates of the conversion factors for CO vary by factors of 3 for the Solar Neighborhood and at least an order of magnitude at low metallicity and by at least half an order of magnitude for our own Galactic Center and for extreme systems such as ULIRGs. Dividing by the area of the galaxy or the beam, one gets Σ_{mol}, which should be thought of as an area-filling factor of the structures being probed times some crude estimate of the mass per structure. That estimate depends on conditions in the structures, such as density, temperature, and abundance, and on the external radiation field and the metallicity. Once the L(CO) translates to surface densities above that of individual clouds ($\Sigma_{\mathrm{mol}} \gtrsim 100\ \mathrm{M_\odot\ pc^{-2}}$), the interpretation may change as the area-filling factor can now exceed unity. Large ranges of velocity in other galaxies (if not exactly face-on) allow I(CO) to still count clouds above this threshold, but the clouds may no longer be identical. The full range of molecular surface densities in other galaxies inferred from CO, assuming a constant conversion factor, is a factor of 10^3 (Section 6); given that CO traces Σ_{mol} only over a factor of 10, at best, in well-studied clouds in the MW (Heiderman et al. 2010, Pineda et al. 2010b), this seems a dangerous extrapolation.

2.5. Mass Functions of Stars, Clusters, and Gas Structures

The mass functions of the structures in molecular clouds (Section 2.2) are of considerable interest in relation to the origin of the mass functions of clusters (clumps) and stars (cores). Salpeter

(1955) fit the IMF of stars to a power law in log M_* with exponent $\gamma_* = 1.35$, or $\alpha_* = 2.35$ (see Section 1.2 for definitions). More recent determinations over a wider range of masses, including brown dwarfs, indicate a clear flattening at lower masses, either as broken power laws (Kroupa, Tout & Gilmore 1993) or a lognormal distribution (Chabrier 2003, Miller & Scalo 1979). A detailed study of the IMF in the nearest massive young cluster, Orion, with stars from 0.1 to 50 $M_\odot$ with a mean age of 2 Myr, shows a peak between 0.1 and 0.3 $M_\odot$, depending on evolutionary models, and a deficit of brown dwarfs relative to the field IMF (Da Rio et al. 2011). Steeper IMFs in massive elliptical galaxies have been suggested by van Dokkum & Conroy (2011). Zinnecker & Yorke (2007) summarized the evidence for a real (not statistical) cutoff in the IMF around 150 $M_\odot$ for star formation in the MW and Magellanic Clouds. Variations in the IMF with environment are plausible, but convincing evidence for variation remains elusive (Bastian, Covey & Meyer 2010).

The masses of embedded young clusters (Lada & Lada 2003), OB associations (McKee & Williams 1997), and massive open clusters (Elmegreen & Efremov 1997, Zhang & Fall 1999) follow a similar relation with $\gamma_{\rm cluster} \sim 1$. Studies of clusters in nearby galaxies have also found $\gamma_{\rm cluster} = 1 \pm 0.1$, with a possible upper mass cutoff or turnover around 1–2 $\times$ 10^6 $M_\odot$ (Gieles et al. 2006), perhaps dependent on the galaxy (but see Chandar et al. 2011). In contrast, the most massive known open clusters in the MW appear to have a mass of 6–8 $\times$ 10^4 $M_\odot$ (Homeier & Alves 2005; Portegies Zwart, McMillan & Gieles 2010; Davies et al. 2011).

The mass functions of clusters and stars are presumably related to the mass functions of their progenitors, clouds or clumps, and cores. For comparison with structures in clouds, we use the distributions versus mass, rather than logarithmic mass, so our points of comparison are $\alpha_* = 2.3$ and $\alpha_{\rm cluster} = 2$. From surveys of emission from CO $J = 1 \rightarrow 0$ in the outer galaxy, where confusion is less problematic, Heyer, Carpenter & Snell (2001) found a size distribution of clouds, $dN/dr \propto r^{-3.2\pm0.1}$, with no sign of a break from the power-law form from 3 to 60 pc. The mass function, using the definition in Equation 2, was fitted by $\alpha_{\rm cloud} = 1.8 \pm 0.03$ over the range 700 to 1×10^6 $M_\odot$. Complementary surveys of the inner Galaxy found $\alpha_{\rm cloud} = 1.5$ up to $M_{\rm max} = 10^{6.5}$ $M_\odot$ (Rosolowsky 2005). The upper cutoff around 3–6 $\times$ 10^6 $M_\odot$ appears to be real, despite issues of blending of clouds (Williams & McKee 1997, Rosolowsky 2005). Using ^{13}CO $J = 1 \rightarrow 0$, which selects somewhat denser parts of clouds, Roman-Duval et al. (2010) found $\alpha_{^{13}{\rm CO}} = 1.75 \pm 0.23$ for $M_{\rm cloud} > 10^5$ $M_\odot$. Clumps within clouds, identified by mapping ^{13}CO or C^{18}O, have a similar value for $\alpha_{\rm clump} = 1.4$–1.8 (Kramer et al. 1998). All results agree that most clouds are small, but unlike stars or clusters, most mass is in the largest clouds ($\alpha_{\rm cloud} < 2$).

Studies of molecular cloud properties in other galaxies have been recently reviewed (Blitz et al. 2007, Fukui & Kawamura 2010). Mass functions of clouds in nearby galaxies appear to show some differences, though systematic effects introduce substantial uncertainty (Sheth et al. 2008, Wong et al. 2011). Evidence for a higher value of $\alpha_{\rm cloud}$ has been found for the LMC (Fukui et al. 2001, Wong et al. 2011) and M33 (Engargiola et al. 2003, Rosolowsky 2005). Most intriguingly, the mass function appears to be steeper in the interarm regions of M51 than in the spiral arms (E. Schinnerer & A. Hughes, personal communication), possibly caused by the aggregation of clouds into larger structures within arms and disaggregation as they leave the arms (Koda et al. 2009).

Much work has been done recently on the mass function of cores, and *Herschel* surveys of nearby clouds will illuminate this topic (e.g., André et al. 2010). At this point, the mass function of cores seems to be clearly steeper than that of clouds and much closer to that of stars (Motte, Andre & Neri 1998; Enoch et al. 2008; Sadavoy et al. 2010). A turnover in the mass function appears at a mass approximately 3–4 times that seen in the stellar IMF (Alves, Lombardi & Lada 2007; Enoch et al. 2008). The similarity of $\alpha_{\rm core}$ to α_* supports the idea that the cores are the immediate precursors of stars and that the mass function of stars is set by the mass function of cores. In this

picture, the offset of the turnover implies that approximately 0.2 to 0.3 of the core mass winds up in the star, consistent with simulations that include envelope clearing by outflows (e.g., Dunham et al. 2010). Various objections and caveats to this appealing picture have been registered (e.g., Clark, Klessen & Bonnell 2007; Hatchell & Fuller 2008; Swift & Williams 2008; Reid et al. 2010).

Note that no such tempting similarity exists between the mass function of clusters and the mass function of clumps defined by ^{13}CO maps, raising the question of whether that observational definition properly fits the theoretical concept of a clump as a cluster-forming entity. Structures marked by stronger emission in ^{13}CO or C^{18}O (Rathborne et al. 2009) are not always clearly bound gravitationally. Ground- and space-based imaging of submillimeter emission by dust (e.g., Men'shchikov et al. 2010) offer promise in this area, but information on velocity structure will also be needed. The data so far suggest that the structure is primarily filamentary, more similar to that of clouds than cores. CS, HCN, and other tracers of much denser gas (Section 2.4), along with dust-continuum emission (Section 2.3), have identified what may be called dense clumps, which appear to have a mass function similar to that of clusters (Shirley et al. 2003, Reid & Wilson 2005, Beltrán et al. 2006).

The comparison of mass functions supports the idea (McKee & Ostriker 2007) that cores are the progenitors of stars and dense clumps are the progenitors of clusters, with clouds less directly related. Upper limits to the mass function of clumps would then predict upper limits to the mass function of clusters, unless nearby clumps result in merging of clusters. Because most clouds and many clumps are more massive than the most massive stars, it is less obvious that an upper limit to stellar masses results from a limit on cloud or clump masses. If clump masses are limited and if the mass of the most massive star to form depends causally (not just statistically) on the mass of the clump or cloud, the integrated galactic IMF (IGIMF) can be steepened (Kroupa & Weidner 2003, Weidner & Kroupa 2006). We discuss the second requirement in Section 4.2 and consequences of this controversial idea in Sections 3.3 and 6.4.

3. STAR-FORMATION-RATE DIAGNOSTICS: THE IMPACT OF MULTIWAVELENGTH OBSERVATIONS

The influx of new observations over the past decade has led to major improvements in the calibration and validation of diagnostic methods for measuring SFRs in galaxies. Whereas measuring uncertainties of factors of two or larger in SFRs was commonplace ten years ago, new diagnostics based on multiwavelength data are reducing these internal uncertainties by up to an order of magnitude in many instances. These techniques have also reduced the impact of many systematic errors, in particular uncertainties due to dust attenuation, though others such as the IMF (Section 2.5) remain important limiting factors.

A detailed discussion of SFR diagnostics and their calibrations was given by Kennicutt (1998a), and here we highlight progress made since that review was published. In Section 3.8, we compile updated calibrations for the most commonly used indices, based on updated evolutionary synthesis models and IMF compared with those of Kennicutt (1998a). The new challenges that come with spatially resolved measurements of galaxies are discussed in Section 3.9.

3.1. Star Counting and Analysis of the Color-Magnitude Diagram

The most direct way to measure SFRs is to count the number of identifiable stars of a certain age. Ideally, one would have reliable masses and ages for each star and the mean SFR would be given by

$$\langle \dot{M}_* \rangle = \sum_{M_*=M_l}^{M_u} N(M_*, t_*) M_* / t_*, \qquad (8)$$

where $N(M_*, t_*)$ is the number of stars in a mass bin characterized by mass M_* and a lifetime bin (the time since formation) characterized by t_* and the SFR would be averaged over the longest value of t_* in the sum. In practice, complete information is not available, and one needs to limit the allowed lifetimes to find the SFR over a certain period. In particular, for nearby clouds in the MW, nearly complete lists of young stellar objects (YSOs) with IR excesses are available. If one assumes that the YSOs sample the IMF in a typical way, one can derive the mean mass of stars ($\langle M_* \rangle$), and the equation becomes

$$\langle \dot{M}_* \rangle = N(\text{YSOs}) \langle M_* \rangle / t_{\text{excess}}. \quad (9)$$

With currently favored IMFs, $\langle M_* \rangle = 0.5\ M_\odot$. The main source of uncertainty is in t_{excess}, the duration of an IR excess (Section 4.1).

For young clusters, one can determine mean ages from fitting isochrones to a color-magnitude diagram (CMD) and measure $\dot{M}_*$ assuming coeval formation as long as some stars have not yet reached the main sequence. Some clusters have measurements of stars down to very low masses (e.g., the Orion Nebula Cluster) (Hillenbrand 1997), but most need corrections for unseen low-mass stars. For older clusters, one can derive the total mass, but not (directly) the duration of star formation, which has to be assumed.

In principle, similar techniques can be applied on a galaxy-wide basis. Beyond the Magellanic Clouds, current instruments cannot resolve individual YSOs in most regions. As a result, most studies of SFRs in galaxies are based either on measurements of massive O-type and/or Wolf-Rayet stars (see Kennicutt 1998a) or on measurements of the entire CMD. Considerable progress has been made recently using spatially resolved mapping of CMDs to reconstruct spatially and age-resolved maps of star formation in nearby galaxies. Many of these use the distribution of blue helium-burning stars in the CMD (e.g., Dohm-Palmer et al. 2002), but more recent analyses fit the entire upper CMDs to synthetic stellar populations to derive estimates of spatially resolved stellar age distributions with formal uncertainties (e.g., Dolphin 2002, Weisz et al. 2008). This technique does not have sufficient age resolution to determine accurate SFRs for ages less than ~10 Myr, but when applied to high-quality data sets such as those obtained with HST, they can provide sufficient age resolution to constrain the temporal behaviors and changes in the spatial distributions of formation over the past 100 Myr or longer (e.g., Weisz et al. 2008, Williams et al. 2011).

3.2. Ultraviolet Continuum Measurements: The Impact of the *Galaxy Evolution Explorer*

The near-ultraviolet (UV) emission of galaxies longward of the Lyman-continuum break directly traces the photospheric emission of young stars and, hence, is one of the most direct tracers of the recent SFR. For a conventional IMF, the peak contribution to the integrated UV luminosity of a young star cluster arises from stars with masses of several solar masses. Consequently, this emission traces stars formed over the past 10–200 Myr, with shorter timescales at the shortest wavelengths (see **Table 1**).

For extragalactic studies, this subject has been revolutionized by the launch of the GALEX mission (Martin et al. 2005a). It imaged approximately two-thirds of the sky in far-UV (FUV; 155 nm) and near-UV (NUV; 230 nm) channels to limiting-source fluxes $m_{AB} \sim 20.5$, and obtained deeper full-orbit or multiorbit imaging ($m_{AB} \geq 23$) for selected galaxies and fields such as those in the Sloan Digital Sky Survey (SDSS). The spatial resolution (4.5 arcsec to 6 arcsec FWHM) of the imager makes it an especially powerful instrument for integrated measurements of distant galaxies and resolved mapping of the nearest external galaxies. Although most scientific applications of

Table 1 Star-formation-rate calibrations

Band	Age range (Myr)[a]	L_x units	log C_x[b]	$\dot{M}_*/\dot{M}_*$(K98)[c]	Reference(s)
FUV	0-10-100	ergs s^{-1} (νL_ν)	43.35	0.63	Hao et al. (2011), Murphy et al. (2011)
NUV	0-10-200	ergs s^{-1} (νL_ν)	43.17	0.64	Hao et al. (2011), Murphy et al. (2011)
Hα	0-3-10	ergs s^{-1}	41.27	0.68	Hao et al. (2011), Murphy et al. (2011)
TIR	0-5-100[d]	ergs s^{-1} (3–1100 μm)	43.41	0.86	Hao et al. (2011), Murphy et al. (2011)
24 μm	0-5-100[d]	ergs s^{-1} (νL_ν)	42.69		Rieke et al. (2009)
70 μm	0-5-100[d]	ergs s^{-1} (νL_ν)	43.23		Calzetti et al. (2010b)
1.4 GHz	0-100	ergs s^{-1} Hz^{-1}	28.20		Murphy et al. (2011)
2–10 keV	0-100	ergs s^{-1}	39.77	0.86	Ranalli et al. (2003)

[a]Second number gives mean age of stellar population contributing to emission; third number gives age below which 90% of emission is contributed.
[b]Conversion factor between SFR and the relevant luminosity, as defined by Equation 12 in Section 3.8.
[c]Ratio of star-formation rate (SFR) derived using the new calibration to that derived using the relations in Kennicutt (1998a). The lower SFRs now mainly result from the different initial mass function and from updated stellar population models.
[d]Numbers are sensitive to star-formation history; those given are for continuous star formation over 0–100 Myr. For more quiescent regions (e.g., disks of normal galaxies), the maximum age will be considerably longer.
Abbreviations: FUV, far ultraviolet; NUV, near ultraviolet; TIR, total infrared.

GALEX data to date have arisen from its imaging surveys, a series of spectroscopic surveys and pointed observations of varying depths were also carried out (Martin et al. 2005a).

The main impacts of GALEX for this subject are summarized in Section 5. Broadly speaking, its largest impacts were in providing integrated UV fluxes (and, hence, SFR estimates) for hundreds of thousands of galaxies and in exploiting the dark sky from space at these wavelengths to reveal star formation at low-surface brightnesses and intensities across a wide range of galactic environments.

Other spaceborne instruments have also provided important data sets in this wavelength region, including the *XMM Optical Monitor* (Mason et al. 2001) and the *Swift UV/Optical Telescope* (Roming et al. 2005). Although these instruments were primarily designed for follow-up of X-ray and gamma-ray observations, they also have been used to image nearby and distant galaxies, with the advantage of higher spatial resolution (~1 arcsec FWHM). Several important studies have also been published over the past decade from observations made with the *Ultraviolet Imaging Telescope* on the ASTRO missions (Stecher et al. 1997, Marcum et al. 2001). The HST continues to be a steady source of observations (mainly in the NUV) for targeted regions in nearby galaxies.

The primary disadvantage of the UV is its severe sensitivity to interstellar dust attenuation. The availability of new data from GALEX and other facilities has stimulated a fresh look at this problem. If the intrinsic color of the emitting stellar population is known a priori, the FUV-NUV color or the UV spectral slope (usually denoted by β) can be used to estimate the dust attenuation, and numerous calibrations have been published (e.g., Calzetti, Kinney & Storchi-Bergmann 1994; Kong et al. 2004; Seibert et al. 2005; Johnson et al. 2007; Salim et al. 2007; Treyer et al. 2007; Hao et al. 2011). The accuracy of these prescriptions rests heavily on the presumed (but uncertain) intrinsic colors, the shape of the dust extinction curve, and the complicated effects of geometry and scattering when averaging over a large physical region (e.g., Gordon et al. 2001).

The abundance of high-quality far-IR observations of nearby galaxies has made it possible to test how well the UV colors correlate with independent estimates of the dust attenuation from the IR/UV flux ratios. Earlier observations of bright starburst galaxies suggest a tight relation between

the logarithmic IR/UV ratio (often termed the IRX) and UV color (e.g., Meurer, Heckman & Calzetti 1999). Indeed, this IRX-β relation provided the primary means for calibrating the color versus attenuation relation. Subsequent observations of a wider range of galaxies, however, have revealed a much larger scatter in the relation (e.g., Boquien et al. 2012). When galaxies of all types are considered, the scatter in actual FUV attenuations for a fixed FUV-NUV color can easily be two orders of magnitude. Even when the comparison is restricted to galaxies with intrinsically high SFRs (as may be observed at high redshift), the uncertainties can easily reach an order of magnitude. As a result, more weight is being applied to alternative estimates of attenuation corrections and SFRs based on combinations of UV with IR measurements (Section 3.7).

3.3. Emission-Line Tracers

The remaining SFR indicators discussed here rely on measuring starlight that has been reprocessed by interstellar gas or dust or on tracers related to the death of massive stars. The most widely applied of these are the optical and near-IR emission lines from ionized gas surrounding massive young stars. For a conventional IMF, these lines trace stars with masses greater than $\sim$15 $M_\odot$, with the peak contribution from stars in the range 30–40 $M_\odot$. As such, the lines (and likewise the free-free radio continuum) represent a nearly instantaneous measure of the SFR, tracing stars with lifetimes of $\sim$3–10 Myr (**Table 1**).

The application of Hα and other emission-line SFR tracers has expanded dramatically in the past decade, through very large spectroscopic surveys of samples of local and distant galaxies, narrow-band emission-line imaging surveys, and large imaging surveys of nearby galaxies designed to study spatial variations in the SFR. Advances in near-IR instrumentation have also led to the first systematic surveys in the Paschen and Brackett series lines, as well as for Hα observed at high redshifts. Results from several of these surveys are discussed and referenced in Section 5.

The Hα emission line remains the indicator of choice for observations of both local and distant galaxies, but for moderate redshifts, the bluer visible lines have been applied, in particular the [OII] forbidden-line doublet at 372.7 nm. This feature is subject to severe systematic uncertainties from dust attenuation and excitation variations in galaxies. Kennicutt (1998a) published a single SFR calibration for the line, but subsequent analyses (e.g., Jansen, Franx & Fabricant 2001; Kewley, Geller & Jansen 2004; Moustakas, Kennicutt & Tremonti 2006) have shown that the systematic effects must be removed or at least calibrated to first order for reliable measurements. Even then, the uncertainties in the [OII]-based SFRs are much larger than for Hα.

Over the past decade, increasing attention has been given to measurements of the redshifted Lyα line ($\lambda_{\rm rest} = 121.6$ nm) as a tracer of star-forming galaxies, especially at high redshifts where it provides unique sensitivity to both low-mass star-forming galaxies and intergalactic gas clouds or "blobs" (e.g., Ouchi et al. 2009, 2010). The strength of the line (8.7 times stronger than Hα for Case B recombination) makes it an attractive tracer in principle, but in realistic ISM environments, the line is subject to strong quenching from the combination of resonant trapping and eventual absorption by dust, usually quantified in terms of a Lyα escape fraction. As a result, Lyα surveys to date have been mainly used for identifying large samples of distant star-forming galaxies. Applying the line as a quantitative SFR tracer requires an accurate measurement of the escape fraction. Several ongoing studies are quantifying this parameter by comparing Lyα fluxes of galaxies with independent SFR tracers such as Hα or the UV continuum (e.g., Atek et al. 2009, Scarlata et al. 2009, Blanc et al. 2011, Hayes et al. 2011). These show that the escape fraction varies wildly between galaxies with a range of more than two orders of magnitude (order 0.01 to 1), but it also increases systematically with redshift. Lyα may prove to be a powerful SFR tracer for the highest-redshift objects, but in view of the large scatter and systematic uncertainties associated with its use, we have chosen not to include an SFR calibration of the line in this review.

Other workers have investigated the efficacy of the IR fine-structure cooling lines, which arise in HII regions or PDRs, as quantitative SFR tracers. Ho & Keto (2007) compiled data from ISO and *Spitzer* on the [NeII]12.8-μm and [NeIII]15.6-μm lines, and they found that the sum of the line fluxes correlates well with hydrogen recombination line fluxes, with a scatter of ∼0.3 dex. In a similar vein, Boselli et al. (2002) and Rodriguez-Fernandez et al. (2006) have investigated the applicability of the [CII]158-μm line, which also arises in PDRs, as an SFR measure. They found good general correspondence between the [CII] luminosity and other measures of the SFR such as ionized gas and dust emission, but the scatter in the relationships is at least a factor of 10. Even larger variations in $L_{[CII]}/L_{IR}$ were found in a more diverse sample of star-forming galaxies by Malhotra et al. (1997). The availability of a rich new set of [CII] observations from *Herschel*, combined with the detection of redshifted [CII] emission in submillimeter galaxies (SMGs) from ground-based instruments, has sparked a resurgence of interest in this application.

The largest systematic errors affecting Hα-based SFRs are dust attenuation and sensitivity to the population of the upper IMF in regions with low absolute SFRs. For regions with modest attenuations, the ratios of Balmer recombination lines (Balmer decrement) can be used to correct for dust. This method has been applied in a number of large spectrophotometric surveys of nearby galaxies (e.g., Kewley et al. 2002; Brinchmann et al. 2004; Moustakas, Kennicutt & Tremonti 2006). The Balmer decrements offer only approximate corrections for attenuation because of variations on scales smaller than the resolution. These variations may lead to an underestimate of the extinction because lines of sight with low extinction are more heavily weighted within the beam. This problem can be addressed partly by adopting a reddening law that compensates in part for these departures from a pure foreground-scheme geometry (e.g., Charlot & Fall 2000). The attenuation of the emission lines is found to be systematically higher than that of the continuum starlight at the same wavelengths (e.g., Calzetti, Kinney & Storchi-Bergmann 1994), which presumably reflects the higher concentrations of dust in the young star-forming regions.

As is the case with UV-based SFRs, the availability of far-IR maps and luminosities for nearby galaxies has also made it possible to calibrate multiwavelength methods for applying dust-attenuation corrections to these measurements (Section 3.7). They reveal that the Balmer decrement provides reasonably accurate attenuation corrections in normal galaxies, where attenuations are modest (typically 0–1 mag at Hα), and care is taken to correct the emission-line fluxes for underlying stellar absorption. The Balmer decrement method for estimating dust attenuation breaks down badly, however, in circumnuclear starbursts or other dusty galaxies (e.g., Moustakas, Kennicutt & Tremonti 2006). With the advent of large-format integral-field spectrographs, there is promise of applying Balmer decrement measurements on a spatially resolved basis in galaxies (e.g., Blanc 2010, Sánchez et al. 2012).

The accuracy of SFRs derived from emission lines will also degrade in regions where the SFR is so low that one enters the regime of small-number statistics in the population of massive ionizing stars. If the IMF were completely blind to the SFR, we would expect such effects to become apparent below Hα luminosities of order 10^{38} ergs s^{-1} or SFRs of order 0.001 $M_\odot$ $year^{-1}$ (e.g., Cerviño et al. 2003). At the very least, this effect will produce a much larger scatter in ionizing flux per unit SFR in this regime. In low-SFR regions, this sampling noise can be exacerbated by the short lifetimes of the ionizing stars, producing large temporal fluctuations in Hα emission even for a fixed longer-term SFR. As a result, other tracers (e.g., FUV emission) tend to provide more accurate and sensitive measurements of the SFR at low star-formation levels.

Can these effects cause systematic errors in the SFRs? Pflamm-Altenburg, Weidner & Kroupa (2007, 2009) have investigated the effect of an IGIMF (Section 2.5) on SFR tracers and shown that the systematic depletion of massive stars in low-SFR environments could cause Hα to substantially underestimate the actual SFR. Interestingly, a systematic deficit of Hα emission in dwarf galaxies

with low SFRs and in low-SFR density regions is observed (Sullivan et al. 2000, Bell & Kennicutt 2001, Lee et al. 2009a, Meurer et al. 2009). Recent work suggests, however, that the systematic dependence of the Hα/UV ratio may be produced instead by temporal variations in SFRs, without having to resort to modifying the IMF (Fumagalli, da Silva & Krumholz 2011; Weisz et al. 2012).

3.4. Infrared Emission: The Impact of *Spitzer* and *Herschel*

Interstellar dust absorbs approximately half of the starlight in the Universe and re-emits it in the IR, so measurements in the IR are essential for deriving a complete inventory of star formation. This section focuses on the transformational results that have come from the *Spitzer Space Telescope* (Werner et al. 2004) and the *Herschel Space Observatory* (Pilbratt et al. 2010). A review in this journal of extragalactic science from *Spitzer* can be found in Soifer, Helou & Werner (2008).

Three other important space missions are beginning to influence this subject: the AKARI mission (Murakami et al. 2007), the *Wide-Field Infrared Survey Explorer* (WISE) mission (Wright et al. 2010), and the *Planck* mission (Planck Collaboration et al. 2011a). These observatories conducted all-sky surveys, with AKARI imaging in the 2.4–160-μm region, WISE in the range of 3.4–22 μm, and *Planck* at 350–850 μm, respectively (with several bands extending to longer wavelengths). Much of the science from these missions is just beginning to emerge, but they will provide very important results in this subject in the coming decade.

Although early applications of dust-based SFR measurements effectively (and necessarily) assumed a one-component dust model, subsequent observations show that the dust emission is comprised of distinct components, each with different spatial distributions and couplings to the young stars. At wavelengths of ∼5–20 μm, the emission is dominated by molecular bands arising from polycyclic aromatic hydrocarbons (PAHs). Longward of $\lambda \sim 20$ μm, the emission is dominated by thermal continuum emission from the main dust-grain population. Emission from small grains transiently heated by intense radiation fields (usually in or near star-forming regions) is important out to approximately 60 μm, whereas at longer wavelengths, emission from larger grains with steady-state temperatures dominates (Draine 2003).

The distribution of these different emission components is illustrated in **Figure 2**, which shows *Spitzer* and *Herschel* images of the nearby star-forming galaxy NGC 6946 at wavelengths ranging from 3.6–500 μm. At 24 μm, the emission peaks around the youngest star-forming regions and HII regions, with a more diffuse component extending between these regions. As one progresses to longer wavelengths, the prominence of the diffuse component increases. Recent measurements with *Herschel* show that this is mainly a physical change and not an artifact of lower spatial resolution at longer wavelengths (Boquien et al. 2011). This diffuse emission is analogous to the IR cirrus emission observed in our own Galaxy. Interestingly, PAH emission appears to correlate the most strongly with the longer-wavelength component of the thermal dust emission (e.g., Bendo et al. 2008), though it often also appears as resolved shells around the young star-forming regions (Helou et al. 2004).

These variations in the morphologies in the different dust-emission components translate into considerable variations in the dust spectral energy distributions (SEDs) within and between galaxies (e.g., Dale & Helou 2002, Dale et al. 2005, Smith et al. 2007), and as a consequence, the conversion of IR luminosities into SFRs must change for different IR wavelengths. Most early applications of dust emission as an SFR tracer were based on the integrated TIR emission. This parameter has the physical advantage of effectively representing the bolometric luminosity of a completely dust-enshrouded stellar population. The TIR-based SFR calibration derived by Kennicutt (1998a), applicable in the limits of complete dust obscuration and dust heating fully dominated by young stars, is still in widespread use today. For most galaxies, however, this complete

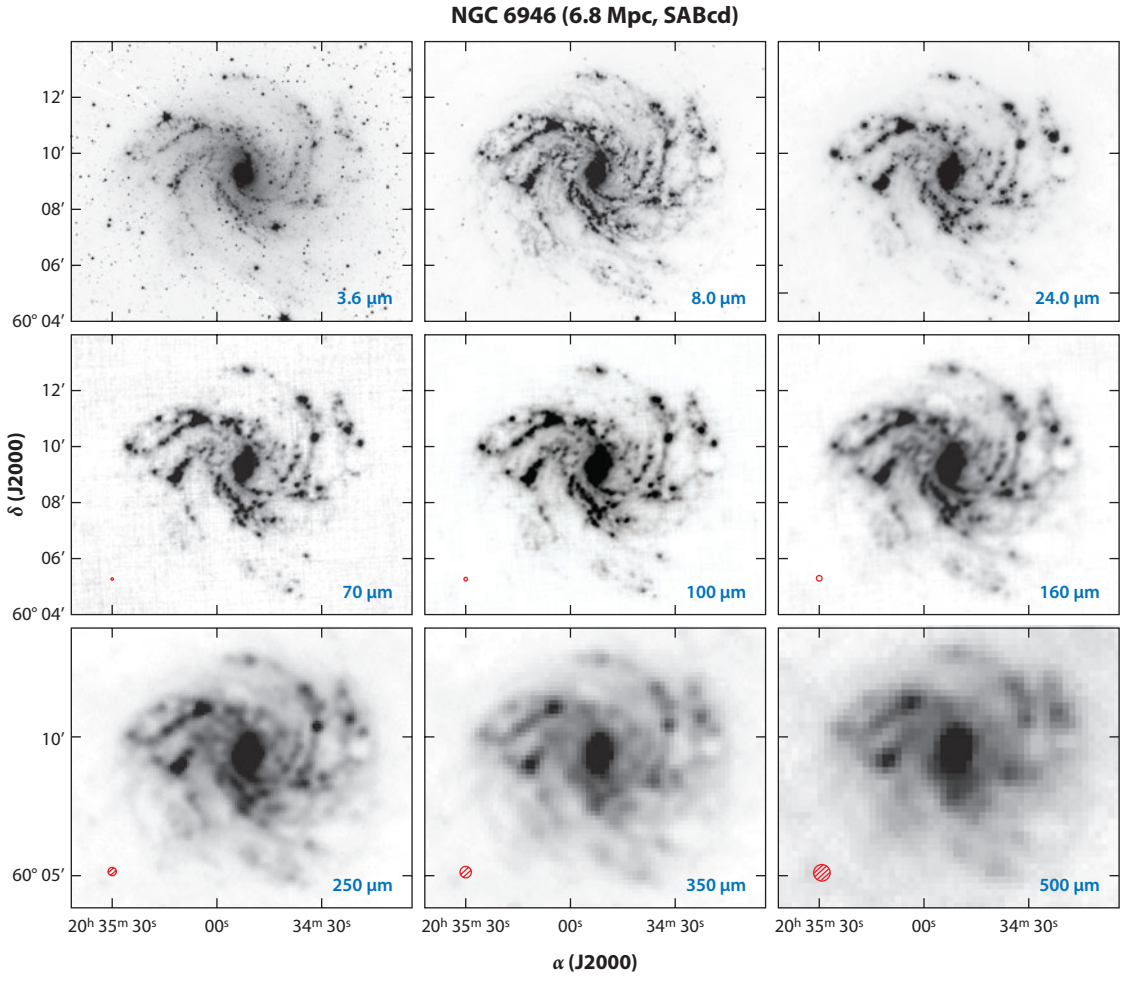

Figure 2

A montage of infrared images of NGC 6946 from *Spitzer* (SINGS) and *Herschel* (KINGFISH). (*Top panels*) *Spitzer* IRAC images at 3.6 μm and 8.0 μm and MIPS image at 24 μm. The emission at these wavelengths is dominated by stars; small, polycyclic aromatic hydrocarbon (PAH) dust grains; and small dust grains heated by intense radiation fields, respectively. (*Middle panels*) *Herschel* PACS images at 70 μm, 100 μm, and 160 μm, processed with the Scanamorphos map-making package. Note the excellent spatial resolution despite the longer wavelengths and the progressive increase in contributions from diffuse dust emission ("cirrus") with increasing wavelength. (*Bottom panels*) *Herschel* SPIRE images at 250 μm, 350 μm, and 500 μm. These bands trace increasingly cooler components of the main thermal dust emission, with possible additional contributions from "submillimeter excess" emission at the longest SPIRE wavelengths. FWHM beam sizes for the respective *Herschel* bands are shown in the lower left corner of each panel in red. [This figure originally appeared in the Publications of the Astronomical Society of the Pacific (Kennicutt et al. 2011). Copyright 2011, Astron. Soc. Pac.; reproduced with permission of the Editors.]

wavelength coverage will not be available, so many workers have calibrated monochromatic SFR indices, usually tuned to one of the *Spitzer* or *Herschel* bands, including 24 μm (e.g., H. Wu et al. 2005, Alonso-Herrero et al. 2006, Calzetti et al. 2007, Relaño et al. 2007, Rieke et al. 2009, and references therein) as well as 70 and 160 μm (Calzetti et al. 2010a). The latter paper contains an excellent discussion comparing the various calibrations in the literature at the time.

As with all SFR indicators, the dust emission is subject to important systematic effects. Just as the UV and visible tracers miss radiation that has been attenuated by dust, the IR emission misses the starlight that is *not* absorbed by dust (e.g., Hirashita et al. 2001). As discussed earlier, dust attenuates only approximately half of the integrated starlight of galaxies on average, so the IR emission will systematically underestimate the SFR if the missing fraction of star formation is not incorporated into the calibrations. This "missing" unattenuated component varies from essentially zero in dusty starburst galaxies to nearly 100% in dust-poor dwarf galaxies and metal-poor regions of more-massive galaxies. Another major systematic error works in the opposite direction; in most galaxies, evolved stars (e.g., ages above ~100–200 Myr) contribute significantly to dust heating, which tends to cause the IR luminosity to overestimate the SFR. The fraction of dust heating from young stars varies by a large factor among galaxies: In extreme circumnuclear starburst galaxies or individual star-forming regions, nearly all the dust heating arises from young stars, whereas in evolved galaxies with low specific SFRs, the fraction can be as low as ~10% (e.g., Sauvage & Thuan 1992, Walterbos & Greenawalt 1996, Cortese et al. 2008). In practical terms, this means that the conversion factor from dust luminosity to SFR—even in the limit of complete dust obscuration—is not fixed, but rather changes as a function of the stellar population mix in galaxies. The difference in conversion factor between starbursts and quiescent galaxies with constant SFR, for example, is approximately a factor of 1.3–2 (e.g., Sauvage & Thuan 1992, Kennicutt et al. 2009, Hao et al. 2011).

The calibration of the mid-IR PAH emission as a quantitative SFR tracer deserves special mention. This index is of particular interest for studies of galaxies at high redshift because the observed-frame 24-μm fluxes of galaxies at $z = 1$–3 tend to be dominated by redshifted PAH emission. A number of studies have shown that the PAH luminosity scales relatively well with the SFR in metal-rich luminous star-forming galaxies (e.g., Roussel et al. 2001; Förster Schreiber et al. 2004; Peeters, Spoon & Tielens 2004; H. Wu et al. 2005; Calzetti et al. 2007; Farrah et al. 2007), but the PAH bands weaken dramatically below metal abundances of approximately 1/4 to 1/3 $Z_{\odot}$ (e.g., Madden 2000, Engelbracht et al. 2005, Calzetti et al. 2007, Smith et al. 2007), rendering them problematic as quantitative SFR tracers in this regime.

The best way to overcome these systematic biases is to combine the IR measurements with UV or visible-wavelength SFR tracers to measure the unattenuated starlight directly and to constrain the dust-heating stellar population (Section 3.7). However, in cases where only IR observations are available, one can attempt to incorporate corrections for these effects into the SFR calibrations. This approach has been taken by most researchers (e.g., Calzetti et al. 2010b, and references therein). Fortunately, for most galaxies with moderate to high specific SFRs, the effects of partial dust attenuation and cirrus dust heating by evolved stars appear to compensate roughly for each other. For example, Kewley et al. (2002) showed that, for a sample of spiral galaxies with integrated emission-line spectra, the TIR-based calibration by Kennicutt (1998a) for dusty starburst galaxies was in good agreement with SFRs based on attenuation-corrected Hα line fluxes. However, one must avoid applying these IR-based recipes in environments where they are bound to fail, for example, in low-metallicity and other largely dust-free galaxies or in galaxies with low specific SFRs and a strong radiation field from more-evolved stars.

3.5. Radio Continuum Emission

The centimeter-wavelength radio continuum emission of galaxies consists of a relatively flat-spectrum, free-free component, which scales with the ionizing luminosity (subject to a weak electron temperature dependence) and a steeper spectrum synchrotron component, which overwhelmingly dominates the integrated radio emission at $\nu \leq 5$ GHz. The free-free component

can be separated with multifrequency radio measurements or high-frequency data (e.g., Israel & van der Hulst 1983; Niklas, Klein & Wielebinski 1997; Murphy et al. 2011) to provide a photoionization-based measure of the SFR without the complications of dust attenuation that are encountered with the Balmer lines.

At lower frequencies, the integrated emission is dominated by the synchrotron emission from charged particles produced by supernovae. An SFR calibration has not been derived from first principles, but observations have repeatedly confirmed a tight correlation between this nonthermal emission and the far-IR emission of galaxies, which favors its application as an SFR tracer (e.g., Condon 1992; Helou, Soifer & Rowan-Robinson 1985). Moreover, improvements to receiver technology with the Expanded Very Large Array (EVLA) and other instruments have made the radio continuum a primary means of identifying star-forming galaxies at high redshift and estimating their SFRs. As a result, the radio continuum is properly included in this discussion of SFR tracers.

Current calibrations of the radio continuum versus SFR relation are bootstrapped from the far-IR calibrations, using the tight radio–IR correlation. The steep synchrotron spectrum makes this calibration strongly wavelength dependent, and most are referenced to 1.4 GHz (e.g., Condon 1992; Yun, Reddy & Condon 2001; Bell 2003). The calibration adopted here in Section 3.8 is derived in similar fashion but adapted to the Kroupa IMFs.

As described above, the IR-based SFR calibrations break down severely in faint galaxies with low dust contents, yet the radio-IR correlation remains tight and nearly linear over the entire luminosity range. How can this arise? The likely explanation can be found in Bell (2003) and references therein, where the decrease in dust opacity in low-mass galaxies is shown to be accompanied by a decline in synchrotron emission relative to other tracers of the SFR. This is seen most directly as a decline in the ratio of nonthermal radio emission (still dominant in the 1–5-GHz region) to the free-free thermal radio emission. Because the thermal radio emission is directly coupled to the stellar ionization rate and SFR, the relative decline in synchrotron luminosity must reflect a physical decline per unit SFR. If correct, then the continuity of the radio-IR relation to low luminosities is the result of a "cosmic conspiracy" (Bell 2003), and one should beware of applying the method in galaxies fainter than $\sim$0.1 L^*.

3.6. X-Ray Emission

Over the past decade, the integrated hard X-ray emission of galaxies has been increasingly applied as an SFR tracer. The component of X-ray emission that does not arise from AGN accretion disks is dominated by massive X-ray binaries, supernovae and supernova remnants, and massive stars, all associated with young stellar populations and recent star formation. Furthermore, the observed 2–10 keV fluxes of galaxies are observed to be strongly correlated with their IR and nonthermal radio continuum fluxes (e.g., Bauer et al. 2002; Ranalli, Comastri & Setti 2003; Symeonidis et al. 2011), thereby strengthening the link to the SFR.

Because the relation between X-ray luminosity and SFR cannot be calibrated from first principles, this calibration is usually bootstrapped from the IR or radio. Ranalli, Comastri & Setti (2003) derived such a calibration for integrated 2–10-keV X-ray luminosities, referenced to Kennicutt's (1998a) calibrations and IMF; this relation is still widely applied today. Persic et al. (2004) derived an alternate calibration in terms of the hard X-ray binary luminosity alone, which is useful for nearby resolved galaxies. Calibrations of the SFR in terms of X-ray luminosity and stellar mass have been published by Colbert et al. (2004) and Lehmer et al. (2010). For simplicity, we have listed in **Table 1** the widely applied relation of Ranalli, Comastri & Setti (2003) but adjusted it to the Kroupa IMF used for the other calibrations.

3.7. Composite Multiwavelength Tracers

Large multiwavelength surveys of galaxies allow tests and calibrations of SFR indices that combine information from more than one tracer and exploit the complementary strengths of different wavelengths. Currently, this capability is mainly limited to nearby galaxies, but with the expansion of far-IR and millimeter surveys of high-redshift galaxies, opportunities to apply multiwavelength diagnostics to distant galaxies should expand in the coming decade (e.g., Overzier et al. 2011, Reddy et al. 2011).

The most widely explored of these methods have combined UV (usually FUV) observations with IR measurements to construct dust-corrected SFRs, using an approximate energy-balancing approach. In its simplest form, one can use a linear combination of UV and IR luminosities to correct the UV fluxes for dust attenuation:

$$L_{\rm UV}({\rm corr}) = L_{\rm UV}({\rm observed}) + \eta\ L_{\rm IR}, \tag{10}$$

where the luminosities are usually calculated from flux densities using the definition $L = \nu L_\nu$ and the coefficient η is dependent on the band passes chosen for the UV and IR measurements. The most common form of this correction uses GALEX FUV (155 nm) and TIR luminosities. Hence,

$$L_{\rm FUV}({\rm corr}) = L_{\rm FUV}({\rm observed}) + \eta_{\rm FUV}\ L_{\rm TIR}. \tag{11}$$

Other prescriptions sometimes adopt a higher-order polynomial dependence on $L_{\rm IR}$ (e.g., Buat et al. 2005), but for brevity, we discuss only the linear combinations here. In most cases, $\eta < 1$ because only part of the dust-heating radiation is contained in the FUV band and in many galaxies there is significant dust heating and TIR emission arising from stars other than the UV-emitting population (IR cirrus). The coefficient η can be calibrated theoretically using evolutionary synthesis models or empirically using independent measurements of dust-corrected SFRs (e.g., Treyer et al. 2010, Hao et al. 2011).

Early applications of this method were largely restricted to luminous starburst galaxies and star-forming regions, for which UV and IR data could be obtained prior to the advent of GALEX, *Spitzer*, and *Herschel* (e.g., Buat et al. 1999; Meurer, Heckman & Calzetti 1999; Gordon et al. 2000), yielding values of $\eta \sim 0.6$. Subsequent analyses extending to normal star-forming galaxies (e.g., Hirashita, Buat & Inoue 2003; Kong et al. 2004; Buat et al. 2005; Burgarella, Buat & Iglesias-Páramo 2005; Treyer et al. 2010; Hao et al. 2011) typically produce values of η that are somewhat lower (e.g., 0.46 for Hao et al. 2011), which almost certainly reflects the larger contribution to dust heating from starlight longward of the FUV. Considering the wide differences in dust-heating populations between starburst and normal galaxies, however, this difference of ∼30% is hardly crippling, especially when it reduces dramatically the much larger systematic errors from UV or IR-based SFRs alone.

A similar energy-balancing approach has been applied to derive dust-corrected emission-line luminosities of galaxies (Calzetti et al. 2007, Zhu et al. 2008, Kennicutt et al. 2009, Treyer et al. 2010). Here the equivalent parameter to η above is calibrated using independent estimates of the Hα attenuation, usually the recombination line decrement as measured from the Paα/Hα or Hα/Hβ ratio. Kennicutt et al. (2009) have shown that this approach can be more broadly applied to estimate attenuation corrections for other emission lines (e.g., [OII]), and it can be calibrated using TIR fluxes, single-band IR fluxes, or even 1.4-GHz radio continuum fluxes. An illustration of the effectiveness of the method is shown in **Figure 3**, taken from Kennicutt et al. (2009).

These composite SFR indicators are not without systematic uncertainties of their own. Questions remain about the systematic reliability of the independent attenuation calibrations (in particular with the effects of dust geometry on the Balmer decrements), and most of the recipes still

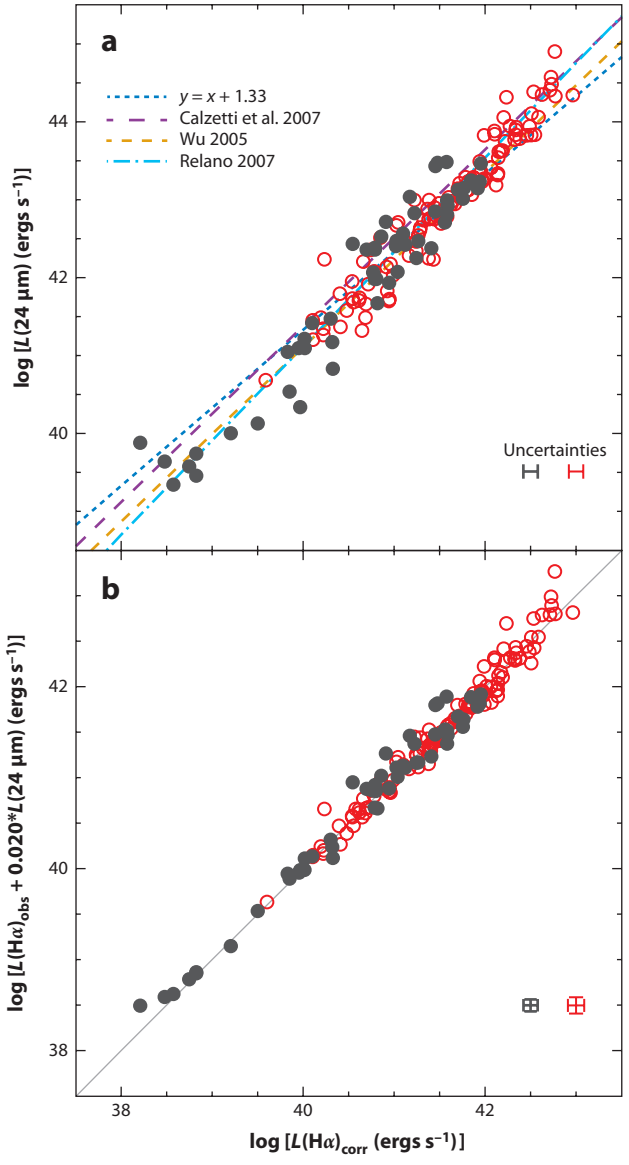

Figure 3

(*a*) Relation between observed 24-μm infrared (IR) luminosity and dust-corrected Hα luminosity (via the integrated Balmer decrement) for nearby galaxies. There is a general correlation but considerable scatter and a pronounced nonlinearity, which reflects a general correlation of average dust attenuation with the star-formation rate. The dust corrections were derived from the absorption-corrected Hα/Hβ ratios in optical spectra. The dotted blue line shows a linear relation for comparison, whereas the other lines show published fits to other samples of galaxies. (*b*) Linear combination of (uncorrected) Hα and 24-μm luminosities compared with the same Balmer-decrement-corrected Hα luminosities. The scatter between the tracers now is reduced severalfold, and the nonlinearity in the comparison with IR luminosities alone is essentially removed. Also note the tightness and linearity of the relation over nearly the entire luminosity range. Taken from Kennicutt et al. (2009); reproduced by permission of the AAS.

Table 2 Multiwavelength dust corrections for normal galaxies

Composite tracer	Reference
$L(\mathrm{FUV})_{\mathrm{corr}} = L(\mathrm{FUV})_{\mathrm{obs}} + 0.46\,L(\mathrm{TIR})$	Hao et al. (2011)
$L(\mathrm{FUV})_{\mathrm{corr}} = L(\mathrm{FUV})_{\mathrm{obs}} + 3.89\,L(25\ \mu\mathrm{m})$	Hao et al. (2011)
$L(\mathrm{FUV})_{\mathrm{corr}} = L(\mathrm{FUV})_{\mathrm{obs}} + 7.2 \times 10^{14}\,L(1.4\ \mathrm{GHz})$[a]	Hao et al. (2011)
$L(\mathrm{NUV})_{\mathrm{corr}} = L(\mathrm{NUV})_{\mathrm{obs}} + 0.27\,L(\mathrm{TIR})$	Hao et al. (2011)
$L(\mathrm{NUV})_{\mathrm{corr}} = L(\mathrm{NUV})_{\mathrm{obs}} + 2.26\,L(25\ \mu\mathrm{m})$	Hao et al. (2011)
$L(\mathrm{NUV})_{\mathrm{corr}} = L(\mathrm{NUV})_{\mathrm{obs}} + 4.2 \times 10^{14}\,L(1.4\ \mathrm{GHz})$[a]	Hao et al. (2011)
$L(\mathrm{H}\alpha)_{\mathrm{corr}} = L(\mathrm{H}\alpha)_{\mathrm{obs}} + 0.0024\,L(\mathrm{TIR})$	Kennicutt et al. (2009)
$L(\mathrm{H}\alpha)_{\mathrm{corr}} = L(\mathrm{H}\alpha)_{\mathrm{obs}} + 0.020\,L(25\ \mu\mathrm{m})$	Kennicutt et al. (2009)
$L(\mathrm{H}\alpha)_{\mathrm{corr}} = L(\mathrm{H}\alpha)_{\mathrm{obs}} + 0.011\,L(8\ \mu\mathrm{m})$	Kennicutt et al. (2009)
$L(\mathrm{H}\alpha)_{\mathrm{corr}} = L(\mathrm{H}\alpha)_{\mathrm{obs}} + 0.39 \times 10^{13}\,L(1.4\ \mathrm{GHz})$[a]	Kennicutt et al. (2009)

[a]Radio luminosity in units of ergs s^{-1} Hz^{-1}.
Abbreviations: FUV, far ultraviolet; NUV, near ultraviolet; TIR, total infrared.

retain a dependence on stellar population age, via the IR term; for example, the best-fitting values of η for HII regions and young starbursts differ from those of normal star-forming galaxies by a factor of ~1.5, consistent with expectations from evolutionary synthesis models, as discussed in Section 3.8 (Kennicutt et al. 2009). Nevertheless, they represent a major improvement over single-wavelength tracers and provide a valuable testing ground for calibrating and exploring the uncertainties in the monochromatic indicators (e.g., Calzetti et al. 2010b).

Table 2 lists examples of dust-attenuation corrections using combinations of FUV and Hα fluxes with various IR and radio tracers, taken from Hao et al. (2011) and Kennicutt et al. (2009), respectively. These can be applied in combination with the monochromatic SFR zero-point calibrations listed in **Table 2** (Section 3.8) to derive dust-corrected SFR measurements.

3.8. An Updated Compendium of Calibrations of Integrated Star-Formation Rates

Kennicutt (1998a) presented calibrations for SFRs derived from UV-continuum, TIR, Hα emission-line, and [OII] emission-line luminosities, which have come into common usage in the field. The considerable expansion of the subject to other wavelengths and SFR diagnostics since that time motivates a reexamination of these calibrations.

Nearly all these calibrations are based on evolutionary synthesis models in which the emergent SEDs are derived for synthetic stellar populations with a prescribed age mix, chemical composition, and IMF. Kennicutt's (1998a) calibrations employed a mix of models from the literature and assumed a single power-law IMF (Salpeter 1955) with mass limits of 0.1 and 100 $M_\odot$. This IMF gave satisfactory SFR calibrations relative to those of more realistic IMFs for Hα, but for other wavelengths, the relative calibrations using different tracers are sensitive to the precise form of the IMF. Today, most workers calibrate SFR tracers using a modern IMF with a turnover below ~1 $M_\odot$, for example, the IMF of Kroupa & Weidner (2003), with a Salpeter slope ($\alpha_* = -2.35$) from 1 to 100 $M_\odot$ and $\alpha_* = -1.3$ for 0.1–1 $M_\odot$. The calibrations presented here use this IMF, but the IMF fit from Chabrier (2003) yields nearly identical results (e.g., Chomiuk & Povich 2011). The past decade has also seen major improvements in the stellar evolution and atmospheric models that are used to generate the synthetic SEDs. The results cited here use the Starburst99 models of Leitherer et al. (1999), which are regularly updated in the online version of the package.

Table 1 presents in compact form calibrations for a suite of SFR tracers in the form

$$\log \dot{M}_*(\mathrm{M}_\odot\ \mathrm{year}^{-1}) = \log L_x - \log C_x. \quad (12)$$

The table lists for each tracer the units of luminosity (L_x), the logarithmic SFR calibration constant C_x, and the primary reference(s) for the calibration. For methods presented by Kennicutt (1998a), we also list the scaling constant between the new (Kroupa IMF, Starburst99 model) SFRs and those from Kennicutt (1998a). As was true for Kennicutt (1998a), the recipes for IR dust emission are in the limit of complete dust attenuation and continuous star formation over a period of 0–100 Myr, which is appropriate for a typical dust-obscured starburst galaxy. Virtually all the SFR calibrations presented in **Table 1** are taken from the literature, and we strongly encourage users of these calibrations to cite the primary sources, regardless of whether they choose to cite this review as well.

The second column of **Table 1** lists the approximate age sensitivity of the different star-formation tracers. These were estimated using the Starburst99 models in the approximation of constant star formation. The second number lists the mean stellar age producing the relevant emission, and the third column lists the age below which 90% of the relevant emission is produced. For the dust emission in the IR, these ages can only be estimated because they depend on the detailed star-formation history over periods of up to 100 Myr and longer and they are also convolved with the level of dust attenuation as a function of stellar age. The numbers are given for the assumed starburst timescales above; for normal galaxies, the 90th percentile age can be 500 Myr or longer.

All results were calculated for solar metal abundances, and readers should beware that all the calibrations are sensitive to metallicity. These have been estimated using evolutionary synthesis models (e.g., Smith, Norris & Crowther 2002; Raiter, Schaerer & Fosbury 2010), but the precise dependences are sensitive to the details of the input stellar models, in particular how effects of stellar rotation are modeled. The models cited above (which do not adopt a dependence of rotation on metallicity) show that a decrease in metal abundance by a factor of 10 increases the FUV luminosity of a fixed mass and IMF population by $\sim 0.07 \pm 0.03$ dex (for the IMFs assumed here), but the ionizing luminosity is more sensitive, increasing by $\sim 0.4 \pm 0.1$ dex for a tenfold decrease in $Z/Z_\odot$. The change in IR luminosities for completely obscured regions should roughly track that for the FUV luminosity, but in most low-metallicity environments, the dust opacity will be severely reduced, producing a sharp fall in IR emission for a given SFR.

3.9. The Challenge of Spatially Resolved Star-Formation Rates in Galaxies

Nearly all the diagnostic methods described up to now have been designed for measuring integrated SFRs of galaxies or for regions such as starbursts containing thousands (or more) of massive stars. The resulting SFR prescriptions implicitly assume that local variations in stellar-age mix, IMF population, and gas/dust geometry largely average out when the integrated emission of a galaxy is measured.

With the advent of high-resolution maps of galaxies in the UV, IR, emission lines, and radio (and integral-field spectroscopic maps in the visible and near-IR), one would like to extend these diagnostic methods to create fully sampled, spatially resolved "SFR maps" of galaxies. This extrapolation to much smaller regions within galaxies (or to galaxies with extremely low SFRs), however, is not at all straightforward. At smaller linear scales, nearly all the statistical approximations cited above begin to break down.

First, when the SFR in the region studied drops below ~ 0.001–$0.01\ \mathrm{M}_\odot\ \mathrm{year}^{-1}$ (depending on the SFR tracer used), incomplete sampling of the stellar IMF will lead to large fluctuations

in the tracer luminosity for a fixed SFR. These begin to become problematic for luminosities of order 10^{38}–10^{39} ergs s^{-1} for emission-line, UV, or IR tracers, and they are especially severe for the ionized-gas tracers, which are most sensitive to the uppermost parts of the stellar IMF. For actively star-forming normal disk galaxies, this onset of stochasticity typically occurs on spatial scales of order 0.1–1 kpc, but the region can be considerably larger in galaxies, or parts of galaxies, with lower SFRs. Note that this breakdown on local scales occurs regardless of whether the IMF varies systematically.

As a prime example of this stochasticity, consider what astronomers in M51 would observe if they examined the Solar Neighborhood in the MW from a distance of 10 Mpc. In a pixel of 100-pc radius centered on the Sun, they would observe no molecular gas and no star formation. If they degraded their resolution to a radius of 300 pc, they would pick up all the Gould Belt clouds but no localized Hα emission. Within a slightly larger radius of 500 pc, their beam would include Orion, with its O stars and HII region. (For this example, we consider only the stars and emission from the Orion Nebula Cluster, for which we have good numbers, not the full Orion clouds and OB associations.) This roughly doubles the number of YSOs. Our M51 observers would measure $\Sigma_{\rm mol} = 0.11\ M_\odot\ {\rm pc}^{-2}$, but if they applied the relation between SFR and Hα luminosity from Kennicutt (1998a), they would derive Σ(SFR) a factor of 10 lower than the actual SFR in Orion, based on the actual stellar content of the Orion Nebula Cluster and a relatively long timescale of 3 Myr (Chomiuk & Povich 2011). They would also miss the total SFR within 500 pc by a factor of 20 because the other clouds produce no O stars. This severe underestimate for Orion from Hα emission results because the Orion cluster is too small to populate fully the IMF; its earliest spectral type is O7 V, so the star cluster produces relatively little ionizing luminosity relative to its total mass and SFR. If the distant observers instead used the TIR emission of Orion, they would still underestimate its SFR by a factor of 8 (Lada et al. 2012) (a factor of 10 with the newer conversions in **Table 1**).

A second measuring bias exists because, when the spatial resolution of the SFR measurements encompass single young clusters, such as Orion, the assumption of continuous star formation that is embedded in the global SFR recipes breaks down severely. In such regions, that emission at all wavelengths will be dominated by a very young population with ages of typically a few million years, which will be shorter than the averaging times assumed for all but the emission-line tracers. These changes affect both the relative luminosities of star-formation tracers in different bands as well as the interpretation of the SFR. Technically speaking, the luminosities of young star-forming clusters provide information on only the masses of the regions studied, and converting these to SFRs requires independent information on the ages and/or age spreads of the stars in the region.

A third measuring bias will set in if the resolution of the measurements becomes smaller than the Strömgren diameters of HII regions or the corresponding dust-emission nebulae, which tend to match or exceed those of the HII regions (e.g., Prescott et al. 2007, Watson et al. 2008). This scale varies from <100 pc in the MW to 200–500 pc in actively star-forming galaxies such as NGC 6946 (**Figure 2**). On these small scales, indirect tracers of the SFR (e.g., Hα, IR) tend to trace the surfaces and bubbles of clouds rather than the young stars. By the same token, much of the Hα and dust emission in galaxies, typically 30–60%, is emitted by diffuse ionized gas and dust located hundreds of parsecs or more from any young stars (e.g., Dale et al. 2007, Oey et al. 2007). Such emission produces a false-positive signal of star formation, and care is needed to account for its effects when mapping the SFR within galaxies.

Taken together, these factors complicate, but do not prevent, the construction of two-dimensional maps of SFRs, so long as the methodology is adapted to the astrophysical application. For example, radial profiles of SFR distributions in galaxies may still be reliably derived using the integrated SFR calibrations, provided that large enough annuli are used to assure that the IMF

is fully populated in aggregate and the SFR is regarded to be averaged over timescales of order 100 Myr. Likewise, a two-dimensional distribution of star formation over the past 5 Myr or so can be derived from a short-lived tracer such as Hα emission, if the spatial coverage is limited to very young regions and structure on scales smaller than individual HII regions is ignored. Maps of integrated Hα and IR emission can be used to study the population of star-forming regions and the star-formation law, when restricted to young regions where the physical association of gas and stars is secure (Section 6.4). An alternative approach is to apply direct stellar photospheric tracers, such as the UV continuum emission on large scales (bearing in mind the variable 10–300 Myr timescales traced by the UV), or resolved stellar tracers, such as YSOs or deep visible-wavelength CMDs, to map the distributions of young stars directly (Section 3.1). Likewise, it should be possible to use pixel-resolved SEDs of galaxies in the UV-visible wavelength region to derive dust-corrected UV maps and possibly apply local corrections for age in the maps. With such a multiplicity of approaches, we anticipate major progress in this area, which will be invaluable to understand in detail the patterns of star formation in galaxies and to connect the findings to detailed studies within the MW.

4. THE LOCAL PERSPECTIVE: FROM THE INSIDE LOOKING OUT

4.1. Outline of Low-Mass Star Formation

The formation of low-mass stars can be studied in greatest detail because it occurs in relatively nearby clouds and sometimes in isolation from other forming stars. The established paradigm provides a point of comparison for more massive, distant, and clustered star formation. Physically, an individual star-forming event, which may produce a single star or a small-number multiple system, proceeds from a prestellar core, which is a gravitationally bound starless core (for definitions, see Section 2.2 as well as di Francesco et al. 2007), a dense region, usually within a larger molecular cloud. Prestellar cores are centrally condensed and can be modeled as Bonnor-Ebert spheres (Ward-Thompson, Motte & André 1999; Evans et al. 2001; Kirk, Ward-Thompson & André 2005), which have nearly power-law [$n(r) \propto r^{-2}$] envelopes around a core with nearly constant density.

Collapse leads to the formation of a first hydrostatic core in a small region where the dust-continuum emission becomes optically thick; this short-lived core is still molecular and grows in mass by continued infall from the outer layers (Larson 1969, Boss & Yorke 1995, Stahler & Palla 2005, Omukai 2007). When the temperature reaches 2,000 K, the molecules in the first hydrostatic core collisionally dissociate, leading to a further collapse to the true protostar, still surrounded by the bulk of the core, often referred to as the envelope. Rotation leads to flattening and a centrifugally supported disk (Terebey, Shu & Cassen 1984). Magnetic fields plus rotation lead to winds and jets (Pudritz et al. 2007; Shang, Li & Hirano 2007), which drive molecular outflows from young stars of essentially all masses (Wu et al. 2004, Arce et al. 2007).

Stage 0 sources have protostars, disks, jets, and envelopes with more mass in the envelope than in the star plus disk (Andre, Ward-Thompson & Barsony 1993). Stage I sources are similar to Stage 0, but with less mass in the envelope than in star plus disk. Stage II sources lack an envelope but have a disk. Stage III sources have little or no disk left. There are several alternative quantitative definitions of the qualitative terms used here (Robitaille et al. 2006, Crapsi et al. 2008).

Stages I through III are usually associated with SED Classes I through III defined by SED slopes rising, falling slowly, and falling more rapidly from 2 to 25 μm (Lada & Wilking 1984). A class intermediate between I and II with a slope near zero (Flat SED) was added by Greene et al. (1994). In fact, orientation effects in the earlier stages can confuse the connection between

class and stage; without detailed studies of each source, one cannot observationally determine the stage without ambiguity. For this reason, most of the subsequent discussion uses classes despite their questionable correspondence to physical configurations. Evans et al. (2009) gave a historical account of the development of the class and stage nomenclature.

For our present purposes, the main point is to establish timescales for the changing observational signatures, so the classes are useful. Using the boundaries between classes from Greene et al. (1994), Evans et al. (2009) found that the combined Class 0/I phases last ~0.5 Myr, with a similar duration for Flat SEDs, assuming a continuous flow through the classes for at least the Class II duration of 2 ± 1 Myr (e.g., Mamajek 2009), which is essentially the age when approximately half the stars in a dated cluster lack IR excesses; hence, all durations can be thought of as half-lives.

To summarize, we would expect a single star-forming core to be dominated by emission at far-IR and submillimeter wavelengths for approximately 0.5 Myr, near-IR and mid-IR radiation for approximately 1.5 Myr, and near-IR to visible light thereafter. However, the duration of emission at longer wavelengths can be substantially lengthened by material in surrounding clumps or clouds not directly associated with the forming star.

The SFRs and efficiencies can be calculated for a set of 20 nearby clouds ($\langle d \rangle = 275$ pc) with uniform data from *Spitzer*. The SFR was calculated from Equation 9 and the assumptions in Section 3.1 by Heiderman et al. (2010), who found a wide range of values for $\dot{M}_*$, with a mean value for the 20 clouds of $\dot{M}_* = 39 \pm 18$ $M_\odot$ Myr^{-1}. The star-formation efficiency [$\epsilon = M_\star/(M_{\rm star} + M_{\rm gas})$] can be calculated over only the past 2 Myr because surveys are incomplete at larger ages; averaging over all 20 clouds, only 2.6% of the cloud mass has turned into YSOs in that period and $\langle \Sigma({\rm SFR}) \rangle = 1.2$ $M_\odot$ year^{-1} kpc^{-2} (Heiderman et al. 2010). For individual clouds, ϵ ranges from 2% to 8% (Evans et al. 2009, Peterson et al. 2011). The final efficiency will depend on how long the cloud continues to form stars before being disrupted. Cloud lifetimes are poorly constrained (Bergin & Tafalla 2007, McKee & Ostriker 2007), and they may differ for clouds where massive stars form. For comparison to extragalactic usage, the mean $t_{\rm dep} = 1/\epsilon'$ (Section 1.2) is approximately 82 Myr for seven local clouds, longer than most estimates of cloud lifetime and much longer than either $\langle t_{\rm ff} \rangle$ (1.4 Myr) or $\langle t_{\rm cross} \rangle$ (5.5 Myr) (Evans et al. 2009). By contrast, the $\langle t_{\rm dep} \rangle$ for local clouds is approximately 10% of the $t_{\rm dep}$ for the MW molecular gas as a whole (Section 5.1).

4.2. Formation of Clusters and High-Mass Stars

The study of young clusters provides some distinct opportunities. By averaging over many stars, a characteristic age can be assigned with, perhaps, more reliability than can be achieved for a single star. As noted (Section 4.1), the set point for ages of all SED classes is determined by the fraction of mid-IR excesses in clusters. This approach does implicitly assume that the cluster forms "coevally," by which one really means that the spread in times of formation is small compared with the age of the cluster. Because objects ranging from prestellar cores to Class III objects often coexist (Rebull et al. 2007), this assumption is of dubious reliability for clusters with ages less than approximately 5 Myr, exactly the ones used to set the timescales for earlier classes. Note also that assuming coeval formation in this sense directly contradicts the assumption of continuous flow through the classes. We live with these contradictions.

Most nearby clusters do not sample very far up the IMF. The nearest young cluster that has formed O stars is 415–430 pc away in Orion (Hirota et al. 2007, Menten et al. 2007), and most lie at much larger distances, making study of the entire IMF difficult. Theoretically, the birthplace of a cluster is a clump (Williams, Blitz & McKee 2000). The clumps identified by ^{13}CO maps in nearby clouds are dubious candidates for the reasons given in Section 2.5. The structures identified by

Kainulainen et al. (2009) in the power-law tail of the probability distribution function are better candidates, but most are still unbound. Objects found in some surveys of dust-continuum emission (Section 2.3) appear to be still better candidates. For example, analysis (Dunham et al. 2011b, Schlingman et al. 2011) of the sources found in millimeter-wave continuum emission surveys of the MW (Section 2.3) indicates typical volume densities of a few $\times$ 10^3 cm^{-3}, compared with $\sim$200 cm^{-3} for ^{13}CO structures. Mean surface densities are $\sim$180 $M_\odot$ pc^{-2} higher than those of gas in the power-law tail ($\Sigma_{gas} \sim$ 40–80 $M_\odot$ pc^{-2}). These structures have a wide range of sizes, with a median of 0.75 to 1 pc.

Studies of regions with signposts of massive star formation, using tracers requiring higher densities (e.g., Plume, Jaffe & Evans 1992; Beuther et al. 2002) or millimeter continuum emission from dust (e.g., Beuther et al. 2002, Mueller et al. 2002), have identified slightly smaller structures ($r \sim 0.5$ pc) that are much denser, indeed, denser on average than cores in nearby clouds. In addition to having a mass distribution consistent with that of clusters (Section 2.5), many have far-IR luminosities consistent with the formation of clusters of stars with masses ranging up to those of O stars. The properties of the sample provided by Plume, Jaffe & Evans (1992) have been studied in a series of papers (Plume et al. 1997, Mueller et al. 2002, Shirley et al. 2003), with the most recent summary in Wu et al. (2010a). The properties of the clumps depend on the tracer used. Because the HCN $J = 1 \rightarrow 0$ line is used in many extragalactic studies, we give the properties as measured in that line. The mean and median FWHM are 1.13 and 0.71 pc, the mean and median IR luminosities are 4.7 $\times$ 10^5 and 1.06 $\times$ 10^5 $L_\odot$, the mean and median virial mass are 5,300 and 2,700 $M_\odot$, the mean and median surface densities are 0.29 and 0.28 g cm^{-2}, and the mean and median of the average volume densities (n) are 3.2 $\times$ 10^4 and 1.6 $\times$ 10^4 cm^{-3}. As lines tracing higher densities are used, the sizes and masses decrease, while the surface densities and volume densities increase, as expected for centrally condensed regions. Very similar results were obtained from studies of millimeter continuum emission from dust (Faúndez et al. 2004) toward a sample of Southern Hemisphere sources surveyed in CS $J = 2 \rightarrow 1$ (Bronfman, Nyman & May 1996).

Embedded clusters provide important testing grounds for theories of star formation. Using criteria of 35 members with a stellar density of 1 $M_\odot$ pc^{-3} for a cluster, Lada & Lada (2003) argued that most stars form in clusters and 90% of those are in rich clusters with more than 100 stars. They added that almost all clusters (>93%) dissipate as the gas is removed, a process they call infant mortality. With more complete surveys enabled by *Spitzer*, the distributions of numbers of stars in clusters and stellar densities are being clarified. Allen et al. (2007) found that $\sim$60% of young stars within 1 kpc of the Sun are in clusters with more than 100 members, but this number is heavily dominated by the Orion Nebula Cluster. Drawing on the samples from *Spitzer* surveys of nearly all clouds within 0.5 kpc, Bressert et al. (2010) found a continuous distribution of surface densities and no evidence for a bimodal distribution, with distinct "clustered" and "distributed" modes. They found that the fraction of stars that form in clusters ranged from 0.4 to 0.9, depending on which definition of clustered was used. Even regions of low-mass star formation, often described as distributed star formation, are quite clustered and the youngest objects (Class I and Flat SED sources; see Section 4.1) are very strongly concentrated to regions of high extinction, especially after the samples have been culled of interlopers (**Figure 4**) (Section 6.4). Similarly, studies of three clouds found that 75% of prestellar cores lay above thresholds in A_V of 8, 15, and 20 mag, even though most of the cloud mass was at much lower extinction levels (Enoch et al. 2007).

A *Spitzer* study (Gutermuth et al. 2009) of 2548 YSOs in 39 nearby ($d < 1.7$ kpc), previously known [primarily from the compilation by Porras et al. (2003)] young clusters, but excluding Orion and NGC 2264, found the following median properties: 26 members, core radius of 0.39 pc, stellar surface density of 60 pc^{-2}, and embedded in a clump with $A_K = 0.8$ mag, which corresponds to

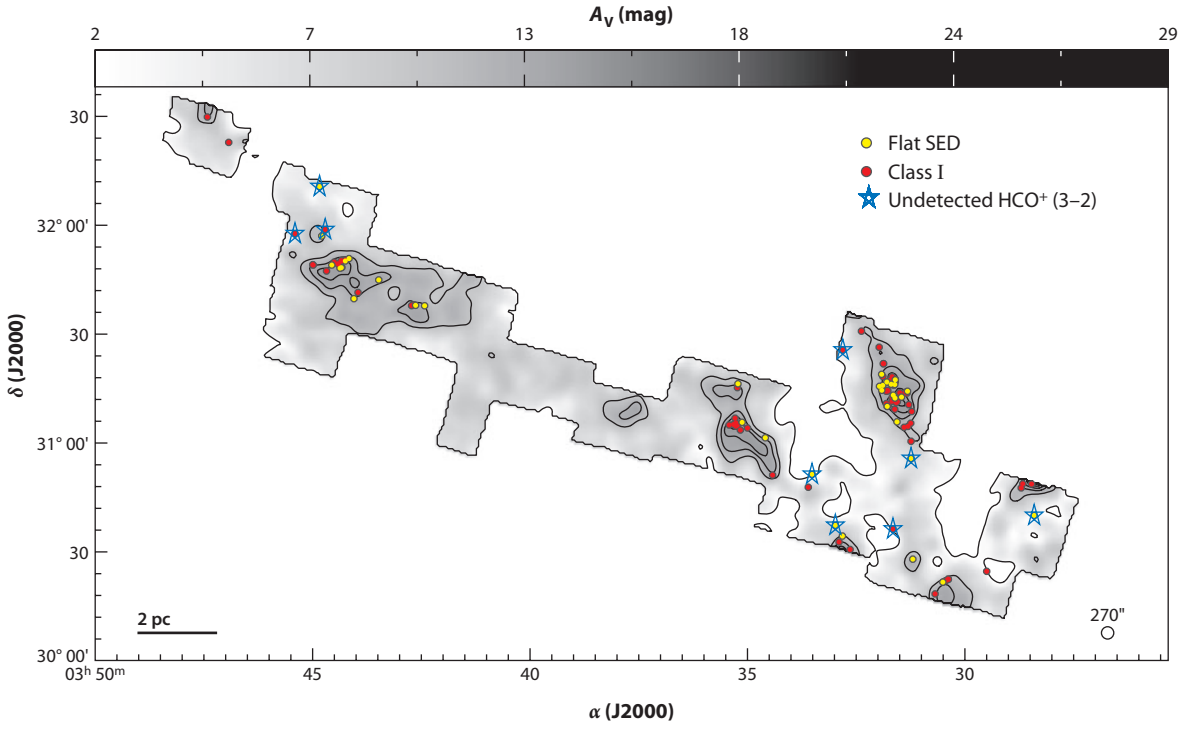

Figure 4

Example of the strong concentration of star formation in regions of high extinction or mass surface density in the Perseus molecular cloud. The gray-scale with black contours is the extinction map ranging from 2 to 29 mag in intervals of 4.5 mag. The yellow-filled circles are Flat SED sources, and the red-filled circles are Class I sources. Sources with a blue open star were not detected in HCO^+ $J = 3 \rightarrow 2$ emission and are either older sources that may have moved from their birthplace or background galaxies. Essentially, all truly young objects lie within the contours of $A_V \geq 8$ mag. Taken from Heiderman et al. (2010); reproduced by permission of the AAS.

$A_V = 7.1$ mag. Translating to mass surface density using $\langle M_\star \rangle = 0.5$ $M_\odot$, the median stellar mass surface density would be 30 $M_\odot$ pc^{-2} and the gas surface density would be 107 $M_\odot$ pc^{-2}. The distributions are often elongated, with a median aspect ratio of 1.82. The median spacing between YSOs, averaged over all 39 clusters, is 0.072 ± 0.006 pc, comparable to the size of individual cores and a plausible scale for Jeans fragmentation. The distributions are all skewed toward low values, with a tail to higher values.

Although various definitions of clustered have been used, one physically meaningful measure is a surface density of ~200 YSOs pc^{-2} (Gutermuth et al. 2005), below which individual cores are likely to evolve in relative isolation (i.e., the timescale for infall is less than the timescale for core collisions). With their sample, Bressert et al. (2010) found that only 26% were likely to interact faster than they collapse. However, that statistic did not include the Orion cluster, which exceeds that criterion.

The fact that the Orion cluster dominates the local star formation warns us that our local sample may be unrepresentative of the Galaxy as a whole. Leaving aside globular clusters, some young clusters are much more massive than Orion. Portegies Zwart, McMillan & Gieles (2010) have cataloged massive ($M_\star \geq 10^4$ $M_\odot$), young (age ≤100 Myr) clusters (12 in all) and associations (13 in all), but none of these are more distant than the Galactic Center, so they are clearly undercounted. The mean half-light radius of the 12 clusters is 1.7 ± 1.3 pc compared with

11.2 ± 6.4 pc for the associations. For the clusters, $\langle \log M_\star(M_\odot) \rangle = 4.2 \pm 0.3$. Three of the massive dense clumps from the Wu et al. (2010a) study have masses above 10^4 $M_\odot$ and are plausible precursors of this class of clusters. Still more massive clusters can be found in other galaxies, and a possible precursor ($M_{\rm cloud} > 1 \times 10^5$ $M_\odot$ within a 2.8 pc radius) has recently been identified near the center of the MW (Longmore et al. 2012).

The topic of clusters is connected to the topic of massive stars because 70% of O stars reside in young clusters or associations (Gies 1987). Furthermore, most of the field population can be identified as runaways (de Wit et al. 2005), with no more than 4% with no evidence of having formed in a cluster. Although there may be exceptions (for discussion, see Zinnecker & Yorke 2007), the vast majority of massive stars form in clusters. The most massive star with a dynamical mass (NGC 3603-A1) weighs in at 116 ± 31 $M_\odot$ and is a 3.77-day binary with a companion at 89 ± 16 $M_\odot$ (Schnurr et al. 2008). Higher initial masses (105–170 $M_\odot$) for the stars in NGC 3603 and even higher in R136 (165–320 $M_\odot$) have been suggested (Crowther et al. 2010). Many of the most massive stars exist in tight (orbital periods of a few days) binaries (Zinnecker & Yorke 2007). For a recent update on massive binary properties, see Sana & Evans (2010).

There is some evidence, summarized by Zinnecker & Yorke (2007), that massive stars form only in the most massive molecular clouds, with $max(M_\star) \propto M_{\rm cloud}^{0.43}$ suggested by Larson (1982). Roughly speaking, it takes $M_{\rm cloud} = 10^5$ $M_\odot$ to make a 50 $M_\odot$ star. Recognizing that clumps are the birthplaces of clusters and that efficiencies are not unity could make the formation of massive stars even less likely. The question (see Section 2.5) is whether the absence of massive stars in clumps or clusters of modest total mass is purely a sampling effect (Calzetti et al. 2010a; Fumagalli, da Silva & Krumholz 2011, and references therein) or a causal relation (Weidner & Kroupa 2006). If causal, differences in the upper mass limit to clouds or clumps (Section 2.5) in a galaxy could limit the formation of the most massive stars. Larson (1982) concluded that his correlation could be due to sampling. As a concrete example, is the formation of a 50 $M_\odot$ star as likely in an ensemble of 100 clouds, each with 10^3 $M_\odot$, as it is in a single 10^5 $M_\odot$ cloud? Unbiased surveys of the MW for clumps and massive stars (Section 5.1) could allow a fresh look at this question, with due regard for the difficulty of distinguishing "very rarely" from "never."

4.3. Theoretical Aspects

The fundamental problem presented to modern theorists of star formation has been to explain the low efficiency of star formation on the scale of molecular clouds. Early studies of molecular clouds concluded that they were gravitationally bound and should be collapsing at free fall (e.g., Goldreich & Kwan 1974). Zuckerman & Palmer (1974) pointed out that such a picture would produce stars at 30 times the accepted average recent rate of star formation in the MW (Section 5.1) if stars formed with high efficiency. Furthermore, Zuckerman & Evans (1974) found no observational evidence for large-scale collapse and suggested that turbulence, perhaps aided by magnetic fields, prevented overall collapse. This suggestion led eventually to a picture of magnetically subcritical clouds that formed stars only via a redistribution of magnetic flux, commonly referred to as ambipolar diffusion (Shu, Adams & Lizano 1987; Mouschovias 1991), which resulted in cloud lifetimes approximately 10 times the free-fall time. If, in addition, only 10% of the cloud became supercritical, a factor of 100 decrease in SFR could be achieved.

Studies of the Zeeman effect in OH have now provided enough measurements of the line-of-sight strength of the magnetic field to test that picture. Despite continuing controversies, the data indicate that most clouds (or, more precisely, the parts of clouds with Zeeman measurements) are supercritical or close to critical, but not strongly subcritical (Crutcher et al. 2010). Pictures of static clouds supported by magnetic fields are currently out of fashion (McKee & Ostriker 2007),

but magnetic fields almost certainly play some role (for a current review, see Crutcher 2012, in this volume). Simulations of turbulence indicate a fairly rapid decay, even when magnetic fields are included (Stone, Ostriker & Gammie 1998). As a result, there is growing support for a more dynamical picture in which clouds evolve on a crossing time (Elmegreen 2000). However, this picture must still deal with the Zuckerman-Palmer problem.

There are two main approaches to solving this problem at the level of clouds, and they are essentially extensions of the two original ideas, magnetic fields and turbulence, into larger scales. One approach, exemplified by Vázquez-Semadeni et al. (2011), argues that clouds are formed in colliding flows of the warm, neutral medium. They simulate the outcome of these flows with magnetic fields but without feedback from star formation. Much of the mass is magnetically subcritical and star formation happens only in the supercritical parts of the cloud. A continued flow of material balances the mass lost to star formation so that the star-formation efficiency approaches a steady value, in rough agreement with the observations.

A second picture, exemplified by Dobbs, Burkert & Pringle (2011), is that most clouds and most parts of clouds are not gravitationally bound but are transient objects. Their simulations include feedback from star formation but not magnetic fields. During cloud collisions, material is redistributed, clouds may be shredded, and feedback removes gas. Except for a few very massive clouds, most clouds lose their identity on the timescales of a few million years. In this picture, the low efficiency simply reflects the fraction of molecular gas that is in bound structures.

It is not straightforward to determine observationally if clouds are bound, especially when they have complex and filamentary boundaries. Heyer, Carpenter & Snell (2001) argued that most clouds in the outer galaxy with $M > 10^4$ $M_\odot$ were bound, but clumps and clouds with $M < 10^3$ $M_\odot$ were often not bound. Heyer et al. (2009) addressed the issues associated with determining accurate masses for molecular clouds. In a study on the inner Galaxy, Roman-Duval et al. (2010) concluded that 70% of molecular clouds (in both mass and number) were bound.

If molecular clouds are bound and last longer than a few crossing times, feedback or turbulence resulting from feedback is invoked. For low-mass stars, outflows provide the primary feedback (e.g., Li & Nakamura 2006). High-mass stars add radiation pressure and expanding HII regions (e.g., Murray 2011). In addition, the efficiency is not much higher in most clumps, so the problem persists to scales smaller than that of clouds.

Another longstanding problem of star-formation theory has been to explain the IMF (Section 2.5). This topic has been covered by many reviews, so we emphasize only two aspects. The basic issue is that the typical conditions in star-forming regions suggest a characteristic mass, either the Jeans mass or the Bonnor-Ebert mass, around 1 $M_\odot$ (e.g., Bonnell, Larson & Zinnecker 2007). Recently, Krumholz (2011) derived a very general expression for a characteristic mass of 0.15 $M_\odot$, with only a very weak dependence on pressure. However, we see stars down to the hydrogen-burning limit and a continuous distribution of brown dwarfs below that, extending down to masses lower than those seen in extrasolar planets (Allers et al. 2006). An extraordinarily high density would be required to make such a low-mass region unstable.

On the other end, making a star with mass greater than 100 times the characteristic mass is challenging. Beuther et al. (2007a) provide a nice review of both observations and theory of massive star formation. Although dense clumps with mass much greater than 100 $M_\odot$ are seen, they are likely to fragment into smaller cores. Fragmentation can solve the problem of forming low-mass objects, but it makes forming massive objects difficult. In fact, simulations of unstable large clumps tend to fragment so strongly as the mean density increases that they overproduce brown dwarfs, but no massive stars (e.g., Klessen, Burkert & Bate 1998; Martel, Evans & Shapiro 2006). This effect is caused by the assumed isothermality of the gas because the Jeans mass is proportional to $(T_K^3/n)^{0.5}$. Simulations including radiative feedback, acting on a global scale, have shown that

fragmentation can be suppressed and massive stars formed (e.g., Bate 2009; Krumholz et al. 2010; Urban, Martel & Evans 2010). Krumholz & McKee (2008) have argued that a threshold clump surface density of 1 g cm^{-2} is needed to suppress fragmentation, allowing the formation of massive stars.

Radiative feedback, acting locally, can, in principle, also limit the mass of the massive stars through radiation pressure. This can be a serious issue for the formation of massive stars in spherical geometries, but more realistic aspherical simulations show that the radiation is channeled out along the rotation axis, allowing continued accretion through a disk (Yorke & Sonnhalter 2002, Krumholz et al. 2009, Kuiper et al. 2011).

The overall picture discussed so far is basically a scaled-up version of the formation of low-mass stars by accretion of material from a single core (sometimes called core accretion). An alternative picture, called competitive accretion, developed by Klessen, Burkert & Bate (1998), Bate, Bonnell & Bromm (2003), and Bonnell, Bate & Vine (2003), builds massive stars from the initial low-mass fragments. The pros and cons of these two models are discussed in a joint paper by the leading protagonists (Krumholz & Bonnell 2009). They agree that the primary distinction between the two is the original location of the matter that winds up in the star: In core-accretion models, the star gains the bulk of its mass from the local dense core, continuing the connection of the core mass function to the initial stellar mass function to massive stars. In competitive-accretion models, the more massive stars collect most of their mass from the larger clump by out-competing other, initially low-mass, fragments. A hybrid picture in which a star forms initially from its parent core but then continues to accrete from the surrounding clump has been advanced (Myers 2009, 2011) with some observational support (e.g., Longmore et al. 2011).

Observational tests of these ideas are difficult. The core-accretion model requires that clumps contain a core mass function extending to massive cores. Some observations of massive dense clumps have found substructure on the scale of cores (Beuther et al. 2007b, Brogan et al. 2009), but the most massive cores identified in these works are 50–75 $M_\odot$. Discussions in those references illustrate the difficulties in conducting these studies with our current capabilities. ALMA will make this kind of study much more viable, but interpretation will always be tricky. The competitive-accretion model relies on a continuous flow of material to the densest parts of the clump to feed the growing oligarchs. Evidence for overall inward flow in clumps is difficult; it has been found in some surveys (Wu & Evans 2003; Fuller, Williams & Sridharan 2005; Reiter et al. 2011a), but not in others (Purcell et al. 2006). Because special conditions are required to produce an inflow signature, the detection rates may underestimate the fraction with inflow. The dense clumps are generally found to be centrally condensed (van der Tak et al. 2000, Beuther et al. 2002, Mueller et al. 2002), which can also suppress overfragmentation.

Other possible tests include the coherence of outflows in clusters, as these should be distorted by sufficiently rapid motions. The kinematics of stars in forming clusters, which should show more velocity dispersion in the competitive accretion models, provide another test. Astrometric studies are beginning to be able to constrain these motions (Rochau et al. 2010), along with providing cleaner separation of cluster members from field objects. Relative motions of cores within clumps appear to be very low (<0.1 km s^{-1}), challenging the competitive-accretion model (Walsh, Myers & Burton 2004).

Theoretical studies include evolutionary tracks of pre-main-sequence stars (e.g., Chabrier & Baraffe 2000 for low-mass stars and substellar objects). These evolutionary calculations are critical for determining the ages of stars and clusters. For more massive stars, it is essential to include accretion in the evolutionary calculations (Palla & Stahler 1992), as high accretion rates strongly affect a star's evolution (Zinnecker & Yorke 2007, Hosokawa & Omukai 2009). Assumptions about accretion and initial conditions may also have substantial consequences for the usual methods of

determining ages of young stars (Baraffe, Chabrier & Gallardo 2009; Baraffe & Chabrier 2010; Hosokawa, Offner & Krumholz 2011).

4.4. Summary Points from the Local Perspective

The main lessons to retain from local studies of star formation as we move to the scale of galaxies are summarized here.

1. Star formation is not distributed smoothly over molecular clouds, but instead it is highly concentrated into regions of high extinction or mass surface density, plausibly associated with the theoretical idea of a cluster-forming clump. This is particularly apparent when prestellar cores or the youngest protostars are considered (e.g., **Figure 4**). In contrast, most of the mass in nearby molecular clouds is in regions of lower extinction.
2. By counting YSOs in nearby clouds, one can obtain reasonably accurate measures of SFR and efficiency without the uncertainties of extrapolation from the high-mass tail of the IMF. The main source of uncertainty is the ages of YSOs.
3. There is no obvious bimodality between "distributed" and "clustered" star formation, but dense clusters with massive stars tend to form in regions of higher mean density and turbulence, which are centrally condensed. Plausible precursors of quite massive (up to 10^4 or perhaps 10^5 $M_\odot$) clusters can be found in the MW.
4. Despite much theoretical progress, the challenge of explaining the low efficiency of star formation, even in regions forming only low-mass stars, remains. Similarly, an understanding of the full IMF, from brown dwarfs to the most massive stars, remains elusive.

5. THE GALACTIC PERSPECTIVE: FROM THE OUTSIDE LOOKING IN

5.1. The Milky Way as a Star-Forming Galaxy

As our nearest example, the MW has obvious advantages in studies of star formation in galaxies. However, living inside the MW presents serious problems of distance determination and selection effects, complementary to the problems associated with studies of other galaxies. We can "look in from the outside" only with the aid of models. After reviewing surveys briefly, we consider properties of gas and star formation within the MW, bearing in mind the issues raised in Sections 2.4 and 3, first as a whole, and then with respect to the radial distribution. Finally, we provide some notes on nonaxisymmetric structure.

5.1.1. Surveys. Recent and ongoing surveys of the Galactic plane at multiple wavelengths are revitalizing the study of the MW as a galaxy. Surveys of HI from both the Northern (Taylor et al. 2003) and Southern (McClure-Griffiths et al. 2005) Hemispheres, along with a finer-resolution survey of parts of the Galactic plane (Stil et al. 2006), have given a much clearer picture of the atomic gas in the MW (for a review of HI surveys, see Kalberla & Kerp 2009). On the basis of these surveys, properties of the cool atomic clouds have been analyzed by Dickey et al. (2003).

Numerous surveys of the MW have been obtained in CO $J = 1 \rightarrow 0$ (e.g., Bronfman et al. 1988; Clemens, Sanders & Scoville 1988; Dame, Hartmann & Thaddeus 2001). A survey of the inner part of the MW in ^{13}CO (Jackson et al. 2006) has helped address some problems caused by optical depth in the main isotopologue.

Surveys for tracers of star formation have been made in radio continuum (free-free) emission (Altenhoff et al. 1970) and recombination lines (Lockman 1989, Anderson et al. 2011), in water masers (Cesaroni et al. 1988, Walsh et al. 2011), and in methanol masers (Pestalozzi, Minier &

Booth 2005; Green et al. 2009). In addition to being signposts of (mostly massive) star formation, the masers provide targets for astrometric studies using very long baseline interferometry (VLBI).

Complementary surveys of clouds have also been done using mid-IR extinction (e.g., Perault et al. 1996, Egan et al. 1998, Peretto & Fuller 2009), which can identify infrared dark clouds against the Galactic background emission. The MIPSGAL survey (Carey et al. 2009) should also provide a catalog of very opaque objects. At longer wavelengths, the dust is usually in emission, and millimeter continuum emission from dust (e.g., Schuller et al. 2009, Rosolowsky et al. 2010, Aguirre et al. 2011) provides a different sample of objects.

Each method has its own selection effects, and efforts are ongoing to bring these into a common framework. A key ingredient is to determine the distances, using spectral lines and methods to break the distance ambiguity in the inner galaxy; initial work is under way (Dunham et al. 2011b, Foster et al. 2011, Russeil et al. 2011, Schlingman et al. 2011). Ultimately, these studies should lead to a better definition of the total amount and distribution of dense gas (Section 1.2). The *Herschel* HIGAL survey (Molinari et al. 2010) will add wavelengths into the far-IR and lead to a far more complete picture. Quantities such as $L_{\rm FIR}/M_{\rm cloud}$ and $L_{\rm FIR}/M_{\rm dense}$, as used in extragalactic studies, can be calculated for large samples.

5.1.2. The Milky Way as a whole. The MW is a barred spiral galaxy (Burton 1988; Dame, Hartmann & Thaddeus 2001; Benjamin et al. 2005). The number and position of the spiral arms are still topics for debate, but the best currently available data favor a grand-design, two-armed, barred spiral with several secondary arms. A conception of what the MW looks like from the outside (Churchwell et al. 2009) is shown in **Figure 5**. We can expect continuing improvements in the model of the MW as VLBI astrometry improves distance determinations of star-forming regions across the MW (Reid et al. 2009, Brunthaler et al. 2011). Because we compare the MW to NGC 6946 in following sections, we also show images of that galaxy at Hα, 24 μm, HI, and CO $J = 2 \rightarrow 1$ in **Figure 6**.

Based on a model including dark matter (Kalberla et al. 2007, Kalberla & Dedes 2008, Kalberla & Kerp 2009), the MW mass within 60 kpc of the center is $M\,({\rm tot}) = 4.6 \times 10^{11}$ $M_\odot$, with $M\,({\rm baryon}) = 9.5 \times 10^{10}$ $M_\odot$. The total mass of atomic gas (HI plus He) is $M\,({\rm atomic}) = 8 \times 10^9$ $M_\odot$, and the warm ionized medium contains $M\,({\rm WIM}) = 2 \times 10^9$ $M_\odot$. The mass fraction of the hot ionized medium (Section 2.1) is negligible. With a (perhaps high) estimate for the molecular mass of $M\,({\rm mol}) = 2.5 \times 10^9$ $M_\odot$, Kalberla & Kerp (2009) derived a gas to baryon ratio of 0.13. As explained in Section 5.1.3, for consistent comparison to the radial distribution in NGC 6946, we use a constant $X({\rm CO}) = 2.0 \times 10^{20}$, correct for helium, and assume an outer radius of the star-forming disk of 13.5 kpc to define masses, surface densities, etc. Within $R_{\rm gal} = 13.5$ kpc, $M\,({\rm mol}) = 1.6 \times 10^9$ $M_\odot$ and $M\,({\rm atomic}) = 5.0 \times 10^9$ $M_\odot$ with these conventions.

The volume-filling factor of the CNM is ∼1% (Cox 2005) and that of molecular clouds, as traced by the ^{13}CO survey (Roman-Duval et al. 2010), has been estimated at ∼0.5% (M. Heyer, personal communication) in the inner galaxy but much lower overall. Denser ($n \sim$ few $\times$ 10^3 cm^{-3}) structures found in millimeter continuum surveys, roughly corresponding to clumps, appear to have a surface-filling factor of 10^{-4} and a volume-filling factor of approximately 10^{-6} (M.K. Dunham, personal communication), but better estimates should be available soon.

The SFR of the MW has been estimated from counting HII regions, which can be seen across the MW, and extrapolating to lower-mass stars (Mezger 1987, McKee & Williams 1997, Murray & Rahman 2010). These methods average, over the effective lifetime of massive stars, approximately 3–10 Myr (**Table 1**). Estimates of $\dot{M}_*$ from a model of the total far-IR emission of the MW (e.g., Misiriotis et al. 2006) are somewhat less sensitive to the high end of the IMF (Section 3) and average over a longer time. An alternative approach based on counting likely YSOs in the

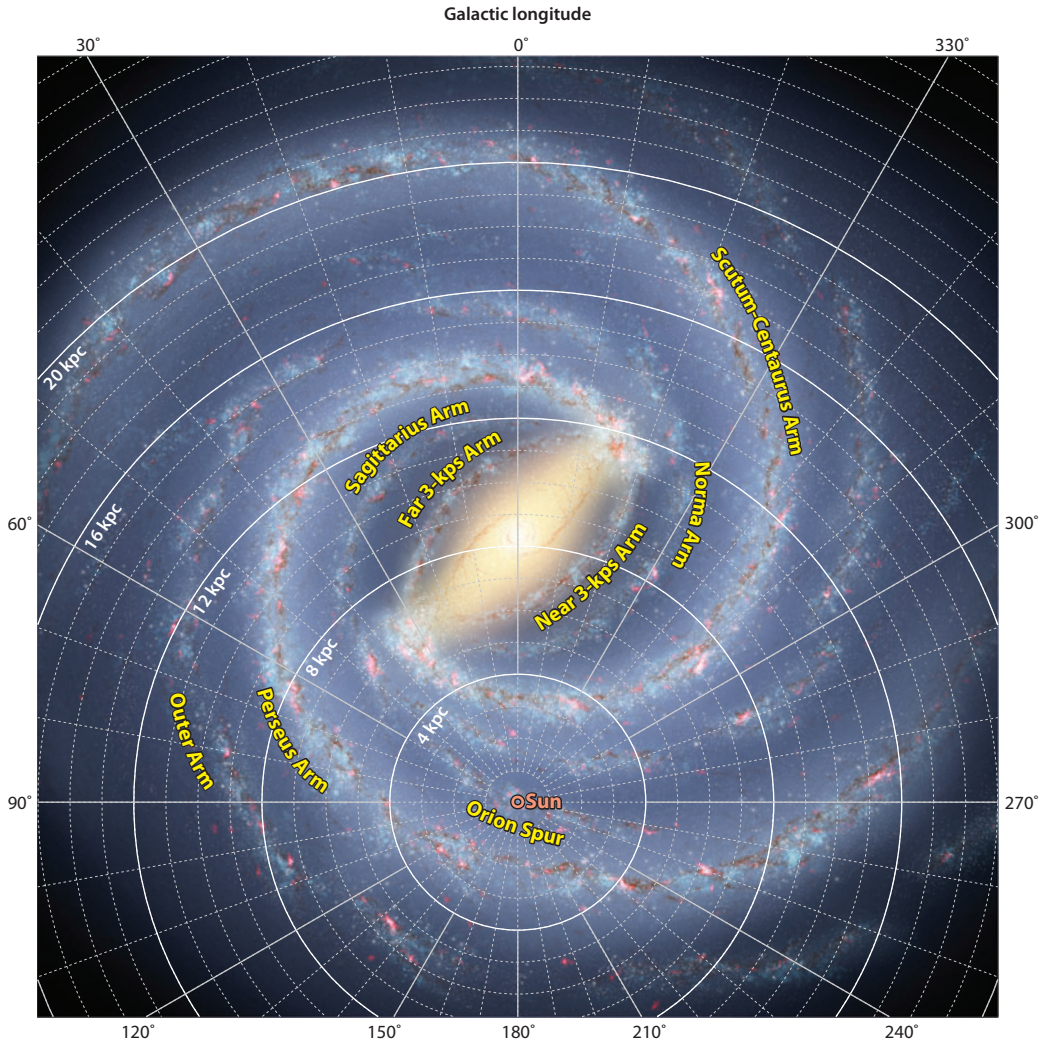

Figure 5

Sketch of approximately how the Galaxy is likely to appear viewed face-on, with Galactic coordinates overlaid and the locations of spiral arms and the Sun indicated. The image is based on data obtained from the literature at radio, infrared, and visible wavelengths. As viewed from a great distance, our Galaxy would appear to be a grand-design two-armed barred spiral with several secondary arms: The main arms are the Scutum-Centaurus and Perseus, and the secondary arms are Sagittarius, the outer arm, and the 3-kpc expanding arm. Adapted by R. Benjamin from a figure originally made by R. Hurt of the Spitzer Science Center in consultation with R. Benjamin at the University of Wisconsin-Whitewater and available in Churchwell et al. (2009). The original figure appeared in the *Publications of the Astronomical Society of the Pacific*, Copyright 2009, Astron. Soc. Pac.; reproduced with permission of the Editors.

GLIMPSE survey of the Galactic plane (Robitaille & Whitney 2010) is much less biased toward the most massive stars but is limited by sensitivity, issues of identification of YSOs, and models of extinction. Chomiuk & Povich (2011) have recently reviewed all methods of computing $\dot{M}_*$ for the MW and concluded that they are consistent with $\dot{M}_* = 1.9 \pm 0.4\ M_\odot\ \mathrm{year}^{-1}$. However, they also concluded that resolved star counts give SFRs that are factors of 2–3 times higher (see Section 6.4 for further discussion).

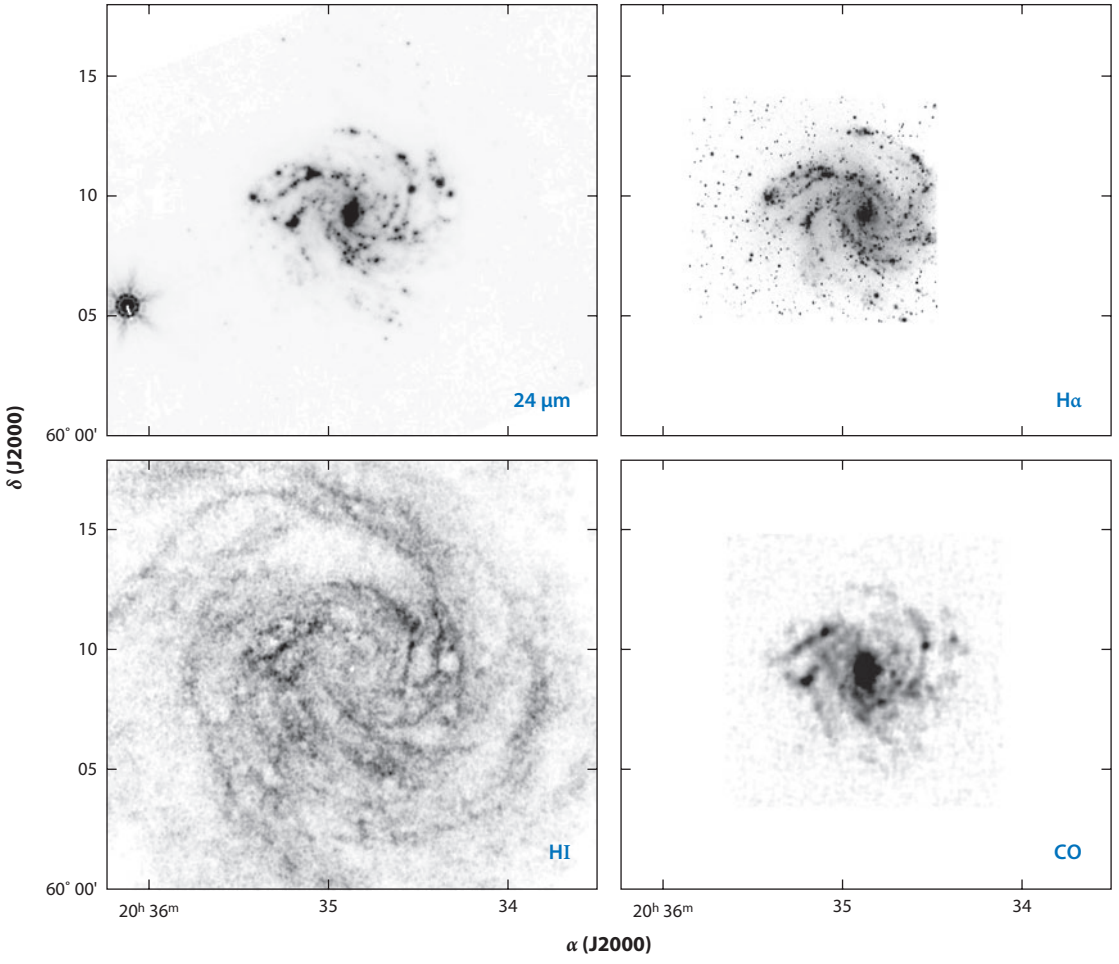

Figure 6

High-resolution maps of star-formation tracers and cold-gas components in NGC 6946. (*Top left*) *Spitzer* 24-μm dust emission from the SINGS/KINGFISH Project (Kennicutt et al. 2011), (*top right*) Hα emission from Knapen et al. (2004), (*bottom left*) HI emission from the VLA THINGS Survey (Walter et al. 2008), and (*bottom right*) CO $J = 2 \rightarrow 1$ emission from the HERACLES Survey (Walter et al. 2008). Note that the HI map extends over a much wider area than the CO, Hα, and 24-μm observations.

With a radius of active star formation of 13.5 kpc (Section 5.1.3), $\dot{M}_* = 1.9\ M_\odot\ \text{year}^{-1}$ yields $\langle \Sigma(\text{SFR}) \rangle = 3.3 \times 10^{-3}\ M_\odot\ \text{year}^{-1}\ \text{kpc}^{-2}$. Taking $M(\text{mol}, R_{\text{gal}} < 13.5) = 1.6 \times 10^9\ M_\odot$, $t_{\text{dep}} = 0.8$ Gyr, 10 times longer than $\langle t_{\text{dep}} \rangle$ in local clouds (Section 4.1). For all the gas in the (60 kpc) MW, $t_{\text{dep}} = 6.6$ Gyr, or 5.5 Gyr if the WIM is excluded. If we attribute all nongaseous baryons in the model by Kalberla & Kerp (2009) ($8.25 \times 10^{10}\ M_\odot$) to stars and stellar remnants, ignore recycling, and take an age of 1×10^{10} years, we would derive an average SFR of $8.25\ M_\odot\ \text{year}^{-1}$, approximately four times the current rate.

5.1.3. Radial distributions. The MW also offers a wide range of conditions, from the far outer Galaxy to the vicinity of the Galactic Center, for detailed study. The hurdle to overcome, especially in the inner MW, is to assign accurate distances. The radial distributions of atomic and molecular gas, along with the SFR surface density (here in units of $M_\odot\ \text{Gyr}^{-1}\ \text{pc}^{-2}$), are plotted in

Figure 7, along with a similar plot for NGC 6946 (Schruba et al. 2011). For consistency, we have used the same X(CO) and correction for helium (for both molecular and atomic gas) as did Schruba et al. (2011). These distributions for the MW have considerable uncertainties and should be taken with appropriate cautions, especially in the innermost regions, as discussed below. Misiriotis et al. (2006) presented a collection of estimates of Σ(SFR) and a model, all of which show a steady decline outward from a peak at $R_{gal} \sim 5$ kpc. However, the situation in the innermost galaxy is unclear. The data on HII regions that form the basis of most estimates are very old, and a fresh determination of $\Sigma(\mathrm{SFR})(R_{gal})$ is needed.

In comparison, NGC 6946 has a similar, rather flat, distribution of atomic gas, with Σ (atomic) $\sim$10 $M_\odot$ pc^{-2}. The molecular-gas distribution is similar to that of the MW, except for a clearer and stronger peak within $R_{gal} = 2$ kpc. The distribution of Σ(SFR) follows the molecular gas in both galaxies, more clearly so in NGC 6946.

We discuss the MW distributions from the outside, moving inward. The average surface density of molecular gas drops precipitously beyond 13.5 kpc, after a local peak in the Perseus arm (Heyer et al. 1998), as does the stellar density (Ruphy et al. 1996), thereby defining the far outer Galaxy and radius used in our whole Galaxy quantities (Section 5.1.2). The atomic surface density also begins to drop around 13–17 kpc, following an exponential with scale-length 3.74 kpc (Kalberla & Kerp 2009). Molecular clouds in the far outer Galaxy are rare but can be found with large-scale surveys. Star formation does continue in the rare molecular clouds (Wouterloot & Brand 1989). Although **Figure 7** would suggest a higher ratio of star formation to molecular gas, there are issues of incompleteness in the outer Galaxy. A study of individual regions (Snell, Carpenter & Heyer 2002) found a value of L_{FIR}/M similar to that for the inner Galaxy. They concluded that the star-formation process within a cloud is not distinguishable from that in the inner Galaxy; the low global rate of star formation is set by the inefficient conversion of atomic to molecular gas in the far outer Galaxy. This result is consistent with the results of Schruba et al. (2011) for other galaxies, as exemplified by NGC 6946.

Inside approximately 13 kpc, the atomic surface density is roughly constant at 10–15 $M_\odot$ pc^{-2}, but the average molecular surface density increases sharply, passing 1 $M_\odot$ pc^{-2} somewhere near the Solar Neighborhood (Dame, Hartmann & Thaddeus 2001) to a local maximum around $R_{gal} =$ 4–5 kpc (Nakanishi & Sofue 2006). After a small decrease inside 4 kpc, the surface density rises sharply within $R_{gal} = 1$ kpc. Nakanishi & Sofue (2006) and, thus, **Figure 7** use a constant X(CO), which could overestimate the molecular mass near the center (Section 2.4).

The innermost part of the MW, $R_{gal} < 250$ pc, known as the Central Molecular Zone (CMZ), potentially provides an opportunity for a close look at conditions in galactic nuclei without current AGN activity, provided that the issues of noncircular motions, foreground and background confusion, and possible changes in X(CO) (Oka et al. 1998) can be overcome. Despite their conclusion that X(CO) is lower, Oka et al. (1998) argued that the CMZ has a molecular mass of 2–6 $\times$ 10^7 $M_\odot$. Analysis of dust emission yields a mass of 5 $\times$ 10^7 $M_\odot$ (Pierce-Price et al. 2000), which leads to $\Sigma_{gas} = 250$ $M_\odot$ pc^{-2} for the CMZ. A TIR luminosity of 4 $\times$ 10^8 $L_\odot$ (Sodroski et al. 1997) for the CMZ would imply $\dot{M}_* \sim 0.06$ $M_\odot$ year^{-1} using the conversion in **Table 1**, roughly consistent with other recent estimates (Immer et al. 2012) based on analysis of point IR sources, but new data from the surveys mentioned above should allow refinement of these numbers. Evidence for variations in SFR on short timescales is discussed by Yusef-Zadeh et al. (2009). Using $\dot{M}_* = 0.06$ $M_\odot$ year^{-1} and $R_{gal} = 0.25$ kpc for the CMZ, $\Sigma(\mathrm{SFR}) = 300$ $M_\odot$ Gyr^{-1} pc^{-2}. These values of Σ_{mol} and Σ(SFR) for the CMZ are plotted separately in **Figure 7** and identified as CMZ. If correct, the CMZ of the MW begins to look a bit more like the inner few kpc of NGC 6946. The CMZ provides an excellent place to test scaling relations, including those for dense gas, in detail, if the complicating issues can be understood. Preliminary results suggest that Σ(SFR) is

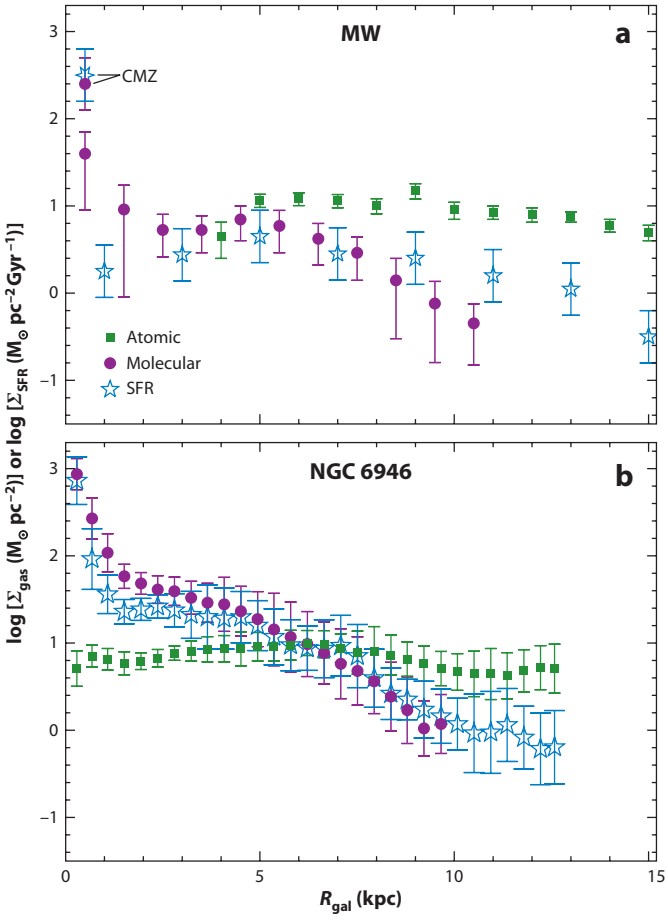

Figure 7

(*a*) The radial distribution of surface densities of atomic gas, molecular gas, and star-formation rate (SFR) for the Milky Way (MW). The atomic data were supplied by P. Kaberla, (Kalberla & Dedes 2008), but we corrected for helium. The discontinuity around 8.5 kpc reflects the inability to model HI near the solar circle. The molecular data are taken from table 1 in Nakanishi & Sofue (2006) but scaled up to be consistent with the bottom panel, using $X(\mathrm{CO}) = 2.0 \times 10^{20}$ and multiplying by 1.36 to include helium. The molecular surface density in the innermost bin is highly uncertain and may be overestimated by using a constant value of X(CO) (Section 2.4). The Σ(SFR) is read from figure 8 in Misiriotis et al. (2006), but it traces back through a complex history to Guesten & Mezger (1982), who used radio continuum emission from HII regions. That result was then scaled to the latest estimate of total SFR in the MW of 1.9 $M_\odot$ year^{-1} (Chomiuk & Povich 2011). Separate points for Σ_{mol} and Σ(SFR) are plotted for the Central Molecular Zone (CMZ) ($R_{\mathrm{gal}} < 250$ pc). An uncertainty of 0.3 was assigned arbitrarily to the values of log Σ(SFR). (*b*) Same as panel *a*, but for NGC 6946. It is based on a figure in Schruba et al. (2011) but modified by A. Schruba to show radius in kiloparsecs for ready comparison to the plot for the MW. Reproduced by permission of the AAS. All gas distributions for both galaxies include a correction for helium.

similar to that expected from Σ_{mol} (see **Figure 7**) but lower than expected from dense-gas relations (S. Longmore, personal communication).

The properties of clouds and clumps also may vary with R_{gal}. Heyer et al. (2009) reanalyzed cloud properties in the inner Galaxy using CO and ^{13}CO surveys. For the area of the cloud defined roughly by the 1-K CO detection threshold, they found a median $\Sigma_{\mathrm{mol}}(\mathrm{cloud}) = 42\ M_\odot\ \mathrm{pc}^{-2}$,

substantially less than originally found by Solomon et al. (1987), and only a few clouds have Σ_{mol}(cloud) > 100 $M_\odot$ pc^{-2}. Analysis based on detection thresholds for ^{13}CO yield a median Σ_{mol}(^{13}CO clump) = 144 $M_\odot$ pc^{-2} for ^{13}CO clumps (Roman-Duval et al. 2010, who refer to them as clouds). The mean in 0.5 kpc bins of surface density per ^{13}CO clump is roughly constant at 180 $M_\odot$ pc^{-2} from R_{gal} = 3 to 6.6 kpc, beyond which it drops sharply toward the much lower values in the Solar Neighborhood. Assuming the region sampled is representative, Roman-Duval et al. (2010) plotted the azimuthally averaged surface density of ^{13}CO clumps versus Galactocentric radius; it peaks at 2.5 $M_\odot$ pc^{-2} at 4.5 kpc, declining to <0.5 $M_\odot$ pc^{-2} beyond 6.5 kpc. The clouds appear to be associated with spiral arms, so azimuthal averaging should be taken with caution. The cloud mass function of 246 clouds in the far outer Galaxy has a power-law slope of $\alpha_{cloud} = -1.88$, similar to but slightly steeper than that found inside the solar circle (Section 2.5) and a maximum mass of approximately 10^4 $M_\odot$ (Snell, Carpenter & Heyer 2002). The lower value for the maximum mass of a cloud seems to result in a concomitant limit on the number of stars formed in a cluster, but no change is inferred for the intrinsic IMF (Casassus et al. 2000). A piece of a spiral arm at R_{gal} = 15 kpc has been recently identified in HI and CO, containing a molecular cloud with $M = 5 \times 10^4$ $M_\odot$ (Dame & Thaddeus 2011).

5.1.4. Nonaxisymmetric structure. The molecular-gas surface density shows a strong local maximum around R_{gal} = 4.5 kpc in the northern surveys (Galactic quadrants I and II), whereas southern surveys (quadrants III and IV) show a relatively flat distribution of Σ_{mol} from approximately 2 to 7 kpc (Bronfman et al. 2000). This asymmetry is likely associated with a spiral structure (Nakanishi & Sofue 2006) and a long (half-length of 4.4 kpc) bar (Benjamin et al. 2005). The SFR measured from L_{FIR} does not, however, reflect this asymmetry. In fact, it is larger in quadrant IV than in I, suggesting a star-formation efficiency up to twice as high, despite the lower peak Σ_{mol} (Bronfman et al. 2000). Interestingly, the distribution of denser gas, traced by millimeter-wave dust-continuum emission (Beuther et al. 2011), is also symmetric on kpc scales, but asymmetries appear within the CMZ region (Bally et al. 2010). Major concentrations of molecular clouds with very active star formation appear to be associated with regions of low shear (Luna et al. 2006) and with the junction of the bar and spiral arms (Nguyen Luong et al. 2011).

5.2. Demographics of Star-Forming Galaxies Today

The recent influx of multiwavelength data has expanded the richness of information available on global star-formation properties of galaxies and transformed the interpretive framework from one based on morphological types to a quantitative foundation based on galaxy luminosities, masses, and other physical properties.

The role of galaxy mass as a fundamental determinant of the star-formation history of a galaxy has been long recognized (e.g., Gavazzi & Scodeggio 1996), but data from SDSS and subsequent surveys have reshaped our picture of the population of star-forming galaxies (e.g., Kauffmann et al. 2003; Baldry et al. 2004, 2006; Brinchmann et al. 2004). The integrated colors of galaxies, which are sensitive to their star-formation histories, show a strongly bimodal dependence on stellar mass, with a relatively tight "red sequence" populated by galaxies with little or no current star formation and a somewhat broader "blue sequence" or "blue cloud" of actively star-forming galaxies. The dominant population shifts from blue to red near a transition stellar mass of $\sim 3 \times 10^{10}$ $M_\odot$ (Kauffmann et al. 2003). The relative dearth of galaxies in the "green valley" between the red and blue sequences suggests a deeper underlying physical bimodality in the galaxy population and a rapid evolution of galaxies from blue to red sequences.

A similar bimodality characterizes the mass dependence of the SFR per unit galaxy mass (SSFR). The mass dependence of the SSFR has been explored by numerous investigators (e.g., Brinchmann et al. 2004, Lee et al. 2007, Salim et al. 2007, Schiminovich et al. 2007). **Figure 8** shows an example from Schiminovich et al. (2007) using dust-corrected FUV measurements of SDSS galaxies.

A clear separation between the blue and red sequences is evident, and the dispersion of SSFRs within the blue sequence is surprisingly small, suggesting that some kind of self-regulation mechanism may be at work among the actively star-forming galaxies. The bimodality is not absolute; there is a clear tail of less active but significantly star-forming galaxies between the two sequences. These represent a combination of relatively inactive (usually early-type) disk galaxies and unusually active spheroid-dominated systems (Section 5.4). The sharp increase in the fraction of inactive galaxies above stellar masses of order a few $\times 10^{10}$ $M_\odot$ is also seen.

The blue sequence in **Figure 8** is not horizontal; the SSFR clearly increases with decreasing galaxy mass. The slope (-0.36 for the data in **Figure 8**) varies somewhat between different studies, possibly reflecting the effects of different sampling biases. The negative slope implies that lower-mass galaxies are forming a relatively higher fraction of their stellar mass today and thus must have formed relatively fewer of their stars (compared with more massive galaxies) in the past. The most straightforward explanation is that the dominant star-forming galaxy population in the Universe has gradually migrated from more massive to less massive galaxies over cosmic time.

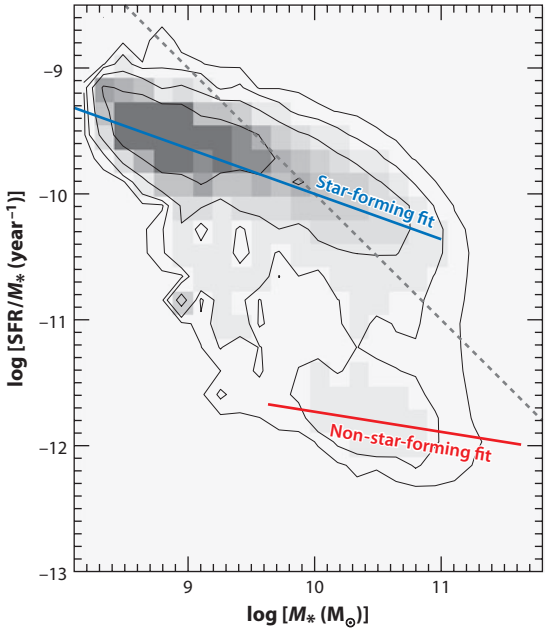

Figure 8

Relation between a specific star-formation rate (SFR) ($\dot{M}_*/M_*$) and galaxy mass for galaxies in the Sloan Digital Sky Survey (SDSS) spectroscopic sample and with SFRs measured from GALEX ultraviolet luminosities. Gray contours indicate the ($1/V_{max}$-weighted) number distribution of galaxies in this bivariate plane. The blue solid line shows the fit to the star-forming sequence, and the red line shows the approximate position of the non-star-forming red sequence on this diagram. The gray dotted line shows the locus of constant $SFR = 1$ $M_\odot$ year^{-1}. Figure adapted from Schiminovich et al. (2007); reproduced by permission of the AAS.

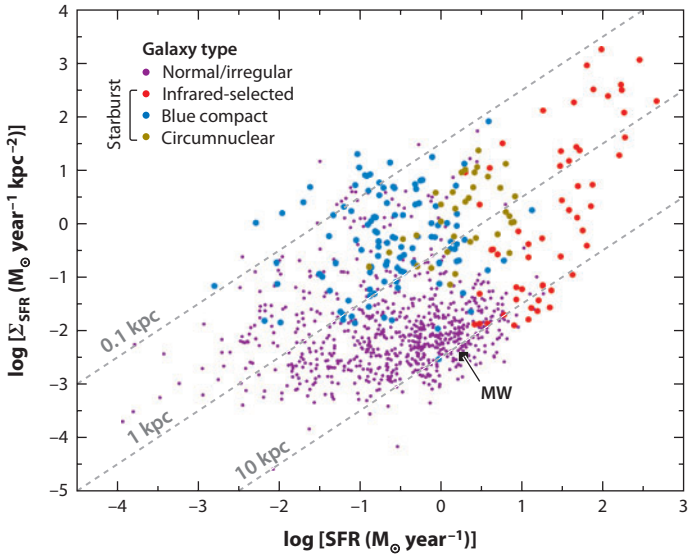

Figure 9

Distribution of integrated star-formation properties of galaxies in the local Universe. Each point represents an individual galaxy or starburst region, with the average star-formation rate (SFR) per unit area (SFR intensity) plotted as a function of the absolute SFR. The SFR intensities are averaged over the area of the main star-forming region rather than the photometric area of the disk. Diagonal gray lines show loci of constant star-formation radii, from 0.1 kpc (*top*) to 10 kpc (*bottom*). Several subpopulations of galaxies are shown: normal disk and irregular galaxies measured in Hα and corrected for dust attenuation (*solid purple points*) from the surveys of Gavazzi et al. (2003), James et al. (2004), Hameed & Devereux (2005), and Kennicutt et al. (2008); luminous and ultraluminous infrared galaxies (LIRGs and ULIRGs, respectively) (*red points*) from Dopita et al. (2002) and Scoville et al. (2000); blue compact starburst galaxies measured in Hα (*blue points*) from Pérez-González et al. (2003) and Gil de Paz et al. (2005); and circumnuclear star-forming rings in local barred galaxies measured in Paα (*dark yellow points*) as compiled by Kormendy & Kennicutt (2004). The position of the Milky Way (*black square*) lies near the high end of normal spirals in total SFR, but it is near the average in Σ(SFR) (Section 5.1). The relative numbers of galaxies plotted does not reflect their relative space densities. In particular, the brightest starburst galaxies are extremely rare.

Direct evidence for this "downsizing" is seen in observations of the SSFR versus mass relation in high-redshift galaxies (e.g., Noeske et al. 2007).

Another instructive way to examine the statistical properties of star-forming galaxies is to compare absolute SFRs and SFRs normalized by mass or area. An example is shown in **Figure 9**, which plots integrated measurements of the SFR per unit area as a function of the absolute SFRs. Several interesting trends can be seen in the data in **Figure 9**. For example, note the extraordinary range in SFRs, more than seven orders of magnitude, whether measured in absolute terms or normalized per unit area or (not shown) galaxy mass. Much of this range is contributed by nonequilibrium systems (starbursts). Normal galaxies occupy a relatively tight range of SFRs per unit area, reminiscent of the tightness of the blue sequence when expressed in terms of SSFRs. The total SFRs of the quiescent star-forming galaxies are also tightly bounded below a value of $\sim$20 $M_\odot$ year^{-1}. Starburst galaxies as well as IR-luminous and ultraluminous systems, in particular, comprise most of the galaxies in the upper 2–3 decades of absolute SFRs and Σ(SFR).

The distribution of SFRs along the X-axis of **Figure 9** (after correcting for volume completeness biases) is simply the SFR distribution function (e.g., Gallego et al. 1995, Martin et al. 2005b). **Figure 10** shows a recent determination of this distribution from Bothwell et al. (2011)

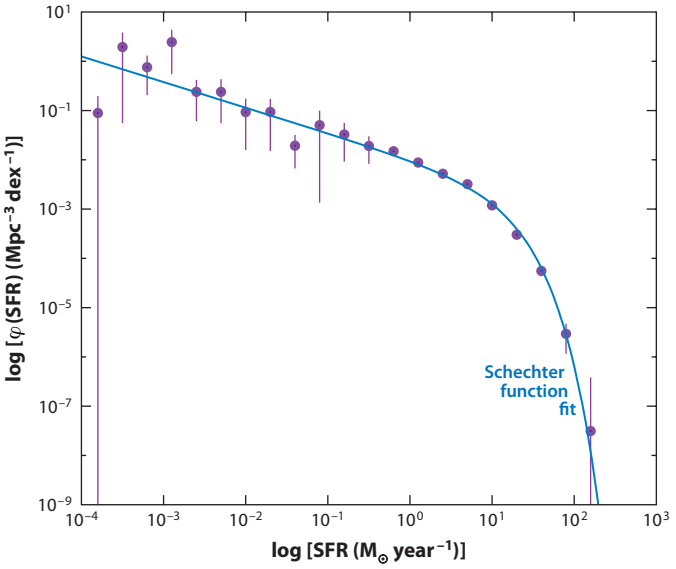

Figure 10

Volume-corrected star-formation-rate (SFR) distribution function for disk and irregular galaxies in the local Universe, as derived from a combination of large flux-limited ultraviolet and infrared catalogs and a multiwavelength survey of the local 11-Mpc volume. Vertical lines indicate uncertainties due to finite sampling; these are especially important for low SFRs where the statistics are dominated by dwarf galaxies that can be observed only over small volumes. Statistics on gas-poor (elliptical, dwarf spheroidal) galaxies are not included in this study. The blue line shows a maximum-likelihood Schechter function fit, as described in the text. Figure is original, but similar to one in Bothwell et al. (2011).

based on flux-limited UV and TIR samples of galaxies and SFRs derived using the methods of Hao et al. (2011) and corrections for AGN contamination following Wu et al. (2010b, 2011). The SFR function is well fitted by a Schechter (1976) exponentially truncated power law, with a faint-end slope $\alpha = -1.5$ and characteristic SFR, $SFR^* = 9\ M_\odot$. Although SFRs as high as $\sim$1,000 $M_\odot$ year^{-1} are found in present-day ULIRGs, the contribution of LIRGs and ULIRGs to the aggregate star formation today is small (<10%) (also see Goto et al. 2011). Steady-state star formation in galaxies dominates today. The value of SFR* increases rapidly with z, and galaxies with $L_{bol} > 10^{11}\ L_\odot$ (i.e., LIRGs) become dominant by redshifts $z > 1$ (e.g., Le Floc'h et al. 2005). This change partly reflects an increase in merger-driven star formation at higher redshift, but at early epochs, even the steady-state star formation in massive galaxies attained levels of order tens to hundreds of solar masses per year, thus placing those galaxies in the LIRG and ULIRG regime. This suggests that most of the decrease in the cosmic SFR in recent epochs has been driven by downsizing in the level of steady-state star formation (e.g., Bell et al. 2005, Jogee et al. 2009).

5.3. The High-Density Regime: Starbursts

As highlighted in Section 1.2, the starburst phenomenon encompasses a wide range of physical scales and host galaxy properties, and no precise physical definition of a starburst has been placed into wide use. Part of the explanation can be seen in **Figure 9**. Although the most extreme starburst galaxies have properties that are well separated from those of normal star-forming galaxies, there is no clear physical break in properties. Instead, starbursts define the upper tails of the overall distributions in SFRs within the general galaxy population.

Much of the attention in this area continues to be focused on the IR-luminous and ultraluminous systems because they probe star formation in the most extreme high-density circumnuclear environments seen in the local Universe. A major breakthrough in recent years has been the use of mid-IR spectroscopy to distinguish dust heated by massive stars from that heated by a buried AGN (e.g., Genzel et al. 1998, Laurent et al. 2000, Dale et al. 2006, Armus et al. 2007). Regions heated by AGNs are distinguished by the appearance of highly ionized atomic species, as well as suppressed mid-IR PAH emission relative to stellar-heated dust. Application of these diagnostics has made it possible to construct clean samples of LIRGs and ULIRGs that are dominated by star formation.

With the *Spitzer* and *Herschel* observatories, it has been possible to extend imaging and spectroscopy of the most luminous IR-emitting galaxies to intermediate redshifts (e.g., Elbaz et al. 2005, Yan et al. 2007). As mentioned above, the fraction of star formation in LIRGs and ULIRGs increases sharply with redshift, but imaging and spectroscopy of these objects reveals a marked shift in the physical characteristics of the population. At low redshift, ULIRGs (and many LIRGs) are dominated by very compact circumnuclear starbursts triggered by mergers. At higher redshifts, the LIRG/ULIRG population becomes increasingly dominated by large disk galaxies with extended star formation. As a consequence of cosmic downsizing (i.e., "upsizing" with increasing redshift), by redshifts $z \sim 1$ the populations of LIRGs and ULIRGs become increasingly dominated by the progenitors of present-day normal galaxies, rather than by the transient merger-driven starbursts that dominate the present-day populations of ULIRGs. Nevertheless, examples of the latter are still found, especially in the population of submillimeter galaxies (SMGs) (e.g., Chapman et al. 2005).

Visible-wavelength observations of these high-redshift galaxies with IFU (integral field unit) instruments, both with and without adaptive optics correction, have revealed many insights into the physical nature of this population of starburst galaxies (e.g., Genzel et al. 2008, 2011; Förster Schreiber et al. 2009, and references therein). The Hα kinematics show a wide range of properties, from normal, differentially rotating disks to disturbed disks, and a subset have signatures of ongoing or recent mergers. The disks tend to be characterized by unusually high velocity dispersions, which have been interpreted as reflecting a combination of dynamical instability and, possibly, energy injection into the ISM from young stars. Further discussion of high-redshift galaxies is beyond the scope of this article, but we return to the cold ISM properties and SFRs of these galaxies in Section 6.

5.4. The Low Star-Formation Rate and Low-Density Regimes

One of the most important discoveries from the GALEX mission was the detection of low levels of star formation in environments that were often thought to have been devoid of star formation. These include early-type galaxies, dwarf galaxies, low-surface-brightness galaxies, and the extreme outer disks of many normal galaxies.

Although star formation had been detected occasionally in nearby elliptical and S0 galaxies (e.g., Pogge & Eskridge 1993), most of these galaxies have historically been regarded as being "red and dead" in terms of recent star formation. Deep GALEX imaging of E/S0 galaxies (e.g., Kaviraj et al. 2007), however, has revealed that approximately 30% of these early-type galaxies exhibit near-UV emission in excess of what could reasonably arise from an evolved stellar population (e.g., Kaviraj et al. 2007). Confirmation of the star formation has come from visible-wavelength IFU spectroscopy, as exploited, for example, by the SAURON Survey (Shapiro et al. 2010). The SFRs in these galaxies tend to be very low, with at most 1–3% of the stellar mass formed over the past 10^9 years. High-resolution UV imaging with HST often reveals extended star-forming rings or spiral arms in these galaxies (Salim & Rich 2010). Follow-up CO observations of these galaxies

reveals significant detections of molecular gas in a large fraction of the galaxies with detected star formation, with molecular gas masses of 10^7–10^{10} $M_\odot$ (Combes, Young & Bureau 2007; Crocker et al. 2011) and with SFRs roughly consistent with the Schmidt law seen in normal galaxies.

The GALEX images also reveal that star formation in more gas-rich disk galaxies often extends much farther in radius than had previously been appreciated. In exceptional cases (e.g., NGC 5236 = M83, NGC 4625), the star formation extends to 3–4 times the normal R_{25} optical radius, out to the edge of the HI disk (Gil de Paz et al. 2005, Thilker et al. 2005). A systematic study by Thilker et al. (2007) revealed that extended "XUV disks" are found in ~20% of spiral galaxies, with less distinct outer UV structures seen in another ~10% of disk galaxies. Follow-up deep Hα imaging and/or spectroscopy revealed extended disks of HII regions that trace the UV emission in most cases (e.g., Christlein, Zaritsky & Bland-Hawthorn 2010; Goddard, Kennicutt & Ryan-Weber 2010; Zaritsky & Christlein 2007), confirming the earlier detection of HII regions at large radii (e.g., Ferguson et al. 1998, Ryan-Weber et al. 2004). Individual examples of extended UV features without Hα counterparts are sometimes found, however (Goddard, Kennicutt & Ryan-Weber 2010). The GALEX images also have led to a breakthrough in measurements of star formation in low-surface-brightness spiral galaxies. These provide a homogeneous body of deep measurements of star formation and the nature of the star-formation law at low surface densities (Section 6) (Wyder et al. 2009). Comparison to the outer MW (Section 5.1) suggests that deep searches for molecular gas will find few clouds, which will nonetheless be the sites of star formation.

The other low-density star-formation regime can be found in dwarf irregular galaxies. Drawing general inferences about the star-formation properties of these galaxies requires large samples with well-defined (ideally volume-limited) selection criteria. Studies of this kind (based on UV, visible, and/or Hα observations) have been carried out by several groups (e.g., Karachentsev et al. 2004; Blanton et al. 2005; Meurer et al. 2006; Kennicutt et al. 2008; Dalcanton et al. 2009; Hunter, Elmegreen & Ludka 2010). One perhaps surprising result is the near ubiquity of star formation in the dwarf galaxies. Kennicutt et al. (2008) observed or compiled Hα luminosities for galaxies within the local 11 Mpc, which included ~300 dwarf galaxies ($M_B > -17$). Excluding a handful of dwarf spheroidal galaxies that have no cold gas, only 10 of these (~3%) were not detected in Hα, meaning that star formation had taken place over the past 3–5 Myr in the other 97% of the systems. Moreover, many of the handful of Hα nondetections show knots of UV emission, demonstrating that even fewer of the galaxies have failed to form stars over the past ~100 Myr (Lee et al. 2011). Recent star formation is seen in all the galaxies with $M_B < -13$ and $M(\mathrm{HI}) > 5 \times 10^7$ $M_\odot$. For less-massive galaxies, it is possible for star formation to cease for timescales that are longer than the ionization lifetime of an HII region (up to 5 Myr), but examples of galaxies with extended periods of no star formation are extremely rare.

These data also provide a fresh look at the temporal properties of the star formation in dwarf galaxies in general. The distribution of SSFRs shows a marked increase in dispersion for galaxies with $M_B > -14.5$ or circular velocity of 50 km s^{-1} (Lee et al. 2007; Bothwell, Kennicutt & Lee 2009). The corresponding neutral gas fraction does not show a similar increase in dispersion (Bothwell, Kennicutt & Lee 2009), suggesting an increased short-term fluctuation of integrated SFRs in low-mass galaxies. Lee et al. (2009b) analyzed the statistics of the SFRs in more depth and confirmed a larger fraction of stars formed in bursts in low-mass galaxies (~25%), but these still represent only a small fraction of the total stars formed—even in the dwarfs the majority of stars appear to form in extended events of duration longer than ~10 Myr. Recent modeling of the statistics of Hα and UV emission by Weisz et al. (2012) and Fumagalli, da Silva & Krumholz (2011) as well as analysis of resolved stellar populations (e.g., Weisz et al. 2008) confirm the importance of fluctuations in the SFR.

6. STAR-FORMATION RELATIONS

The immense dispersion in SFR properties seen in **Figure 9** collapses to a remarkably tight scaling law when the SFR surface densities Σ(SFR) are plotted against mean gas surface densities ($\Sigma_{\rm gas}$) (Kennicutt 1998b). This emergent order reflects the fact that gas is the input driver for star formation. The concept of a power-law relation between SFR density and gas density dates to Schmidt (1959, 1963), and relations of this kind are commonly referred to as Schmidt laws. On physical grounds, we may expect the most fundamental relation to be between the volume densities of star formation and gas, but because most observations of external galaxies can measure only surface densities integrated along the line of sight, the most commonly used relation, often called a Kennicutt-Schmidt (KS) law, is in terms of surface densities:

$$\Sigma_{\rm SFR} = A\,\Sigma_{\rm gas}^{N}. \tag{13}$$

The precise form of this relation depends on assumptions about how $\Sigma_{\rm gas}$ is derived from the observations (Section 2.4), but a strong correlation is clearly present.

6.1. The Disk-Averaged Star-Formation Law

Kennicutt (1998a) presented a review of observations of the Schmidt law up to the time, and nearly all that work characterized the relation between the disk-averaged SFR and gas surface densities in galaxies. **Figure 11** presents an updated version of the global Schmidt law in galaxies. Each point is an individual galaxy with the surface density defined as the total gas mass (molecular plus atomic) or SFR normalized to the radius of the main star-forming disk, as measured from Hα, Paα, or IR maps. For simplicity, a constant X(CO) factor [2.3×10^{20} (K km s^{-1})$^{-1}$ with no correction for helium; see Section 2.4] has been applied to all the galaxies; the consequences of a possible breakdown in this assumption are discussed below. The sample of galaxies has been enlarged from that studied by Kennicutt (1998b), and all the Hα-based SFR measurements have been improved by incorporating individual (IR-based) corrections for dust attenuation and [NII] contamination. Most of the galaxies form a tight relation, and with the improved data set, even the normal galaxies (**Figure 11**, *purple points*) follow a well-defined Schmidt law on their own. The dispersion of the normal galaxies overall from the average relation (± 0.30 dex rms) is considerably higher than can be attributed to observational uncertainties, which suggests that much of the dispersion is physical. The form of this integrated Schmidt law appears to be surprisingly insensitive to the SFR environment and parameters such as the atomic versus molecular fraction, but some metal-poor galaxies (defined as $Z < 0.3\ Z_{\odot}$) deviate systematically from the main relation (**Figure 11*a***). These deviations could arise from a physical change in the star-formation law but more likely reflect a breakdown in the application of a constant X(CO) factor (Section 2.4) (Leroy et al. 2011, and references therein). Adopting higher values of X(CO) for metal-poor galaxies brings the galaxies much more into accord with the main relation in **Figure 11*a***.

Recent observations of low-surface-brightness spiral galaxies by Wyder et al. (2009) extend the measurements of the integrated star-formation law to even lower mean surface densities (**Figure 11*a***). A clear turnover is present, which is consistent with breaks seen in spatially resolved observations of the star-formation law (Section 6.2).

The slope of the integrated Schmidt law is nonlinear, with $N \simeq 1.4$–1.5 (Kennicutt 1998b) when a constant X(CO) factor is applied. This uncertainty range does not include all possible systematic errors, arising, for example, from changes in X(CO) or the IMF with increasing surface density or SFR. Major systematic changes in either of these could easily change the derived value of N by as much as 0.2–0.3. For example, if X(CO) were five times lower in the dense starburst

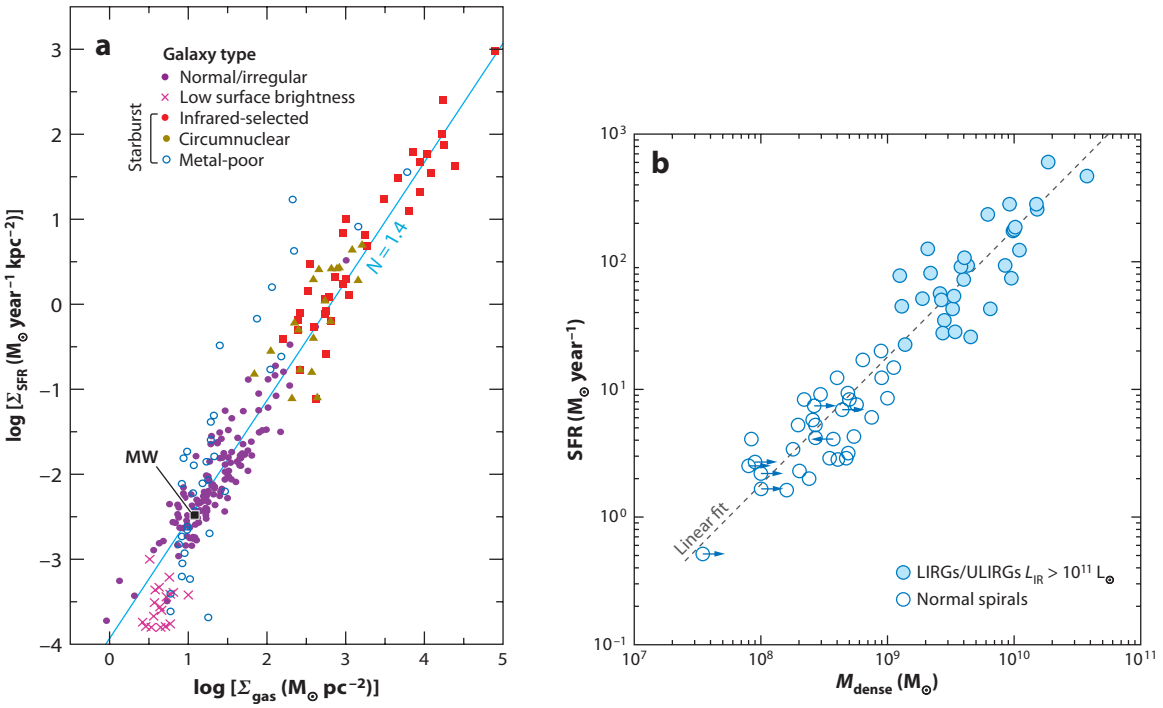

Figure 11

(*a*) Relationship between the disk-averaged surface densities of star formation and gas (atomic and molecular) for different classes of star-forming galaxies. Each point represents an individual galaxy, with the SFRs and gas masses normalized to the radius of the main star-forming disk. Colors are used similarly as in **Figure 9**: Purple points represent normal spiral and irregular galaxies, red points infrared-selected starburst galaxies [mostly luminous and ultraluminous infrared galaxies (LIRGs and ULIRGs, respectively)], and dark yellow points denote circumnuclear starbursts with star-formation rates (SFRs) measured from Paα measurements. The Milky Way (*black square*) fits well on the main trend seen for other nearby normal galaxies. Magenta crosses represent nearby low-surface-brightness galaxies, as described in the text. Open blue circles denote low-mass irregular and starburst galaxies with estimated metal (oxygen) abundances less than 0.3 $Z_{\odot}$, indicating a systematic deviation from the main relation. For this plot, a constant X(CO) factor was applied to all galaxies. The light blue line shows a fiducial relation with slope $N = 1.4$ (not intended as a fit to these data). The sample of galaxies has been enlarged from that studied in Kennicutt (1998b), with many improved measurements as described in the text. (*b*) Corresponding relation between the total (absolute) SFR and the mass of dense molecular gas as traced in HCN. The dashed gray line is a linear fit, which contrasts with the nonlinear fit in panel *a*. Figure adapted from Gao & Solomon (2004). Reproduced by permission of the AAS.

galaxies (Section 2.4), the slope of the overall Schmidt law would increase from 1.4–1.5 to 1.7–1.9 (Narayanan et al. 2011).

Usually, the Schmidt law is parameterized in terms of the total (atomic plus molecular) gas surface density, but one can also explore the dependences of the disk-averaged SFR densities on the mean atomic and molecular surface densities individually. Among normal galaxies with relatively low mean surface densities, the SFR density is not particularly well correlated with either component, though variations in X(CO) could partly explain the poor correlation between SFR and derived H_2 densities (e.g., Kennicutt 1998b). In starburst galaxies with high gas surface densities, however, the gas is overwhelmingly molecular, and a strong nonlinear Schmidt law is observed (**Figure 11*a***).

A similar nonlinear dependence is observed for total SFR (as opposed to SFR surface density) versus total molecular gas mass (e.g., Solomon & Sage 1988, Gao & Solomon 2004). This

similarity presumably reflects another manifestation of the same underlying physical correlation. The dependence of the SFR on dense molecular gas mass is markedly different, however. The right panel of **Figure 11**, taken from Gao & Solomon (2004), shows the relation between the integrated SFRs and the dense molecular gas masses, as derived from HCN $J = 1 \rightarrow 0$ measurements (Section 2.4) for a sample of normal and starburst galaxies. In contrast to the correlation with total molecular mass from CO $J = 1 \rightarrow 0$, this relation is linear, implying a strong coupling between the masses of dense molecular clumps and stars formed, which is largely independent of the galactic star-forming environment. J. Wu et al. (2005) have subsequently shown that this linear relation extends down to the scales of individual star-forming molecular clouds and dense clumps in the Galaxy. Combined with the MW studies (Section 4), these dense gas relations for galaxies suggest that dense clumps are plausible fundamental star-forming units. If so, the mass fraction of the ISM (and fraction of the total molecular gas) residing in dense clumps must increase systematically with the SFR.

Because $L_{\rm HCN}$ in the $J = 1 \rightarrow 0$ line is only an approximate tracer for dense gas (Section 2.4.3) and because the definition of a dense clump is by no means precise (Section 2.5), one should be careful not to overinterpret these trends. Similar comparisons of the SFR with the emission from other molecular tracers suggest that the slope of the SFR versus gas mass relation changes continuously as one proceeds from lower-density tracers such as CO $J = 1 \rightarrow 0$ to higher-excitation (and higher-density) CO transitions and further to high-density tracers such as HCN and HCO^+ and to higher transitions of those molecules (e.g., Juneau et al. 2009). Multitransition studies along with realistic modeling will help to refine the interpretation of line luminosities of dense gas tracers (e.g., Graciá-Carpio et al. 2008, Juneau et al. 2009).

The data shown in **Figure 11** all come from observations of nearby galaxies ($z < 0.03$), but recently, a number of studies have addressed the form of the molecular-gas Schmidt law for starburst galaxies extending to redshifts $z \geq 2$ (e.g., Bouché et al. 2007, Daddi et al. 2010, Genzel et al. 2010). The interpretation of these results is strongly dependent on the assumptions made about X(CO) in these systems. When a Galactic X(CO) conversion is applied, the high-redshift galaxies tend to fall roughly on the upper parts of the Schmidt law seen locally (e.g., **Figure 11**). However, if a lower X(CO) factor is applied to the most compact starburst and SMGs, as suggested by many independent analyses of X(CO) (Section 2.4), the Schmidt relations shift leftward by the same factor, forming a parallel relation (Daddi et al. 2010, Genzel et al. 2010).

Taken at face value, these results suggest the presence of two distinct modes of star formation with different global efficiencies, which separate the extended star-forming disks of normal galaxies from those in the densest circumnuclear starbursts; this distinction is likely to be present both in the present-day Universe and at early cosmic epochs. This inferred bimodality, however, is a direct consequence of the assumption of two discrete values for X(CO) in the two modes. A change in the interpretation of CO emission is certainly plausible when the derived molecular surface density is similar to that of an individual cloud ($\Sigma_{\rm mol} > 100\ M_\odot\ {\rm pc}^{-2}$), but the behavior of X(CO) may be complex (Section 2.4). Variation of X(CO) over a continuous range would indicate a steeper Schmidt law, rather than a bimodal law (Narayanan et al. 2011).

Daddi et al. (2010) also note that the higher concentration of gas in the ULIRGs/SMGs is consistent with an enhanced fraction of dense gas and the dense gas relations of Gao & Solomon (2004). However, the SFR also appears to be larger for a given mass of dense gas in extreme starbursts (Garcia-Burillo et al. 2011 and references therein), especially when a lower value of $\alpha_{\rm HCN}$ is used. As with CO, one can interpret these as bimodal relations or as steeper than linear dependences on the gas-tracer lines. These results, together with evidence for lower SFR per mass of dense gas in the CMZ of the MW (Section 5.1), warn against an overly simplistic picture of dense clumps as the linear building blocks for massive star formation, with no other variables in the picture.

The correlations between SFR and gas surface densities (and masses) are not the only scaling laws that are observed. Kennicutt (1998b) pointed out that the SFR surface densities also correlate tightly with the ratio of the gas surface density to the local dynamical time, defined in that case to be the average orbit time. This prescription is especially useful for numerical simulations and semianalytical models of galaxy evolution. Interestingly, Daddi et al. (2010) and Genzel et al. (2010) found that the bifurcation of Schmidt laws between normal galaxies and ULIRGs/SMGs described above does not arise in the dynamical form of this relation.

Blitz & Rosolowsky (2006) discovered another strong scaling relation between the ratio of molecular to atomic hydrogen in disks and the local hydrostatic pressure. The relation extends over nearly three orders of magnitude in pressure and H_2/HI ratio and is nearly linear (slope = 0.92). Technically speaking, this scaling relation applies only to the phase balance of cold gas rather than the SFR, but it can be recast into a predicted star-formation law if assumptions are made about the scaling between the SFR and the molecular gas components (e.g., Blitz & Rosolowsky 2006, Leroy et al. 2008). Recent work by Ostriker, McKee & Leroy (2010) and Ostriker & Shetty (2011) provides a theoretical explanation for these relations.

Finally, a number of workers have explored the scaling between SFR surface density and a combination of gas and stellar surface densities. For example, Dopita (1985) and Dopita & Ryder (1994) proposed a scaling between the SFR density and the product of gaseous and stellar surface densities; the latter scales with the disk hydrostatic pressure and, hence, bears some relation to the picture provided by Blitz & Rosolowsky (2006). More recently Shi et al. (2011) showed that the scatter in the star-formation law is minimized with a relation of the form $\Sigma_{\rm SFR} \propto \Sigma_{\rm gas}\Sigma_*^{0.5}$.

Determining which of these different formulations of the star-formation law is physical and which are mere consequences of a more fundamental relation is difficult from observations alone. Some of the degeneracies between these various relations can be understood if most gas disks lie near the limit of gravitational stability ($Q \sim 1$) (Kennicutt 1989), and the critical column densities for the formation of cold gas phase, molecule formation, and gravitational instability lie close to each other (e.g., Elmegreen & Parravano 1994, Schaye 2004). In such conditions, it can be especially difficult to identify which physical process is most important from observations. We return to this topic below.

We conclude this section by mentioning that there are other SFR scaling laws that can be understood as arising from an underlying Schmidt law. The best known of these is a strong correlation between characteristic dust attenuation in a star-forming galaxy and the SFR, with the consequence that galaxies with the highest absolute SFRs are nearly all dusty LIRGs and ULIRGs (e.g., Wang & Heckman 1996, Martin et al. 2005b, Bothwell et al. 2011). This opacity versus SFR relation is partly a manifestation of the Schmidt law because we now know that the most intense star formation in galaxies takes place in regions with abnormally high gas surface densities and, thus, also in regions with abnormally high dust surface densities. The other factor underlying the SFR versus opacity correlation is the prevalence of highly concentrated circumnuclear star formation in the most intense starbursts observed in the present-day Universe (Section 5.3); this may not necessarily be the case for starburst galaxies at early cosmic epochs.

6.2. Radial Distributions of Star Formation and Gas

Over the past few years, major progress has been made in characterizing the spatially resolved star-formation law within individual galaxies. This work has been enabled by large multiwavelength surveys of nearby galaxies such as the Spitzer Infrared Nearby Galaxies Survey (SINGS) (Kennicutt et al. 2003), the GALEX Nearby Galaxies Survey (Gil de Paz et al. 2007), the Spitzer/GALEX Local Volume Legacy Survey (Dale et al. 2009, Lee et al. 2011), and the Herschel KINGFISH

Survey (Kennicutt et al. 2011). The resulting data sets provide the means to measure spatially resolved and dust-corrected SFRs across a wide range of galaxy properties (Section 3). These surveys, in turn, have led to large spin-off surveys in HI [e.g., THINGS (Walter et al. 2008), FIGGS (Begum et al. 2008), Local Volume HI Survey (Koribalski 2010), LITTLE THINGS (Hunter et al. 2007)] and in CO [e.g., BIMA-SONG (Helfer et al. 2003), IRAM HERACLES (Leroy et al. 2009), JCMT NGLS (Wilson et al. 2009), CARMA/NRO Survey (Koda & Nearby Galaxies CO Survey Group 2009), CARMA STING (Rahman et al. 2011, 2012)]. The capabilities of these new data sets are illustrated in **Figure 6**, which shows *Spitzer* 24-μm, Hα, VLA HI, and CO (in this case from HERACLES) maps of NGC 6946 (see **Figure 7** for the corresponding radial distributions of gas and star formation).

The first step in exploiting the spatial resolution of the new observations is to analyze the azimuthally averaged radial profiles of the SFR and gas components (as illustrated, for example, in **Figure 7**) and the resulting SFR versus gas surface density correlations. This approach has the advantage of spatially averaging over large physical areas, which helps to avoid the systematic effects that are introduced on smaller spatial scales (Section 3.9). Radial profiles also have limitations arising from the fact that a single radial point represents an average over subregions with often wildly varying local gas and SFR densities, and changes in other radially varying physical parameters may be embedded in the derived SFR versus gas density relations.

Large-scale analyses of the star-formation law derived in this way have been carried out by numerous researchers (e.g., Kennicutt 1989, Martin & Kennicutt 2001, Wong & Blitz 2002, Boissier et al. 2003, Heyer et al. 2004, Komugi et al. 2005, Schuster et al. 2007, Leroy et al. 2008, Gratier et al. 2010, Schruba et al. 2011). A strong correlation between SFR and gas surface density is seen in nearly all cases, with a nonlinear slope when plotted in terms of total (atomic + molecular) density. The best-fitting indices N vary widely, however, ranging from 1.4 to 3.1 for the dependence on total gas density and from 1.0 to 1.4 for the dependence on molecular gas surface density alone for constant X(CO). The measurements of the MW range from $N = 1.2 \pm 0.2$, when only molecular gas is used (Luna et al. 2006), to 2.18 ± 0.20 when total (atomic and molecular) gas is used (Misiriotis et al. 2006).

Some of the differences between these results can be attributed to different schemes for treating dust attenuation, different CO line tracers, different metallicities [which may influence the choice of X(CO)], and different fitting methods. The influence of a metallicity-dependent X(CO) factor is investigated explicitly by Boissier et al. (2003). Because any variation in X(CO) is likely to flatten the radial molecular density profiles, a variable conversion factor tends to steepen the slope of the derived Schmidt law; for the prescription they use, the best-fitting slope can increase to as high as $N = 2.1$–3.6, underscoring once again the critical role that assumptions about X(CO) play in the empirical determination of the star-formation law. Despite these differences in methodology, real physical variation in the SFR versus gas density relation on these scales cannot be ruled out.

This body of work also confirms the presence of a turnover or threshold in the star-formation relation at low surface densities in many galaxies. Early work on this problem (e.g., Kennicutt 1989, Martin & Kennicutt 2001, Boissier et al. 2003) was based on radial profiles in Hα, and some questions have been raised about whether these thresholds resulted from breakdowns in the SFR versus Hα calibration in low-surface-brightness regimes, as opposed to real thresholds in the SFR. Subsequent comparisons of UV and Hα profiles appear to confirm the presence of radial turnovers in the SFR in most disks, however, even in galaxies where lower levels of star formation persist to much larger radii (e.g., Thilker et al. 2007, Christlein, Zaritsky & Bland-Hawthorn 2010; Goddard, Kennicutt & Ryan-Weber 2010). This extended star formation can be seen in **Figure 7** ($R >$ 7–8 kpc). Recent studies of nearby galaxies with unusually extended XUV disks

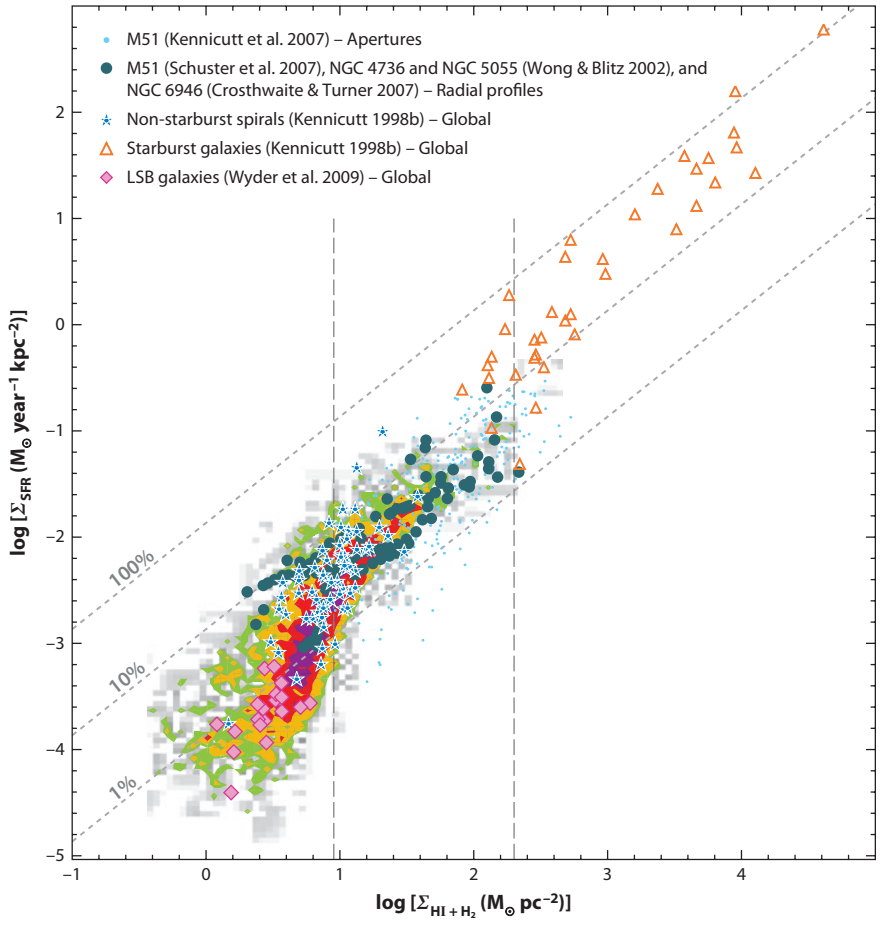

Figure 12

Relation between star-formation-rate (SFR) surface densities and total (atomic and molecular) gas surface densities for various sets of measurements (from Bigiel et al. 2008). Regions colored gray, green, yellow, and red show the distribution of values from measurements of subregions of SINGS galaxies. Overplotted as light blue dots are data from measurements in individual apertures in M51 (Kennicutt et al. 2007). Data from radial profiles from M51 (Schuster et al. 2007), NGC 4736 and NGC 5055 (Wong & Blitz 2002), and NGC 6946 (Crosthwaite & Turner 2007) are shown as dark blue filled circles. The disk-averaged measurements from 61 normal spiral galaxies (*dark blue stars*) and 36 starburst galaxies (*orange triangles*) from Kennicutt (1998b) are also shown. The magenta-filled diamonds show global measurements from 20 low-surface-brightness (LSB) galaxies (Wyder et al. 2009). In all cases, calibrations of initial mass function (IMF), X(CO), etc., were placed on a common scale. The three dotted gray diagonal lines extending from lower left to upper right reflect a constant global star-formation efficiency. The two vertical lines denote regimes that correspond roughly to those discussed in Section 6 of this review. Figure taken from Bigiel et al. (2008). Reproduced by permission of the AAS.

also show that the UV-based SFR falls off much more rapidly than the cold-gas surface density, with global star-formation efficiencies (ϵ') an order of magnitude or more lower than those in the inner disks (Bigiel et al. 2010). Taken together, these recent results and studies of the outer MW (Section 5.1) confirm the presence of a pronounced turnover in the Schmidt law for total gas at surface densities of order a few $M_\odot$ pc^{-2} (**Figure 12**).

6.3. The Star-Formation Law on Subkiloparsec Scales

The same multiwavelength data can be used in principle to extend this approach to point-by-point studies of the star-formation law. The angular resolution of the currently available data sets (optical/UV, mid-far IR, HI, CO) allows for extending this analysis down to angular scales of ~10 arcsec, which correspond to linear scales of 30–50 pc in the local group and 200–1000 pc for the galaxies in the local supercluster targeted by SINGS, THINGS, KINGFISH, and similar surveys. Recent analyses have become available (Kennicutt et al. 2007; Bigiel et al. 2008, 2010, 2011; Leroy et al. 2008; Blanc et al. 2009; Eales et al. 2010; Verley et al. 2010; Liu et al. 2011; Rahman et al. 2011, 2012; Schruba et al. 2011), and several other major studies are ongoing.

The most comprehensive attack on this problem to date is based on a combination of SINGS, THINGS, and HERACLES observations (see papers by Bigiel, Leroy, and Schruba, as cited above), and **Figure 12**, taken from Bigiel et al. (2008), nicely encapsulates the main results from this series of studies. The colored regions are the loci of individual subkiloparsec measurements of SFR surface densities (measured from a combination of FUV and 24-μm IR fluxes) and total gas densities [HI plus H_2 from CO(2–1) with a constant X(CO) factor], for 18 galaxies in the SINGS/THINGS sample. Other data (including Kennicutt 1998b) are overplotted as described in the figure legend and caption. The measurements show at least two distinct regimes, a low-density subthreshold regime where the dependence of the SFR density on gas density is very steep (or uncorrelated with gas density) and a higher-density regime where the SFR is strongly correlated with the gas density. The general character of this relation with a high-density power law and a low-density threshold confirms most of the results presented above.

One can also examine separately the dependence of the SFR density on the atomic and molecular surface densities, and the two relations are entirely different. The local SFR density is virtually uncorrelated with HI density, in part because the range of HI column densities is truncated above $\Sigma_{HI} \sim 10\ M_\odot\ pc^{-2}$ or $N(HI) \sim 10^{21}\ cm^{-2}$. This upper limit to the local HI densities corresponds to the column density where the HI efficiently converts to molecular form. This phase transition also roughly coincides with the turnover in the SFRs in **Figure 12**, which hints that the SFR threshold may be driven in part, if not entirely, by an atomic-molecular phase transition (see Section 7).

In contrast to the HI, the SFR surface density is tightly correlated with the H_2 surface density, as inferred from CO. A recent stacking analysis of the HERACLES CO maps made it possible to extend this comparison statistically to low H_2 column densities, showing a tight correlation between SFR and CO surface brightness that extends into the HI-dominated (subthreshold) regime (Schruba et al. 2011), reminiscent of studies in the outer MW (**Figure 7**) (Section 5.1).

The strong local correlation between Σ(SFR) and Σ_{mol} is seen in all the recent studies that probe linear scales of ~200 pc and larger. This is hardly surprising, given the strong coupling of star formation to dense molecular gas in local clouds (Sections 4 and 6.4). However, on smaller linear scales, the measurements show increased scatter for reasons discussed in Section 3.9. On these scales, we expect the scaling laws to break down, as the stars and gas may arise from separate regions. This effect has been directly observed in high-resolution observations of M33 (Onodera et al. 2010).

The main results described above—the presence of a power-law SFR relation with a low-density threshold, the lack of correlation of the local SFR with HI column density, the strong correlation with H_2 column density, and the rapidly increasing scatter in the Schmidt law on linear scales below 100–200 pc—are seen consistently across most, if not all, recent spatially resolved studies. Most of the recent studies also derive a mildly nonlinear slope for the SFR density versus total gas density Schmidt law in the high-density regime, with indices N falling in the range 1.2–1.6. Less clear from the recent work is the linearity and slope of the Schmidt law on small scales,

especially the dependence of SFR surface density on molecular-gas surface density. The results from the HERACLES/THINGS studies have consistently shown a roughly linear Σ_{SFR} versus Σ_{mol} relation ($N = 1.0$–1.1), and similar results have been reported by Blanc et al. (2009), Eales et al. (2010), and Rahman et al. (2011). Other researchers, however, have reported steeper dependences ($N = 1.2$–1.7), closer to those seen in integrated measurements (e.g., Kennicutt et al. 2007, Verley et al. 2010, Liu et al. 2011, Rahman et al. 2011, Momose 2012). The discrepancies between these results are much larger than the estimated fitting errors and probably arise, in part, from systematic differences in the observations and in the way the data are analyzed (see discussion in, e.g., Blanc et al. 2009). One effect that appears to be quite important is the way in which background diffuse emission is treated in measuring the local SFRs (Section 3.9). Liu et al. (2011) show that they can produce either a linear or nonlinear local molecular SFR law depending on whether the diffuse emission is removed. Another CARMA-based study by Rahman et al. (2011), however, suggests that the effects of diffuse emission may not be sufficient to account for all the differences between different analyses. Another important factor may be the excitation of the CO tracer used (e.g., Juneau et al. 2009).

It is important to bear in mind that nearly all of our empirical knowledge of the form of the local star-formation law is based on observations of massive gas-rich spiral galaxies with near-solar gas-phase metal abundances. Most studies of the star-formation relations in metal-poor dwarf galaxies have been limited to HI data or marginal detections in CO at best (e.g., Bigiel et al. 2008). A recent study of the SMC ($\sim 1/5\ Z_\odot$) offers clues to how these results may change in low-metallicity environments; Bolatto et al. (2011) found that the atomic-dominated threshold regime in the SMC extends up to surface densities that are an order of magnitude higher than in spirals.

6.4. Local Measurements of Star-Formation Relations

With the ongoing large-scale surveys of the Galaxy and the Magellanic Clouds in recent years, it is becoming possible to investigate SFR indicators, the scaling laws, and other star-formation relations for local samples. These can provide valuable external checks on the methods applied on larger scales to external galaxies and probe the star-formation relations on physical scales that are not yet accessible for other galaxies. Local studies of the conversion of CO observations into column density or mass were discussed in Section 2.4.

Comparison of various SFR indicators for the MW (Section 5.1), as would be used by observers in another galaxy, against more direct measures, such as young-star counts, suggests that SFRs based on the usual prescriptions (mid-IR and radio continuum) may be underestimating absolute $\dot{M}_*$ by factors of 2–3 (Chomiuk & Povich 2011). Chomiuk & Povich (2011) suggest that changes to the intermediate-mass IMF, timescale issues, models for O stars, and stochastic sampling of the upper IMF can contribute to the discrepancy. As discussed above, measures of SFR that use ionizing photons (Hα or radio continuum) require regions with a fully populated IMF to be reliable, and they systematically underestimate the SFR in small star-forming clouds (Section 3.9). For example, star formation in clouds near the Sun would be totally invisible to these measures and the SFR would be badly underestimated in the Orion Cluster (Section 3.9). Tests of other SFR tracers, such as 24-μm emission, within the MW would be useful. Changes in the IMF as large as those proposed by Chomiuk & Povich (2011) should also be readily observable in more evolved Galactic star clusters, if not in the field star IMF itself.

Using a YSO-counting method for five giant molecular clouds (GMCs) in the N159 and N44 regions in the LMC, Chen et al. (2010) reached stellar masses of approximately 8 $M_\odot$, below which they needed to extrapolate. The resulting ratios of $\dot{M}_*$ (YSOs) to $\dot{M}_*$ (Hα +24 μm) ranged from 0.37 to 11.6 with a mean of 3.5.

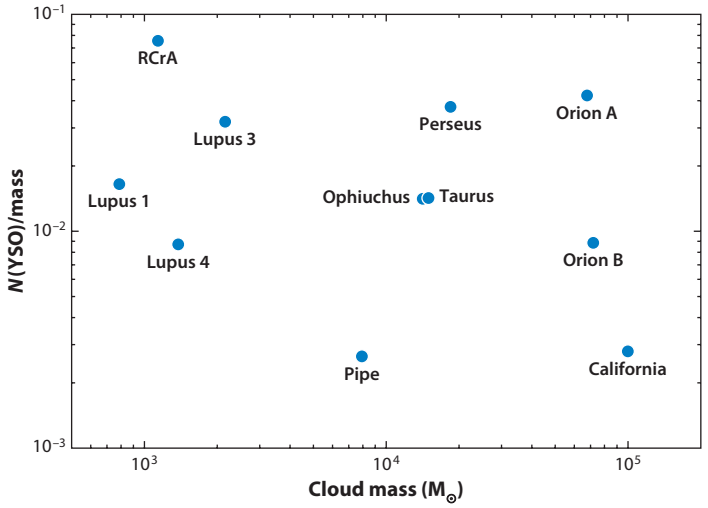

Figure 13

Plot of the ratio of the total number of young stellar objects [*N*(YSOs)] in a cloud to the total cloud mass versus total cloud mass. This is equivalent to a measure of the star-formation efficiency as a function of cloud mass for the local sample. It is also equivalent to the measure of the star-formation rate (SFR) per unit cloud mass as a function of the cloud mass. The plot shows large variations in the efficiency and, thus, the SFR per unit mass for the local cloud sample. Taken from Lada, Lombardi & Alves (2010); reproduced by permission of the AAS.

Recent studies have begun to probe the form of the star-formation relations on scales of clouds and clumps. Using the YSO star-counting method to get $\dot{M}_*$ and extinction maps to get mean mass surface density of individual, nearby clouds, Evans et al. (2009) found that the local clouds all lay well above Kennicutt's (1998b) relation. Taken in aggregate, using the mean Σ_{gas}, they lay a factor of 20 above the Kennicutt (1998a) relation and even farther above the relation of Bigiel et al. (2008).

Subsequent studies show evidence for both a surface-density threshold for star-forming clumps and a $\Sigma(\mathrm{SFR}) - \Sigma_{mol}$ relation in this high-density subcloud regime. Lada, Lombardi & Alves (2010) found a surface-density threshold for efficient star formation in nearby clouds: The SFR per cloud mass scatters widely (**Figure 13**) but is linearly proportional to the cloud mass above a surface-density contour of 116 ± 28 $M_\odot$ pc^{-2} (**Figure 14**). The coefficient also agrees well with the dense-gas relations of Gao & Solomon (2004). Heiderman et al. (2010) studied the behavior of Σ(SFR) on smaller scales using contours of extinction. They limited the YSOs to Class I and Flat SED objects to ensure that they were still closely related to their surrounding gas and found a steep increase in Σ(SFR) with increasing Σ_{gas} up to approximately 130 $M_\odot$ pc^{-2}, above which a turnover was suggested. By adding the dense-clumps data from Wu et al. (2010a), they identified a turnover at 129 ± 14 $M_\odot$ pc^{-2}, where the Σ(SFR) began to match the dense-gas relation but was far above Kennicutt's (1998b) relation for total gas (**Figure 15**). The agreement between these two independent approaches is encouraging, suggesting that a contour of approximately 125 $M_\odot$ pc^{-2} is a reasonable defining level for a star-forming clump (Section 2.2). Other studies have found similar thresholds for efficient star formation or the presence of dense cores (Lada 1992; Li, Evans & Lada 1997; Onishi et al. 1998; Johnstone, Di Francesco & Kirk 2004; Enoch et al. 2007; André et al. 2010). Theoretical explanations for such thresholds can be found by considering magnetic support (Mouschovias & Spitzer 1976) or regulation by photoionization

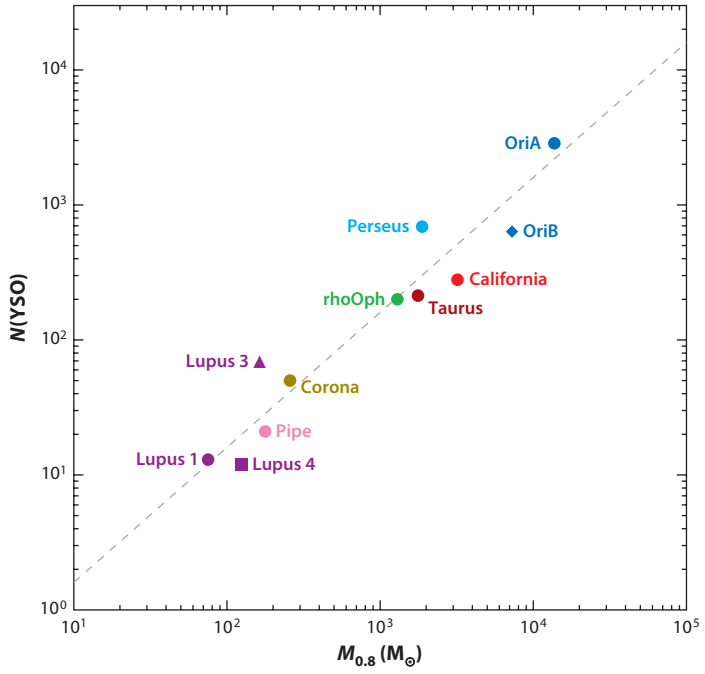

Figure 14

Relation between the total number of young stellar objects [*N*(YSOs)], the number of YSOs in a cloud, and $M_{0.8}$, the integrated cloud mass above the threshold extinction of $A_{K0} = 0.8$ mag. For these clouds, the star-formation rate (SFR) is directly proportional to *N*(YSOs). Thus, this graph also represents the relation between the SFR and the mass of highly extincted and dense cloud material. A line representing the best-fit linear relation is also plotted for comparison. There appears to be a strong linear correlation between *N*(YSOs) (or SFR) and $M_{0.8}$, the cloud mass at high extinction and density. Taken from Lada, Lombardi & Alves (2010); reproduced by permission of the AAS.

(McKee 1989). Alternatively, this threshold may simply correspond to the part of the cloud that is gravitationally bound (cf. Section 4.3).

The SFR density is even higher within clumps. Gutermuth et al. (2011) found a continuation of the steep increase in Σ(SFR) to higher Σ_{gas} in a study including embedded clusters. They found that $\Sigma(\mathrm{SFR}) \propto \Sigma_{gas}^2$ up to several 100 $M_\odot$ pc^{-2}, with no evidence of a threshold. Near the centers of some centrally condensed clumps, Σ_{gas} reaches 1 g cm^{-2}, or approximately 4800 $M_\odot$ pc^{-2} (Wu et al. 2010a), a threshold for the formation of massive stars suggested by theoretical analysis (Krumholz & McKee 2008).

Other studies have identified possible scaling relations in which SFR surface densities are not simply proportional to surface densities of dense gas. One analysis found that clouds forming stars with masses over 10 $M_\odot$ satisfied the following relation: $m(r) \geq 870\ M_\odot (r/pc)^{1.33}$ (Kauffmann & Pillai 2010, Kauffmann et al. 2010), where $m(r)$ is the enclosed mass as a function of radius. This is essentially a criterion they call compactness; it can be thought of as requiring a central condensation, with $\rho(r) \propto r^p$ with $p \geq 1.67$.

Dunham et al. (2011b) compared a subset of clumps in the Bolocam Galactic Plane Survey (BGPS) catalog (Rosolowsky et al. 2010, Aguirre et al. 2011) with kinematic distances to the Heiderman-Lada criterion for efficient star formation and to the Kauffman-Pillai criterion for massive star formation. Approximately half the clumps satisfy both criteria. Interestingly, Dunham

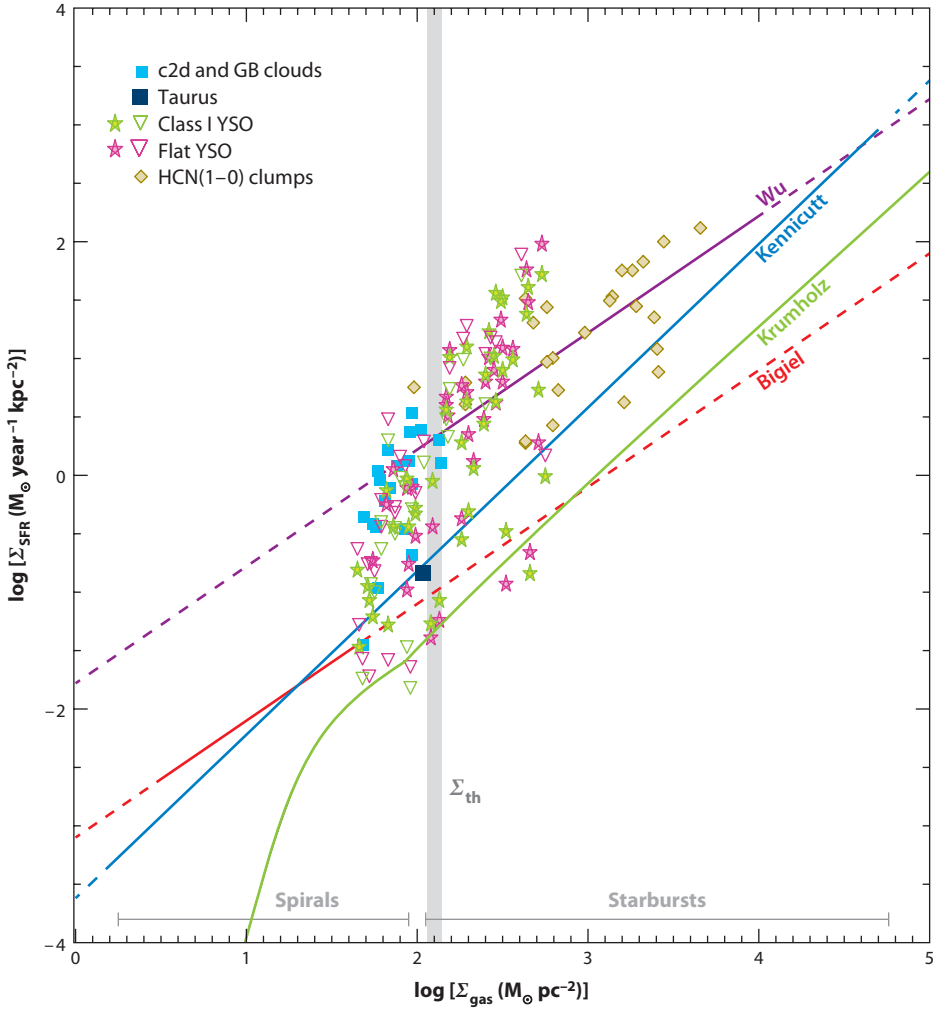

Figure 15

Comparison of Galactic total c2d and Gould Belt (GB) clouds, young stellar objects (YSOs), and massive clumps to extragalactic relations. Star-formation rate (SFR) and gas surfaces densities for the total c2d and GB clouds (*light blue squares*), the Taurus cloud (*black square*), c2d Class I and Flat spectral energy distribution YSOs (*green and magenta stars* or *inverted triangles* for upper limits), and $L_{IR} > 10^{4.5}$ $L_\odot$ massive clumps (*dark yellow diamonds*) are shown. The range of gas surface densities for the spirals and circumnuclear starburst galaxies in the Kennicutt (1998b) sample is denoted by the gray horizontal lines. The gray-shaded region denotes the range for $\Sigma_{th} = 129 \pm 14$ $M_\odot$ pc^{-2}. Taken from Heiderman et al. (2010); reproduced by permission of the AAS.

et al. (2011a) found that approximately half the BGPS sample contained at least one mid-IR source from the GLIMPSE survey. For the clumps most securely identified with star formation, 70% to 80% satisfy the Heiderman-Lada or Kauffman-Pillai criteria.

All these studies consistently show that Σ(SFR), especially for massive stars, is strongly localized to dense gas and is much higher (for $\Sigma_{gas} > 100$ $M_\odot$ pc^{-2}) than in the extragalactic Schmidt relations (Kennicutt 1998b, Bigiel et al. 2008). This offset between the extragalactic and

dense-clump Schmidt laws can be straightforwardly understood as reflecting the mass fraction (or surface-filling factor) of dense clumps in the star-forming ISM. If most or all star formation takes place in dense clumps, but the clumps contain only a small fraction of the total molecular gas, we would expect the characteristic star formation t_{dep} measured for clumps to be proportionally shorter than t_{dep} of the total cloud mass and the efficiency (ϵ) to be higher. Using a threshold of $C^{18}O$ emission to define clumps, Higuchi et al. (2009) found that the star-formation efficiency (ϵ) in clumps varies widely but averages 10%, approximately 4 times that in clouds as a whole (Section 4.1). If this interpretation is correct, we would also expect the relations between SFR and dense gas mass for galaxies (Gao-Solomon relation) to be similar for galaxies and the clumps, and they indeed appear to be roughly consistent (J. Wu et al. 2005).

This conclusion is subject to some caveats, however. Various authors (Krumholz & Thompson 2007, Narayanan et al. 2008, Juneau et al. 2009) have pointed out that lines like those of HCN $J = 1 \rightarrow 0$ are not thermalized at lower densities, so they can result in a linear relation even if the underlying star-formation relation is a local version of a nonlinear KS law that extends to much lower densities. The SFR versus dense-gas relation is based on a correlation between total FIR and HCN luminosities, and L_{FIR} is likely to underestimate the SFR in young clusters (Krumholz & Thompson 2007; Urban, Martel & Evans 2010; Gutermuth et al. 2011), perhaps by up to factors of 3–30. However, Lada et al. (2012) found a similar continuity between the Gao-Solomon starbursts and SFRs measured by counting YSOs in gas above a threshold surface density.

7. TOWARD A SYNTHESIS

7.1. Summary: Clues from Observations

Before we embark on an interpretation of the observed star-formation law, it is useful to collect the main conclusions that can be drawn from the observations of star formation both outside and inside the Galaxy. Beginning on the galactic scale (>1 kpc), we can identify at least two and probably three distinct star-formation regimes (**Table 3**). Whole galaxies may lie in one of these regimes, but a single galaxy may include two or three regimes.

Table 3 Star-formation regimes[a]

Name	Σ_{gas} ($M_\odot$ pc^{-2})	Gas properties	Star formation	Examples
Low Density	<10	Mostly atomic	Low, sparse	Outer disks Early-type galaxies LSB galaxies Dwarf galaxies Solar Neighborhood in MW
Intermediate Density	$10-\Sigma_{dense}$	Atomic → molecular	Moderate	Normal disks Inner MW Molecular clouds
High Density	Σ_{dense}	Molecular → dense	High, concentrated	Some nuclear regions Starbursts Mergers Clumps and cores

[a]The dividing line between intermediate- and high-density regimes (Σ_{dense}) ranges from 100 to 300 $M_\odot$ pc^{-2}.
Abbreviations: LSB, low surface brightness; MW, Milky Way.

7.1.1. The low-density regime. The lowest-density regime (sometimes referred to as the subthreshold regime) is most readily observed in the outer disks of spiral galaxies, but it can also be found in the interarm regions of some spiral galaxies and throughout the disks of some gas-poor galaxies. The Solar Neighborhood lies near the upper end of this low-density regime and the outer disk of the MW is clearly in this regime (Section 5.1).

The cold gas in these regions is predominantly atomic, though local concentrations of molecular gas are often found. Star formation is highly dispersed, with young clusters and HII regions observed only in regions of unusually high cold-gas densities. The global "efficiency" of star formation, ϵ' (defined in Section 1.2), or $\Sigma(\mathrm{SFR})/\Sigma_{\mathrm{gas}}$, is very low and is uncorrelated with Σ_{gas}. The steep, nearly vertical "Schmidt" relation seen in this regime (e.g., **Figure 12**) mainly reflects lack of correlation over a region where the SFR has a much larger dynamic range than the local gas density; any apparent correlation is not physical. Recent stacking analysis of CO maps and studies of the outer MW suggest, however, that there may be a strong correlation with molecular surface density (Section 6) (Schruba et al. 2011).

7.1.2. The intermediate-density regime. The intermediate-density regime is roughly characterized by average gas surface densities of $\Sigma_{\mathrm{gas}} > 10\ \mathrm{M}_{\odot}\ \mathrm{pc}^{-2}$, corresponding roughly to $N(\mathrm{H}) \sim 10^{21}\ \mathrm{cm}^{-2}$, or $A_V \sim 1$ mag, for solar metallicity. The upper limit to this regime is approximately $\Sigma_{\mathrm{gas}} \sim 100$–$300\ \mathrm{M}_{\odot}\ \mathrm{pc}^{-2}$, as discussed in the next section. The intermediate regime applies within the main optical radii (R_{25}) of most gas-rich, late-type spiral and irregular galaxies. The Galactic-ring region of the MW lies at the low end of this regime, whereas the CMZ may lie near the high end (Section 5.1).

The transition from the low-density regime roughly corresponds to the transition between HI-dominated and H_2-dominated ISMs. Above $\Sigma_{\mathrm{gas}} = 10\ \mathrm{M}_{\odot}\ \mathrm{pc}^{-2}$, both the phase balance of the ISM and the form of the star-formation law begin to change. The intermediate range features an increasing filling factor of molecular clouds, and star formation becomes more pervasive. The SFR surface density is strongly and tightly correlated with the cold-gas surface density, whether expressed in terms of the total (atomic plus molecular) or only the molecular surface density. In most massive spiral galaxies, the cold gas in this regime is molecular dominated. In low-mass and irregular galaxies, atomic gas can dominate, though this is somewhat dependent on the value of X(CO) that is assumed. The characteristic depletion time (t_{dep}) (Section 1.2) for the interstellar gas is 1–2 Gyr (e.g., Bigiel et al. 2011).

When expressed in terms of ϵ' (Section 1.2), the SFR per unit total gas mass, nearly all studies suggest that ϵ' increases with gas surface density, with an exponent of 0.2–0.5 (the Schmidt law exponent $N - 1$). When measured against molecular mass (or surface density), some studies suggest ϵ' is constant, but others suggest ϵ' is increasing systematically with surface density.

7.1.3. The high-density regime. The two regimes discussed above were able to reproduce all the early observations of the large-scale star-formation law by Kennicutt (1989, 1998b) and Martin & Kennicutt (2001). However a number of recent observations suggest the presence of a third regime (and second transition) around $\Sigma_{\mathrm{gas}} > 100$–$300\ \mathrm{M}_{\odot}\ \mathrm{pc}^{-2}$, into what may be called the high-density, or starburst, regime. Around this value of Σ_{gas}, the interpretation of I(CO) is likely to change (Section 2.4), and studies of local MW clouds indicate that a similar Σ_{gas} value may correspond to the theoretical notion of a cluster-forming clump, in which the SFR is much higher than in the rest of the cloud (Section 6.4). In the most extreme starburst galaxy environments, if standard values of X(CO) are used, the average surface densities of gas (virtually all molecular) reach 1,000 to $10^4\ \mathrm{M}_{\odot}\ \mathrm{pc}^{-2}$, and the volume-filling factor of clumps could reach unity (Wu et al. 2009). Although the interpretation of molecular emission in these conditions warrants skepticism

(Section 2.4) (Garcia-Burillo et al. 2011), the highest inferred surface density also corresponds to the densest parts of cluster-forming clumps and the theoretical threshold of 1 g cm^{-2} for efficient formation of massive stars (Section 4.3).

Some recent observations strongly hint at the existence of such a transition. As discussed in Section 6, luminous and ultraluminous starburst galaxies (and high-redshift SMGs) have characteristic ratios of $L_{IR}/L(CO)$ that are as much as 1–2 orders of magnitude higher than in normal galaxies, implying that at some point the SFR per molecular mass must increase dramatically. This could be explained by a break in the slope of the Schmidt law at high densities, a continuous nonlinear Schmidt-law slope extending from the intermediate- to high-density regimes, or a second mode of star formation in extreme starbursts with much higher "efficiency" (ϵ'). As discussed in Section 6.3, the constancy of the molecular ϵ' at intermediate surface densities is uncertain. Observations of CO in high-redshift galaxies have been interpreted in terms of just such a bimodal Schmidt law (Daddi et al. 2010, Genzel et al. 2010). This interpretation rests on the assumption of a bimodality in X(CO) (Section 6.1), and a change in ϵ' that follows these changes in X(CO); this is not entirely implausible because the same physical changes in the ISM environment in the densest starbursts could affect both the CO conversion factor and ϵ' if an increasing fraction of the gas is in dense clumps.

Both a Galactic value of X(CO) in the starbursts and a much lower value have their discomforting aspects. Applying a Galactic conversion factor produces total molecular masses that often exceed dynamical mass limits for the regions, whereas adopting values of X(CO) that are factors of several lower than the usually adopted values produces gas consumption times as short as 10 Myr (Daddi et al. 2010, Genzel et al. 2010), with implications for the triggering and duty cycles of these massive starbursts.

The relations between SFR and ISM properties summarized above strictly refer to the correlations with the total cold-gas surface density or in some cases the total HI and total H_2 densities; these are the relations of most interest for applications to galaxy modeling and cosmology. However, the observational picture is quite different when we correlate the SFR with the supply of dense gas, as traced by HCN $J = 1 \rightarrow 0$ and other dense-clump tracers. Here there seems to be a single linear relation that extends across all of the SFR regimes described above, including the star-forming clouds in the MW (Gao & Solomon 2004, J. Wu et al. 2005, Gao et al. 2007, Lada et al. 2012), However, there is still some evidence of bimodality even if tracers of dense gas are used (Garcia-Burillo et al. 2011), and physically based models, rather than simple conversion factors, are needed.

7.1.4. Clues from studies of molecular clouds. The biggest hurdle one confronts when attempting to interpret these observations of galaxies is the severe influences of spatial averaging, both across the sky and along the line of sight. The star-formation law relates surface densities of young stars and interstellar gas—already smoothed along the line of sight—averaged over linear dimensions ranging from order 100 pc to 50 kpc. These are 2–4 orders of magnitude larger than the sizes of the dense-clump regions in which most stars form and 4–8 orders of magnitude larger in terms of the surface areas being measured. This difference in scales means that the "surface densities" measured in extragalactic studies are really characterizing the filling factors of gas clumps and star-forming regions, rather than any measure of physical densities. Understanding how this "active component" of the star-forming ISM works is essential even to an empirical understanding of large-scale star formation, and even more so to understanding its underlying physics. Detailed studies within the MW provide a way to "zoom in" farther than is possible for other galaxies.

A common observed feature across all the density regimes observed in galaxies is that star formation takes place in molecular clouds. In the lowest-density regimes, clouds are rare and

widely separated, but within individual molecular clouds in the MW, which can be probed in detail, star formation seems to be indistinguishable from that in regions of somewhat higher average surface density (Section 5.1).

These observations also reveal that nearly all star formation within molecular clouds is highly localized, taking place in clumps, roughly defined by $\Sigma_{mol} > 125\ M_\odot\ pc^{-2}$, or $n > 10^4\ cm^{-3}$ (Section 6.4). The clumps host young stars, YSOs, and prestellar cores, the sites of individual star formation. This scale is as close to a deterministic environment for star formation as can be found. Once a prestellar core reaches substantial central condensation, approximately one-third of its mass will subsequently turn into young stars within a few million years (Alves, Lombardi & Lada 2007; Enoch et al. 2008). The relatively low global efficiencies (both ϵ and ϵ') within GMCs are largely a reflection of the low-mass fraction in clumps and cores (Section 4.1). The SFR surface density in the clumps is 20–40 times that predicted for the mass surface density from the extragalactic Schmidt relation (Section 6.4); this can also be largely understood as reflecting the low fraction of the molecular gas mass that resides in clumps and cores.

One may be tempted to identify the dense clumps within molecular clouds as a possible fourth density regime, in addition to the three regimes already discussed from observations of galaxies. However, this would be very misleading because so far as is currently known, the formation of most stars in dense clumps is a common feature of star formation across all the ISM environments in galaxies, extending from low-density subthreshold disks to the most intense starbursts. The dense clump may well be the fundamental unit of massive, clustered star formation (J. Wu et al. 2005). If this picture is correct, then the three regimes identified in galaxies and the order-of-magnitude increases in the conversion rate from gas to star formation across them must reflect changes in the fraction of the ISM that is converted to dense clumps, approaching 100% in the densest and most intense starbursts.

7.2. Some Speculations

The observations summarized in this review have stimulated a rich literature of theoretical ideas, models, and simulations aimed at explaining the observed star-formation relations and constructing a coherent picture of galactic-scale star formation. Unfortunately we have neither the space nor the expertise to review that large body of theoretical work here. A review of many of the theoretical ideas can be found in McKee & Ostriker (2007), and an informative summary of the main models in the literature up to 2008 can be found in Leroy et al. (2008). Here we offer some speculations aimed toward explaining the observations, connecting the extragalactic and MW studies, and identifying directions for future work. Many of these speculations reflect ideas being discussed in the literature, and we make no claims for originality in the underlying concepts.

As mentioned in the introduction, the formation of stars represents the end point of a chain of physical processes that begins with cooling and infall of gas from the intergalactic medium onto disks, followed by the formation of a cool atomic phase, contraction to gravitationally bound clouds, the formation of molecules and molecular clouds, the formation of dense clumps within those molecular clouds, and ultimately the formation of prestellar cores, stars, and star clusters. Although the beginning and end points of this process are relatively clear, the sequence of intermediate steps, in particular the respective roles of forming cool atomic gas, molecular gas, and bound clouds, is unclear, and it is possible that different processes dominate in different galactic environments. By the same token, a variety of astrophysical timescales may be relevant, e.g., the free-fall time of the gas within clouds, the crossing time for a cloud, the free-fall time of the gas layer, or the dynamical timescales for the disc and spiral-arm passages. Any of these timescales may be invoked for setting the timescale for star formation and the form of the star-formation law. However, one

can construct two scenarios to explain the observations outlined in Section 7.1, which illustrate the boundaries of fully locally driven versus globally driven approaches. In some sense, these approaches are complementary, but they need to be brought together.

The first approach, which could be called a bottom-up picture, assumes that star formation is controlled locally within molecular clouds (e.g., Krumholz & McKee 2005), building on what we observe in well-studied local regions of star formation. In this picture, one can identify three distinct regimes (Section 7.1) and associate the transitions between them to the crossing of two physically significant thresholds, i.e., the threshold for conversion of atomic to molecular gas and the threshold for efficient star formation in a molecular cloud, identified with the theoretical notion of a clump (Section 2.2). In the purest form of this picture, the SFR is driven completely by the amount and structure of the molecular gas. Current evidence from studies of nearby clouds indicates that the SFR scales linearly with the amount of dense gas in clumps (Lada, Lombardi & Alves 2010), and this relation extends to starburst galaxies if the HCN emission is used as a proxy for the dense gas (J. Wu et al. 2005, Lada et al. 2012). In this picture, the nonlinear slope ($N \sim 1.5$) of the global Schmidt relation would arise from either a decrease in the characteristic timescale (Krumholz, Dekel & McKee 2012) or by an increase in the fraction of gas above the clump threshold ($f_{\rm dense}$), from its typical value in local clouds [$f_{\rm dense} \sim 0.1$ (Lada et al. 2012)] with $f_{\rm dense} \propto \Sigma_{\rm gas}^{0.5}$.

The second approach, which we could call a top-down picture, assumes that star formation is largely controlled by global dynamical phenomena, such as disk instabilities (e.g., Silk 1997), and the dynamical timescales in the parent galaxy. In this picture, the transition between the low-density and higher-density SFR regimes is mainly driven by gravitational instabilities in the disk rather than by cooling or molecular-formation thresholds, and the nonlinear increase in the SFR relative to gas density above this threshold reflects shorter self-gravitational timescales at higher density or the shorter dynamical timescales. In this approach, there is no particular physical distinction between the intermediate-density and high-density regimes; in principle, the same dynamical processes can regulate the SFR continuously across this wide surface-density regime. Likewise, the total surface density of gas, whether atomic or molecular, is what drives the SFR. The asymptotic form of this picture is a self-regulated star-formation model: The disk adjusts to an equilibrium in which feedback from massive star formation acts to balance the hydrostatic pressure of the disk or to produce an equilibrium porosity of the ISM (e.g., Cox 1981; Dopita 1985; Silk 1997; Ostriker, McKee & Leroy 2010).

A comparison of these pictures to the observations shows that each has its particular set of attractions and challenges. The bottom-up picture has the attraction of simplicity, associating nearly all the relevant SFR physics with the formation of molecular-gas and molecular-cloud clumps. It naturally fits with a wide range of observations including the tight correlation of the SFR and molecular-gas surface densities (e.g., Schruba et al. 2011 and references therein), the concentration of star formation within clouds in regions of dense gas (Section 4), and the observation of a linear relation between the dense gas traced by HCN emission and the total SFR in galaxies (Section 6). If the resolved star-formation relation at intermediate surface densities is linear (Section 6) (Bigiel et al. 2008), $f_{\rm dense}$ would be constant in that regime and increase monotonically with $\Sigma_{\rm gas}$ in the higher-density starburst regime, with the transition occurring where $\Sigma_{\rm gas}$ derived from CO is similar to the threshold for dense gas. This picture does not explain why a particular galaxy or part of a galaxy lies in one of these regimes, a question perhaps best answered by the top-down picture.

Aspects of the top-down picture date back to early dynamical models of the ISM and the first observations of star-formation thresholds in disks (e.g., Quirk & Tinsley 1973, Larson 1987, Zasov & Stmakov 1988, Kennicutt 1989, Elmegreen 1991, Silk 1997). There is some observational evidence for associating the observed low-density thresholds in disks with gravitational instabilities in the

disk (e.g., *Q* instabilities), rather than with atomic- or molecular-phase transitions (e.g., Kennicutt 1989, Martin & Kennicutt 2001), but recent observations and theoretical analyses have raised questions about this interpretation (e.g., Schaye 2004, Leroy et al. 2008). At higher surface densities, the global relation between Σ(SFR) and the ratio of gas density to local dynamical time (Σ_{gas}/τ_{dyn}) shows a correlation that is nearly as tight as the conventional Schmidt law (Kennicutt 1998b); it also removes the double sequence of disks and starbursts that results if X(CO) is systematically lower in the starbursts (Section 6) (Daddi et al. 2010, Genzel et al. 2010). In this picture, the higher SFR for a given gas surface density in mergers is caused by the compaction of the gas and the resulting shorter rotation period. However, the efficiency per orbital period is not clearly explained in this picture. Theories of feedback-regulated star formation show promise in explaining the low efficiency per orbit in normal galaxies (Kim, Kim & Ostriker 2011), and they may also explain the less effective role of negative feedback in merger-driven starbursts (e.g., Ostriker & Shetty 2011). This model does not extend to cloud-level star formation. If feedback from massive stars is fundamental, the similarity between the efficiency in local clouds forming only low-mass stars and regions with strong feedback from massive stars (cf. Evans et al. 2009, Murray 2011) remains a mystery.

Both of these scenarios can claim some successes, but neither provides a complete explanation that extends over all scales and environments. As but one example, the large changes in the present-day SFRs and past star-formation histories of galaxies as functions of galaxy mass and type may well be dictated mainly by external influences such as the accretion history of cold gas from the cosmic web and intergalactic medium. Neither the bottom-up nor top-down pictures as articulated above incorporate these important physical processes. On smaller scales, a complete model for star formation may combine features of both scenarios. The dynamical picture is quite attractive on the scales of galaxies, and extending it to smaller scales would be interesting. In doing so, the question of what to use for τ_{dyn} arises. The galaxy rotation period cannot control star formation in individual clouds, so a more local dynamical time is needed. One option is the cloud or clump crossing time (essentially the size over the velocity dispersion) (Elmegreen 2000), which may be particularly relevant in regions of triggered star formation. Because clumps are the star-forming units, their crossing times may be the more relevant quantities.

A popular option is the free-fall time (e.g., Krumholz & McKee 2005). Because $t_{ff} \propto \rho^{-0.5}$, a volumetric star-formation law, $\rho_{SFR} \propto \rho/t_{ff} \propto \rho^{1.5}$, where ρ is the gas density, is a tempting rule. With this rule, the roughly 1.5 power of the KS relation appears to be explained if we ignore the difference between volume and surface density. Indeed, Krumholz, Dekel & McKee (2012) argue that such a volumetric law reproduces observations from the scale of nearby clouds to starburst galaxies. However, the definition of t_{ff} changes for compact starbursts (see equation 9 in their paper), essentially at the boundary between the intermediate- and high-density regimes discussed in Section 7.1. Including the atomic-molecular threshold, as treated in Krumholz, McKee & Tumlinson (2009), clarifies that this "scale-free" picture implicitly recognizes the same three regimes discussed in Section 7.1.

Theories that rely on t_{ff} face two problems. First, no evidence has been found in well-studied molecular clouds for collapse at t_{ff} (Section 4.3) (e.g., Zuckerman & Evans 1974). To match observations, an "efficiency" of approximately 0.01 must be inserted. Why the star-formation density should remain proportional to t_{ff}, while being slowed by a factor of 100, is a challenging theoretical question. Studies of the role of turbulence show some promise in explaining this paradox (Krumholz & McKee 2005, Hennebelle & Chabrier 2011), and magnetic fields may play a role.

The second problem is how to calculate a relevant t_{ff} in a cloud, much less a galaxy, with variations in ρ by many orders of magnitude and much of the gas unlikely to be gravitationally bound. For example, Krumholz, Dekel & McKee (2012) calculate t_{ff} from the mean density of the whole cloud ($t_{ff} \propto 1/\langle\rho\rangle$). A computation of $\langle t_{ff}\rangle$ from $\langle 1/\rho\rangle$ would emphasize the densest

gas, where star formation is observed to occur. In a model that accounts for this, Hennebelle & Chabrier (2011) reproduce at some level the observations of surface-density thresholds for efficient star formation observed in nearby clouds (Heiderman et al. 2010; Lada, Lombardi & Alves 2010). An alternative to the models involving $t_{\rm ff}$ that instead emphasizes the critical role of the dense-gas threshold can be found in Lada et al. (2012). Because both models claim to apply to cloud-level star formation, observations of MW clouds should be able to test them.

7.3. Future Prospects

We hope that this review has conveyed the tremendous progress over the past decade in understanding the systematic behavior of star formation, both in the MW and in other galaxies. As often happens when major observational advances are made, observational pictures that once seemed simple and certain have proven to be more complex and uncertain. We have attempted to inject a dose of skepticism about some well-accepted truisms and to highlight important questions where even the observations do not present a completely consistent picture.

As we return to the key questions outstanding in this subject (see the sidebar, Questions), a few clear themes emerge, many of which lie at the cusp between MW and extragalactic observations and between theory and simulation on the subcloud scale, on the one hand, and the galactic and cosmological scales, on the other. The recent observations within the MW of a near-universal association of stars with dense molecular clumps (Section 6.4) offer the potential key of a fundamental subunit of high-efficiency star formation in all galactic environments, from the low-density and quiescent environments of outer disks and dwarf galaxies to the most intense starbursts. However, this hypothesis needs to be validated observationally in a wider range of environments. Restated from another perspective, we need much better information on the structure (physical structure, substructure) and dynamics of star-forming clouds across the full range of star-forming environments found in galaxies today.

Fortunately, we are on the brink of major progress on multiple fronts. One approach is to assemble more complete and "zoomed-out" views of the MW, while preserving the unparalleled spatial resolution and sensitivity of MW observations to characterize fully the statistical trends in cloud structure, kinematics, mass spectra, and associated star formation for complete, unbiased, and physically diverse samples. In the near term, *Herschel* surveys will deliver images of nearby clouds, the plane of the MW, and many galaxies in bands from 60 to 500 μm. When the MW plane data are combined with higher-resolution surveys of the MW at 0.87 to 1.1 mm from ground-based telescopes, spectroscopic follow-up, and improved distances from ongoing VLBA studies, we will have a much improved and nuanced picture of the gas in the MW, which can then provide a more useful template for understanding similar galaxies. Recent surveys have doubled the number of known HII regions in the MW (Anderson et al. 2011), allowing for study of a wider range of star-formation outcomes. Tests of the limitations on SFR tracers used in extragalactic work will be possible, as will comparisons to KS relations on a variety of spatial scales. The Magellanic Clouds also offer great potential for extending this approach to two sets of environments with different metallicities, ISM environments, and star-formation properties (exploiting, for example, the 30 Doradus region).

This expanded information from MW surveys will then need to be combined with more sensitive and "zoomed-in" observations of other galaxies. For such studies, the weakest link currently is our limited knowledge of the molecular gas. We can trace HI and SFRs to much lower levels than we can detect CO, even with stacked CO maps. When fully commissioned, ALMA will have a best resolution of approximately 13 mas at 300 GHz (0.5 pc at the distance of M51) and approximately 8 times the total collecting area of any existing millimeter facility, allowing us to trace molecular emission to deeper levels and/or to obtain resolution at least 10 times better than the best current

studies. It may be possible to study dense structures within molecular clouds in other galaxies, enabling comparison to dense clumps in the MW clouds. To be most effective, these programs will need to expand beyond the typical surveys in one or two CO rotational transitions to include the high-density molecular tracers and, ideally, a ladder of tracers with increasing excitation and/or critical density. Continuum observations will gain even more because of large bandwidths and atmospheric stability. Maps of millimeter-wave dust emission may become the preferred method to trace the gas in other galaxies, as they are already becoming in the MW, bypassing the issues of X(CO). Observations of radio recombination lines may also provide alternative tracers of SFR in highly obscured regions. It is difficult to exaggerate the potential transformational power of ALMA for this subject.

For molecular line observations of nearby galaxies, large single dishes (the Nobeyama 45-m, the IRAM 30-m, and the future CCAT), along with the smaller millimeter arrays, IRAM PdB and CARMA, will provide complementary characterization of the molecular and dense gas on larger scales than can be efficiently surveyed with ALMA. A substantial expansion of the IRAM interferometer (NOEMA) will provide complementary advances in sensitivity in the Northern Hemisphere. This subject will also advance with a substantial expansion of HI mapping (by e.g., the EVLA) to expand the range of environments probed and, ideally, to attain spatial resolutions comparable to the rapidly improving molecular line observations. Although it is likely that star formation on the local scale concentrates in molecular-dominated regions, the formation of this molecular gas from atomic gas remains a critical (and possibly controlling) step in the entire chain that leads from gas to stars.

Future opportunities for improving our measurements of SFRs in galaxies also await, though the truly transformational phase of that subject may already be passing with the end of the ISO, *Spitzer*, GALEX, and *Herschel* eras. HST continues to break new ground, especially in direct mapping of young stars and their ages via resolved CMDs. *Herschel* surveys of nearby galaxies will provide far-IR data, complementary to the other wavelength regions that trace star formation (Section 3), and multiband imaging with the EVLA will allow better separation of nonthermal from free-free continuum emission, which directly traces the ionization rate and massive SFR. SOFIA offers the opportunity to map the brightest regions of star formation with higher spatial and spectral resolution than provided by *Spitzer*. Further into the future, major potential lies with JWST, which will vastly improve our capabilities for tracing star formation via IR radiation, both on smaller scales in nearby galaxies and in very distant galaxies. SPICA may provide complementary capability at longer wavelengths. As highlighted in the sidebar, Questions, key unknowns in this subject include robust constraints on the ages and lifetimes of star-forming clouds; observations of resolved star clusters, both in the MW and nearby galaxies, offer potential for considerable inroads to this problem.

A number of the questions we have listed can also be attacked with ground-based optical/IR observations. As discussed in Section 3.9, despite the current availability of spatially resolved multiwavelength observations of nearby galaxies, we still do not have an absolutely reliable way to measure dust-corrected SFRs, especially from short-lived tracers that are critical for exploring the local Schmidt law. For observations of normal galaxies where local attenuations are modest, integral-field mapping of galaxies offers the means to produce high-quality Hα maps corrected for dust using the Balmer decrement (e.g., Blanc et al. 2009, 2010; Sánchez et al. 2012). A gold standard for such measurements is also available in the hydrogen recombination lines of the Paschen and Brackett series in the near-IR. The emissivities of these lines are directly related to ionizing luminosities in the same way as are the more widely applied Balmer lines (albeit with somewhat stronger density and temperature dependences), and these lines suffer much lower dust attenuation (readily calibrated by comparing with Hα or other shorter wavelength lines). These lines are much

fainter, however, and are subject to strong interference from telluric OH emission (and thermal emission at longer wavelengths). Continuing advances in near-IR detectors have now brought many of these lines into the accessible range, and soon we should begin to see large-scale surveys that provide high-resolution emission maps and robust SFR maps, at least on spatial scales larger than individual HII regions. These maps, in turn, can be used to test and, we hope, recalibrate other dust-free tracers such as combinations of IR dust emission with UV and optical emission-line maps. Looking further ahead, spectral imaging in the near-IR (and with Hα in the visible) with massively parallel integral-field spectrometers will provide more precise and full views of star formation.

The current, pioneering studies of star formation at $z \sim 1$–3 will become much easier with new instrumentation. Advances in submillimeter-array technology (e.g., SCUBA-2 on the JCMT) and larger dishes at very high altitude, such as CCAT, will allow deep and wide searches for dust-continuum emission from distant galaxies. Many of the biases in current samples can be alleviated, and a more complete picture of star formation through cosmic time can be constructed. Huge surveys of Lyα-emitting galaxies will be undertaken to constrain dark energy, providing as a by-product nearly 1 million star-forming galaxies at $1.9 < z < 3.5$ and a large number of [OII]-emitting galaxies for $z < 0.5$ (e.g., Hill et al. 2008).

As the theoretical side of this subject lies outside the scope of this review, we comment only briefly on this area. Numerical simulations are poised to make major contributions to this subject over the next several years. Simulations with higher resolution and more sophisticated treatments of the heating, cooling, phase balance, and feedback are providing deeper insights into the physical nature of the star-formation scaling laws and thresholds and the life cycles of molecular clouds (e.g., Dobbs 2008, Robertson & Kravtsov 2008, Tasker & Tan 2009, Dobbs & Pringle 2010, Brooks et al. 2011, Tasker 2011). Inclusion of realistic stellar feedback may obviate the need for artificial constraints on efficiency (e.g., Hopkins, Quataert & Murray 2011).

Analytical models that incorporate the wide range of relevant physical processes on the scales of both molecular clouds and galactic disks are also leading to deeper insights into the triggering and regulation of star formation on the galactic scale (e.g., Ostriker, McKee & Leroy 2010; also see papers cited in Section 7.2). Exploring different prescriptions for cloud-scale star formation in galaxy evolution models will illuminate the effects of the cloud-scale prescription on galaxy-scale evolution. At the "microscale" of molecular clouds, inclusion of radiative and mechanical feedback from star formation is producing more realistic models, and perhaps, the relative importance of feeding from the local core and from the greater clump may be quantified (e.g., references in Section 4.3).

We conclude with a hope and a prediction. From the start, this review was designed to exchange ideas between those studying star formation in the MW and those studying star formation in other galaxies. We have benefited immensely from this exchange, and we hope for more of this cross talk between our two communities: People studying star formation within the MW can put their results in a larger context; those studying other galaxies can appreciate that our home galaxy offers unique advantages for understanding galaxies. A common theme across both arenas has been the rapid pace of advancements in both observations and theory. When the next review of this subject is written, we predict that it will focus on observational tests of detailed physical theories and simulations rather than on empirical star-formation laws. We conclude with heartfelt thanks to all of those who are working toward this common goal.

DISCLOSURE STATEMENT

The authors are not aware of any affiliations, memberships, funding, or financial holding that might be perceived as affecting the objectivity of this review.

ACKNOWLEDGMENTS

We acknowledge the many people who have supplied information and preprints in advance of publication. In addition, we thank Alberto Bolatto, Leonardo Bronfman, Peter Kaberla, Jin Koda, Adam Leroy, Yancy Shirley, and Linda Tacconi for useful and stimulating discussions. Henrik Beuther, Guillermo Blanc, Daniela Calzetti, Reinhard Genzel, Rob Gutermuth, Mark Krumholz, Charles Lada, Fred Lo, Steve Longmore, Eve Ostriker, and Jim Pringle provided valuable comments on an early draft. We both express special thanks to our current and former students and postdocs, with whom we have shared countless valuable discussions. N.J.E. thanks the Institute of Astronomy, Cambridge, and the European Southern Observatory, Santiago, for hospitality during extended visits, during which much of his work on the review was done. N.J.E. also acknowledges support from the National Science Foundation grant AST-1109116 to the University of Texas at Austin.

LITERATURE CITED

Abdo AA, Ackermann M, Ajello M, Baldini L, Ballet J, et al. 2010. *Ap. J.* 710:133–49
Aguirre JE, Ginsburg AG, Dunham MK, Drosback MM, Bally J, et al. 2011. *Ap. J. Suppl.* 192:4
Allen L, Megeath ST, Gutermuth R, Myers PC, Wolk S, et al. 2007. See Reipurth, Jewitt & Keil 2007, pp. 361–76
Allers KN, Kessler-Silacci JE, Cieza LA, Jaffe DT. 2006. *Ap. J.* 644:364–77
Alonso-Herrero A, Rieke GH, Rieke MJ, Colina L, Pérez-González PG, Ryder SD. 2006. *Ap. J.* 650:835–49
Altenhoff WJ, Downes D, Goad L, Maxwell A, Rinehart R. 1970. *Astron. Astrophys. Suppl.* 1:319–55
Alves J, Lombardi M, Lada CJ. 2007. *Astron. Astrophys.* 462:L17–21
Anderson LD, Bania TM, Balser DS, Rood RT. 2011. *Ap. J. Suppl.* 194:32
André P, Men'shchikov A, Bontemps S, Könyves V, Motte F, et al. 2010. *Astron. Astrophys.* 518:L102
Andre P, Ward-Thompson D, Barsony M. 1993. *Ap. J.* 406:122–41
Arce HG, Shepherd D, Gueth F, Lee CF, Bachiller R, et al. 2007. See Reipurth, Jewitt & Keil 2007, pp. 245–60
Armus L, Charmandaris V, Bernard-Salas J, Spoon HWW, Marshall JA, et al. 2007. *Ap. J.* 656:148–67
Atek H, Kunth D, Schaerer D, Hayes M, Deharveng JM, et al. 2009. *Astron. Astrophys.* 506:L1–4
Bacmann A, André P, Puget JL, Abergel A, Bontemps S, Ward-Thompson D. 2000. *Astron. Astrophys.* 361:555–80
Baldry IK, Balogh ML, Bower RG, Glazebrook K, Nichol RC, et al. 2006. *MNRAS* 373:469–83
Baldry IK, Glazebrook K, Brinkmann J, Ivezić Ž, Lupton RH, et al. 2004. *Ap. J.* 600:681–94
Bally J, Aguirre J, Battersby C, Bradley ET, Cyganowski C, et al. 2010. *Ap. J.* 721:137–63
Baraffe I, Chabrier G. 2010. *Astron. Astrophys.* 521:A44
Baraffe I, Chabrier G, Gallardo J. 2009. *Ap. J. Lett.* 702:L27–31
Barnard EE. 1908. *Astron. Nachr.* 177:231
Bastian N, Covey KR, Meyer MR. 2010. *Annu. Rev. Astron. Astrophys.* 48:339–89
Bate MR. 2009. *MNRAS* 397:232–48
Bate MR, Bonnell IA, Bromm V. 2003. *MNRAS* 339:577–99
Bauer FE, Alexander DM, Brandt WN, Hornschemeier AE, Vignali C, et al. 2002. *Astron. J.* 124:2351–63
Begum A, Chengalur JN, Karachentsev ID, Sharina ME, Kaisin SS. 2008. *MNRAS* 386:1667–82
Bell EF. 2003. *Ap. J.* 586:794–13
Bell EF, Kennicutt RC Jr. 2001. *Ap. J.* 548:681–93
Bell EF, Papovich C, Wolf C, Le Floc'h E, Caldwell JAR, et al. 2005. *Ap. J.* 625:23–36
Beltrán MT, Brand J, Cesaroni R, Fontani F, Pezzuto S, et al. 2006. *Astron. Astrophys.* 447:221–33
Bendo GJ, Draine BT, Engelbracht CW, Helou G, Thornley MD, et al. 2008. *MNRAS* 389:629–50
Benjamin RA, Churchwell E, Babler BL, Indebetouw R, Meade MR, et al. 2005. *Ap. J. Lett.* 630:L149–52
Bergin EA, Tafalla M. 2007. *Annu. Rev. Astron. Astrophys.* 45:339–96
Beuther H, Churchwell EB, McKee CF, Tan JC. 2007a. See Reipurth, Jewitt & Keil 2007, pp. 165–80
Beuther H, Leurini S, Schilke P, Wyrowski F, Menten KM, Zhang Q. 2007b. *Astron. Astrophys.* 466:1065–76

Beuther H, Schilke P, Menten KM, Motte F, Sridharan TK, Wyrowski F. 2002. *Ap. J.* 566:945–65
Beuther H, Tackenberg J, Linz H, Henning T, Schuller F, et al. 2012. *Ap. J.* 747:A43
Bigiel F, Leroy A, Walter F, Blitz L, Brinks E, et al. 2010. *Astron. J.* 140:1194–213
Bigiel F, Leroy A, Walter F, Brinks E, de Blok WJG, et al. 2008. *Astron. J.* 136:2846–71
Bigiel F, Leroy AK, Walter F, Brinks E, de Blok WJG, et al. 2011. *Ap. J. Lett.* 730:L13
Blanc GA. 2010. In *Proc. From Stars to Galaxies: Connecting our Understanding of Star and Galaxy Formation*, 7–10 April. Gainsville: Univ. Fla.; **http://conference.astro.ufl.edu/STARSTOGALAXIES**
Blanc GA, Adams JJ, Gebhardt K, Hill GJ, Drory N, et al. 2011. *Ap. J.* 736:31
Blanc GA, Gebhardt K, Heiderman A, Evans NJ II, Jogee S, et al. 2010. In *New Horizons in Astronomy: Frank N. Bash Symposium 2009*, ed. LM Stanford, JD Green, L Hao, Y Mao, *ASP Conf.* 432:180–86. San Francisco: Astron. Soc. Pac.
Blanc GA, Heiderman A, Gebhardt K, Evans NJ II, Adams J. 2009. *Ap. J.* 704:842–62
Blanton MR, Lupton RH, Schlegel DJ, Strauss MA, Brinkmann J, et al. 2005. *Ap. J.* 631:208–30
Blitz L, Fukui Y, Kawamura A, Leroy A, Mizuno N, Rosolowsky E. 2007. See Reipurth, Jewitt & Keil 2007, pp. 81–96
Blitz L, Rosolowsky E. 2006. *Ap. J.* 650:933–44
Bloemen H. 1989. *Annu. Rev. Astron. Astrophys.* 27:469–516
Bohlin RC, Savage BD, Drake JF. 1978. *Ap. J.* 224:132–42
Boissier S, Prantzos N, Boselli A, Gavazzi G. 2003. *MNRAS* 346:1215–30
Bok BJ, Reilly EF. 1947. *Ap. J.* 105:255
Bolatto AD, Leroy AK, Jameson K, Ostriker E, Gordon K, et al. 2011. *Ap. J.* 741:12
Bonnell IA, Bate MR, Vine SG. 2003. *MNRAS* 343:413–18
Bonnell IA, Larson RB, Zinnecker H. 2007. See Reipurth, Jewitt & Keil 2007, pp. 149–64
Boquien M, Buat V, Boselli A, Baes M, Bendo GJ, et al. 2012. *Astron. Astrophys.* 539:A145
Boquien M, Calzetti D, Combes F, Henkel C, Israel F, et al. 2011. *Astron. J.* 142:111
Boselli A, Gavazzi G, Lequeux J, Pierini D. 2002. *Astron. Astrophys.* 385:454–63
Boss AP, Yorke HW. 1995. *Ap. J. Lett.* 439:L55–58
Bothwell MS, Kenicutt RC, Johnson BD, Wu Y, Lee JC, et al. 2011. *MNRAS* 415:1815–26
Bothwell MS, Kennicutt RC, Lee JC. 2009. *MNRAS* 400:154–67
Bouché N, Cresci G, Davies R, Eisenhauer F, Förster Schreiber NM, et al. 2007. *Ap. J.* 671:303–9
Bressert E, Bastian N, Gutermuth R, Megeath ST, Allen L, et al. 2010. *MNRAS* 409:L54–58
Brinchmann J, Charlot S, White SDM, Tremonti C, Kauffmann G, et al. 2004. *MNRAS* 351:1151–79
Brogan CL, Hunter TR, Cyganowski CJ, Indebetouw R, Beuther H, et al. 2009. *Ap. J.* 707:1–23
Bronfman L, Casassus S, May J, Nyman LÅ. 2000. *Astron. Astrophys.* 358:521–34
Bronfman L, Cohen RS, Alvarez H, May J, Thaddeus P. 1988. *Ap. J.* 324:248–66
Bronfman L, Nyman LA, May J. 1996. *Astron. Astrophys. Suppl.* 115:81
Brooks AM, Solomon AR, Governato F, McCleary J, MacArthur LA, et al. 2011. *Ap. J.* 728:51
Brunthaler A, Reid MJ, Menten KM, Zheng XW, Bartkiewicz A, et al. 2011. *Astron. Nachr.* 332:461
Buat V, Donas J, Milliard B, Xu C. 1999. *Astron. Astrophys.* 352:371–82
Buat V, Iglesias-Páramo J, Seibert M, Burgarella D, Charlot S, et al. 2005. *Ap. J. Lett.* 619:L51–54
Burgarella D, Buat V, Iglesias-Páramo J. 2005. *MNRAS* 360:1413–25
Burton WB. 1988. In *Galactic and Extragalactic Radio Astronomy*, ed. GL Verschuur, KI Kellermann, pp. 295–358. Berlin: Springer-Verlag
Calzetti D, Chandar R, Lee JC, Elmegreen BG, Kennicutt RC, Whitmore B. 2010a. *Ap. J. Lett.* 719:L158–61
Calzetti D, Kennicutt RC, Engelbracht CW, Leitherer C, Draine BT, et al. 2007. *Ap. J.* 666:870–95
Calzetti D, Kinney AL, Storchi-Bergmann T. 1994. *Ap. J.* 429:582–601
Calzetti D, Wu SY, Hong S, Kennicutt RC, Lee JC, et al. 2010b. *Ap. J.* 714:1256–79
Carey SJ, Noriega-Crespo A, Mizuno DR, Shenoy S, Paladini R, et al. 2009. *Publ. Astron. Soc. Pac.* 121:76–97
Casassus S, Bronfman L, May J, Nyman LÅ. 2000. *Astron. Astrophys.* 358:514–20
Cerviño M, Luridiana V, Pérez E, Vílchez JM, Valls-Gabaud D. 2003. *Astron. Astrophys.* 407:177–90
Cesaroni R, Palagi F, Felli M, Catarzi M, Comoretto G, et al. 1988. *Astron. Astrophys. Suppl.* 76:445–58
Chabrier G. 2003. *Publ. Astron. Soc. Pac.* 115:763–95
Chabrier G, Baraffe I. 2000. *Annu. Rev. Astron. Astrophys.* 38:337–77

Chandar R, Whitmore BC, Calzetti D, Di Nino D, Kennicutt RC, et al. 2011. *Ap. J.* 727:88
Chapman NL, Mundy LG, Lai SP, Evans NJ II. 2009. *Ap. J.* 690:496–511
Chapman SC, Blain AW, Smail I, Ivison RJ. 2005. *Ap. J.* 622:772–96
Charlot S, Fall SM. 2000. *Ap. J.* 539:718–31
Chen CHR, Indebetouw R, Chu YH, Gruendl RA, Testor G, et al. 2010. *Ap. J.* 721:1206–32
Chomiuk L, Povich MS. 2011. *Astron. J.* 142:197
Christlein D, Zaritsky D, Bland-Hawthorn J. 2010. *MNRAS* 405:2549–60
Churchwell E, Babler BL, Meade MR, Whitney BA, Benjamin R, et al. 2009. *Publ. Astron. Soc. Pac.* 121:213–30
Clark PC, Klessen RS, Bonnell IA. 2007. *MNRAS* 379:57–62
Clemens DP, Barvainis R. 1988. *Ap. J. Suppl.* 68:257–86
Clemens DP, Sanders DB, Scoville NZ. 1988. *Ap. J.* 327:139–55
Colbert EJM, Heckman TM, Ptak AF, Strickland DK, Weaver KA. 2004. *Ap. J.* 602:231–48
Combes F, Young LM, Bureau M. 2007. *MNRAS* 377:1795–807
Condon JJ. 1992. *Annu. Rev. Astron. Astrophys.* 30:575–611
Cortese L, Boselli A, Franzetti P, Decarli R, Gavazzi G, et al. 2008. *MNRAS* 386:1157–68
Cox DP. 1981. *Ap. J.* 245:534–51
Cox DP. 2005. *Annu. Rev. Astron. Astrophys.* 43:337–85
Crapsi A, van Dishoeck EF, Hogerheijde MR, Pontoppidan KM, Dullemond CP. 2008. *Astron. Astrophys.* 486:245–54
Crocker AF, Bureau M, Young LM, Combes F. 2011. *MNRAS* 410:1197–222
Crosthwaite LP, Turner JL. 2007. *Astron. J.* 134:1827–42
Crowther PA, Schnurr O, Hirschi R, Yusof N, Parker RJ, et al. 2010. *MNRAS* 408:731–51
Crutcher RM. 2012. *Annu. Rev. Astron. Astrophys.* 50:29–63
Crutcher RM, Wandelt B, Heiles C, Falgarone E, Troland TH. 2010. *Ap. J.* 725:466–79
Daddi E, Elbaz D, Walter F, Bournaud F, Salmi F, et al. 2010. *Ap. J. Lett.* 714:L118–22
Dalcanton JJ, Williams BF, Seth AC, Dolphin A, Holtzman J, et al. 2009. *Ap. J. Suppl.* 183:67–108
Dale DA, Bendo GJ, Engelbracht CW, Gordon KD, Regan MW, et al. 2005. *Ap. J.* 633:857–70
Dale DA, Cohen SA, Johnson LC, Schuster MD, Calzetti D, et al. 2009. *Ap. J.* 703:517–56
Dale DA, Gil de Paz A, Gordon KD, Hanson HM, Armus L, et al. 2007. *Ap. J.* 655:863–84
Dale DA, Helou G. 2002. *Ap. J.* 576:159–68
Dale DA, Smith JDT, Armus L, Buckalew BA, Helou G, et al. 2006. *Ap. J.* 646:161–73
Dame TM, Hartmann D, Thaddeus P. 2001. *Ap. J.* 547:792–813
Dame TM, Thaddeus P. 2011. *Ap. J. Lett.* 734:L24
Da Rio N, Robberto M, Hillenbrand LA, Henning T, Stassun KG. 2012. *Ap. J.* 748:A14
Davies B, Bastian N, Gieles M, Seth AC, Mengel S, Konstantopoulos IS. 2011. *MNRAS* 411:1386–94
Dekel A, Birnboim Y. 2006. *MNRAS* 368:2–20
de Wit WJ, Testi L, Palla F, Zinnecker H. 2005. *Astron. Astrophys.* 437:247–55
Dickey JM, McClure-Griffiths NM, Gaensler BM, Green AJ. 2003. *Ap. J.* 585:801–22
Dickman RL. 1978. *Ap. J. Suppl.* 37:407–27
Dickman RL, Snell RL, Schloerb FP. 1986. *Ap. J.* 309:326–30
di Francesco J, Evans NJ II, Caselli P, Myers PC, Shirley Y, et al. 2007. See Reipurth, Jewitt & Keil 2007, pp. 17–32
Dobbs CL. 2008. *MNRAS* 391:844–58
Dobbs CL, Burkert A, Pringle JE. 2011. *MNRAS* 413:2935–42
Dobbs CL, Pringle JE. 2010. *MNRAS* 409:396–404
Dohm-Palmer RC, Skillman ED, Mateo M, Saha A, Dolphin A, et al. 2002. *Astron. J.* 123:813–31
Dolphin AE. 2002. *MNRAS* 332:91–108
Dopita MA. 1985. *Ap. J. Lett.* 295:L5–8
Dopita MA, Pereira M, Kewley LJ, Capaccioli M. 2002. *Ap. J. Suppl.* 143:47–72
Dopita MA, Ryder SD. 1994. *Ap. J.* 430:163–78
Downes D, Solomon PM. 1998. *Ap. J.* 507:615–54
Downes D, Solomon PM, Radford SJE. 1993. *Ap. J. Lett.* 414:L13–16
Draine BT. 2003. *Annu. Rev. Astron. Astrophys.* 41:241–89

Draine BT. 2011. *Physics of the Interstellar and Intergalactic Medium*. Princeton, NJ: Princeton Univ. Press
Dunham MK, Robitaille TP, Evans NJ II, Schlingman WM, Cyganowski CJ, Urquhart J. 2011a. *Ap. J.* 731:90
Dunham MK, Rosolowsky E, Evans NJ II, Cyganowski C, Urquhart JS. 2011b. *Ap. J.* 741:110
Dunham MM, Evans NJ II, Terebey S, Dullemond CP, Young CH. 2010. *Ap. J.* 710:470–502
Eales SA, Smith MWL, Wilson CD, Bendo GJ, Cortese L, et al. 2010. *Astron. Astrophys.* 518:L62
Egan MP, Shipman RF, Price SD, Carey SJ, Clark FO, Cohen M. 1998. *Ap. J. Lett.* 494:L199
Elbaz D, Le Floc'h, Dole H, Marcillac D. 2005. *Astron. Astrophys.* 434:L1
Elmegreen BG. 1991. *Ap. J.* 378:139–56
Elmegreen BG. 2000. *Ap. J.* 530:277–81
Elmegreen BG, Efremov YN. 1997. *Ap. J.* 480:235
Elmegreen BG, Parravano A. 1994. *Ap. J. Lett.* 435:L121
Engargiola G, Plambeck RL, Rosolowsky E, Blitz L. 2003. *Ap. J. Suppl.* 149:343–63
Engelbracht CW, Gordon KD, Rieke GH, Werner MW, Dale DA, Latter WB. 2005. *Ap. J. Lett.* 628:L29–32
Enoch ML, Evans NJ II, Sargent AI, Glenn J. 2009. *Ap. J.* 692:973–97
Enoch ML, Evans NJ II, Sargent AI, Glenn J, Rosolowsky E, Myers P. 2008. *Ap. J.* 684:1240–59
Enoch ML, Glenn J, Evans NJ II, Sargent AI, Young KE, Huard TL. 2007. *Ap. J.* 666:982–1001
Evans NJ II. 1999. *Annu. Rev. Astron. Astrophys.* 37:311–62
Evans NJ II, Dunham MM, Jørgensen JK, Enoch ML, Merín B, et al. 2009. *Ap. J. Suppl.* 181:321–50
Evans NJ II, Rawlings JMC, Shirley YL, Mundy LG. 2001. *Ap. J.* 557:193–208
Falgarone E, Phillips TG, Walker CK. 1991. *Ap. J.* 378:186–201
Farrah D, Bernard-Salas J, Spoon HWW, Soifer BT, Armus L, et al. 2007. *Ap. J.* 667:149–69
Faúndez S, Bronfman L, Garay G, Chini R, Nyman LÅ, May J. 2004. *Astron. Astrophys.* 426:97–103
Feldmann R, Gnedin NY, Kravtsov AV. 2012. *Ap. J.* 747:A124
Ferguson AMN, Wyse RFG, Gallagher JS, Hunter DA. 1998. *Ap. J. Lett.* 506:L19–22
Field GB, Goldsmith DW, Habing HJ. 1969. *Ap. J. Lett.* 155:L149
Flaherty KM, Pipher JL, Megeath ST, Winston EM, Gutermuth RA, et al. 2007. *Ap. J.* 663:1069–82
Förster Schreiber NM, Genzel R, Bouché N, Cresci G, Davies R, et al. 2009. *Ap. J.* 706:1364–428
Förster Schreiber NM, Roussel H, Sauvage M, Charmandaris V. 2004. *Astron. Astrophys.* 419:501–16
Foster JB, Jackson JM, Barnes PJ, Barris E, Brooks K, et al. 2011. *Ap. J. Suppl.* 197:25
Frerking MA, Langer WD, Wilson RW. 1982. *Ap. J.* 262:590–605
Fukui Y, Kawamura A. 2010. *Annu. Rev. Astron. Astrophys.* 48:547–80
Fukui Y, Mizuno N, Yamaguchi R, Mizuno A, Onishi T. 2001. *Publ. Astron. Soc. Jpn.* 53:L41–44
Fuller GA, Williams SJ, Sridharan TK. 2005. *Astron. Astrophys.* 442:949–59
Fumagalli M, da Silva RL, Krumholz MR. 2011. *Ap. J. Lett.* 741:L26
Gallego J, Zamorano J, Aragon-Salamanca A, Rego M. 1995. *Ap. J. Lett.* 455:L1
Gao Y, Carilli CL, Solomon PM, Vanden Bout PA. 2007. *Ap. J. Lett.* 660:L93–96
Gao Y, Solomon PM. 2004. *Ap. J.* 606:271–90
Garcia-Burillo S, Usero A, Alonso-Herrero A, Gracia-Carpio J, Pereira-Santaella M, et al. 2012. *Astron. Astrophys.* 539:A8
Gavazzi G, Boselli A, Donati A, Franzetti P, Scodeggio M. 2003. *Astron. Astrophys.* 400:451–55
Gavazzi G, Scodeggio M. 1996. *Astron. Astrophys.* 312:L29–32
Genzel R, Burkert A, Bouché N, Cresci G, Förster Schreiber NM, et al. 2008. *Ap. J.* 687:59–77
Genzel R, Lutz D, Sturm E, Egami E, Kunze D, et al. 1998. *Ap. J.* 498:579
Genzel R, Newman S, Jones T, Förster Schreiber NM, Shapiro K, et al. 2011. *Ap. J.* 733:101
Genzel R, Tacconi LJ, Gracia-Carpio J, Sternberg A, Cooper MC, et al. 2010. *MNRAS* 407:2091–108
Gieles M, Larsen SS, Bastian N, Stein IT. 2006. *Astron. Astrophys.* 450:129–45
Gies DR. 1987. *Ap. J. Suppl.* 64:545–63
Gil de Paz A, Boissier S, Madore BF, Seibert M, Joe YH, et al. 2007. *Ap. J. Suppl.* 173:185–255
Gil de Paz A, Madore BF, Boissier S, Swaters R, Popescu CC, et al. 2005. *Ap. J. Lett.* 627:L29–32
Glover SCO, Federrath C, Mac Low MM, Klessen RS. 2010. *MNRAS* 404:2–29
Goddard QE, Kennicutt RC, Ryan-Weber EV. 2010. *MNRAS* 405:2791–809
Goldreich P, Kwan J. 1974. *Ap. J.* 189:441–54
Goldsmith PF, Heyer M, Narayanan G, Snell R, Li D, Brunt C. 2008. *Ap. J.* 680:428–45

Gordon KD, Clayton GC, Witt AN, Misselt KA. 2000. *Ap. J.* 533:236–44
Gordon KD, Misselt KA, Witt AN, Clayton GC. 2001. *Ap. J.* 551:269–76
Goto T, Arnouts S, Inami H, Matsuhara H, Pearson C, et al. 2011. *MNRAS* 410:573–84
Graciá-Carpio J, García-Burillo S, Planesas P, Fuente A, Usero A. 2008. *Astron. Astrophys.* 479:703–17
Gratier P, Braine J, Rodriguez-Fernandez NJ, Schuster KF, Kramer C, et al. 2010. *Astron. Astrophys.* 522:A3
Green JA, Caswell JL, Fuller GA, Avison A, Breen SL, et al. 2009. *MNRAS* 392:783–94
Greene TP, Wilking BA, Andre P, Young ET, Lada CJ. 1994. *Ap. J.* 434:614–26
Griffin MJ, Abergel A, Abreu A, Ade PAR, André P, et al. 2010. *Astron. Astrophys.* 518:L3
Guesten R, Mezger PG. 1982. *Vistas Astron.* 26:159–224
Gutermuth RA, Megeath ST, Myers PC, Allen LE, Pipher JL, Fazio GG. 2009. *Ap. J. Suppl.* 184:18–83
Gutermuth RA, Megeath ST, Pipher JL, Williams JP, Allen LE, et al. 2005. *Ap. J.* 632:397–420
Gutermuth RA, Pipher JL, Megeath ST, Myers PC, Allen LE, Allen TS. 2011. *Ap. J.* 739:84
Hameed S, Devereux N. 2005. *Astron. J.* 129:2597–616
Hao CN, Kennicutt RC Jr, Johnson BD, Calzetti D, Dale DA, Moustakas J. 2011. *Ap. J.* 741:A124
Hatchell J, Fuller GA. 2008. *Astron. Astrophys.* 482:855–63
Hayes M, Schaerer D, Östlin G, Mas-Hesse JM, Atek H, Kunth D. 2011. *Ap. J.* 730:8
Heiderman A, Evans NJ II, Allen LE, Huard T, Heyer M. 2010. *Ap. J.* 723:1019–37
Heiles C, Troland TH. 2003. *Ap. J.* 586:1067–93
Helfer TT, Thornley MD, Regan MW, Wong T, Sheth K, et al. 2003. *Ap. J. Suppl.* 145:259–327
Helou G, Roussel H, Appleton P, Frayer D, Stolovy S, et al. 2004. *Ap. J. Suppl.* 154:253–58
Helou G, Soifer BT, Rowan-Robinson M. 1985. *Ap. J. Lett.* 298:L7–11
Hennebelle P, Chabrier G. 2011. *Ap. J. Lett.* 743:L29
Heyer M, Krawczyk C, Duval J, Jackson JM. 2009. *Ap. J.* 699:1092–103
Heyer MH, Brunt C, Snell RL, Howe JE, Schloerb FP, Carpenter JM. 1998. *Ap. J. Suppl.* 115:241
Heyer MH, Carpenter JM, Snell RL. 2001. *Ap. J.* 551:852–66
Heyer MH, Corbelli E, Schneider SE, Young JS. 2004. *Ap. J.* 602:723–29
Higuchi AE, Kurono Y, Saito M, Kawabe R. 2009. *Ap. J.* 705:468–82
Hill GJ, Gebhardt K, Komatsu E, Drory N, MacQueen PJ, et al. 2008. In *Panoramic Views of Galaxy Formation and Evolution*, ed. T Kodama, T Yamada, K Aoki, *ASP Conf. Ser.* 399:115–18. San Francisco: Astron. Soc. Pac.
Hillenbrand LA. 1997. *Astron. J.* 113:1733–68
Hirashita H, Buat V, Inoue AK. 2003. *Astron. Astrophys.* 410:83–100
Hirashita H, Inoue AK, Kamaya H, Shibai H. 2001. *Astron. Astrophys.* 366:83–90
Hirota T, Bushimata T, Choi YK, Honma M, Imai H, et al. 2007. *Publ. Astron. Soc. Jpn.* 59:897
Ho LC, Keto E. 2007. *Ap. J.* 658:314–18
Hollenbach DJ, Tielens AGGM. 1997. *Annu. Rev. Astron. Astrophys.* 35:179–216
Homeier NL, Alves J. 2005. *Astron. Astrophys.* 430:481–89
Hopkins PF, Quataert E, Murray N. 2011. *MNRAS* 417:950–73
Hosokawa T, Offner SSR, Krumholz MR. 2011. *Ap. J.* 738:140
Hosokawa T, Omukai K. 2009. *Ap. J.* 691:823–46
Hunter DA, Brinks E, Elmegreen B, Rupen M, Simpson C, et al. 2007. *Bull. Am. Astron. Soc.* 38:895
Hunter DA, Elmegreen BG, Ludka BC. 2010. *Astron. J.* 139:447–75
Immer K, Schuller F, Omont A, Menten KM. 2012. *Astron. Astrophys.* 537:A121
Israel FP, van der Hulst JM. 1983. *Astron. J.* 88:1736–48
Jackson JM, Rathborne JM, Shah RY, Simon R, Bania TM, et al. 2006. *Ap. J. Suppl.* 163:145–59
James PA, Shane NS, Beckman JE, Cardwell A, Collins CA, et al. 2004. *Astron. Astrophys.* 414:23–43
Jansen RA, Franx M, Fabricant D. 2001. *Ap. J.* 551:825–32
Jogee S, Miller SH, Penner K, Skelton RE, Conselice CJ, et al. 2009. *Ap. J.* 697:1971–92
Johnson BD, Schiminovich D, Seibert M, Treyer M, Martin DC, et al. 2007. *Ap. J. Suppl.* 173:392–403
Johnstone D, Di Francesco J, Kirk H. 2004. *Ap. J. Lett.* 611:L45–48
Juneau S, Narayanan DT, Moustakas J, Shirley YL, Bussmann RS, et al. 2009. *Ap. J.* 707:1217–32
Kainulainen J, Beuther H, Banerjee R, Federrath C, Henning T. 2011. *Astron. Astrophys.* 530:A64
Kainulainen J, Beuther H, Henning T, Plume R. 2009. *Astron. Astrophys.* 508:L35–38

Kalberla PMW, Dedes L. 2008. *Astron. Astrophys.* 487:951–63
Kalberla PMW, Dedes L, Kerp J, Haud U. 2007. *Astron. Astrophys.* 469:511–27
Kalberla PMW, Kerp J. 2009. *Annu. Rev. Astron. Astrophys.* 47:27–61
Karachentsev ID, Karachentseva VE, Huchtmeier WK, Makarov DI. 2004. *Astron. J.* 127:2031–68
Kauffmann G, Heckman TM, White SDM, Charlot S, Tremonti C, et al. 2003. *MNRAS* 341:54–69
Kauffmann J, Bertoldi F, Bourke TL, Evans NJ II, Lee CW. 2008. *Astron. Astrophys.* 487:993–1017
Kauffmann J, Pillai T. 2010. *Ap. J. Lett.* 723:L7–12
Kauffmann J, Pillai T, Shetty R, Myers PC, Goodman AA. 2010. *Ap. J.* 716:433–45
Kaviraj S, Schawinski K, Devriendt JEG, Ferreras I, Khochfar S, et al. 2007. *Ap. J. Suppl.* 173:619–42
Kennicutt RC, Calzetti D, Aniano G, Appleton P, Armus L, et al. 2011. *Publ. Astron. Soc. Pac.* 123:1347–69
Kennicutt RC Jr. 1989. *Ap. J.* 344:685–703
Kennicutt RC Jr. 1998a. *Annu. Rev. Astron. Astrophys.* 36:189–232
Kennicutt RC Jr. 1998b. *Ap. J.* 498:541
Kennicutt RC Jr, Armus L, Bendo G, Calzetti D, Dale DA, et al. 2003. *Publ. Astron. Soc. Pac.* 115:928–52
Kennicutt RC Jr, Calzetti D, Walter F, Helou G, Hollenbach DJ, et al. 2007. *Ap. J.* 671:333–48
Kennicutt RC Jr, Hao CN, Calzetti D, Moustakas J, Dale DA, et al. 2009. *Ap. J.* 703:1672–95
Kennicutt RC Jr, Lee JC, Funes SJJG, Sakai S, Akiyama S. 2008. *Ap. J. Suppl.* 178:247–79
Kewley LJ, Geller MJ, Jansen RA. 2004. *Astron. J.* 127:2002–30
Kewley LJ, Geller MJ, Jansen RA, Dopita MA. 2002. *Astron. J.* 124:3135–43
Kim CG, Kim WT, Ostriker EC. 2011. *Ap. J.* 743:25
Kirk JM, Ward-Thompson D, André P. 2005. *MNRAS* 360:1506–26
Klessen RS, Burkert A, Bate MR. 1998. *Ap. J. Lett.* 501:L205
Knapen JH, Stedman S, Bramich DM, Folkes SL, Bradley TR. 2004. *Astron. Astrophys.* 426:1135–41
Koda J, Nearby Galaxies CO Survey Group. 2009. In *Am. Astron. Soc. Meet. Abstr.* 213, *Bull. Am. Astron. Soc.* 41:456
Koda J, Scoville N, Sawada T, La Vigne MA, Vogel SN, et al. 2009. *Ap. J. Lett.* 700:L132–36
Komugi S, Sofue Y, Nakanishi H, Onodera S, Egusa F. 2005. *Publ. Astron. Soc. Jpn.* 57:733–41
Kong X, Charlot S, Brinchmann J, Fall SM. 2004. *MNRAS* 349:769–78
Koribalski BS. 2010. In *Galaxies in Isolation: Exploring Nature Versus Nurture*, ed. L Verdes-Montenegro, A del Olmo, J Sulentic, *ASP Conf. Ser.* 421:137. San Francisco, Astron. Soc. Pac.
Kormendy J, Kennicutt RC Jr. 2004. *Annu. Rev. Astron. Astrophys.* 42:603–83
Kramer C, Stutzki J, Rohrig R, Corneliussen U. 1998. *Astron. Astrophys.* 329:249–64
Kroupa P, Tout CA, Gilmore G. 1993. *MNRAS* 262:545–87
Kroupa P, Weidner C. 2003. *Ap. J.* 598:1076–78
Krumholz MR. 2011. *Ap. J.* 743:110
Krumholz MR, Bonnell IA. 2009. In *Structure Formation in Astrophysics*, ed. G Chabrier, pp. 288–320. Cambridge, UK: Cambridge Univ. Press
Krumholz MR, Cunningham AJ, Klein RI, McKee CF. 2010. *Ap. J.* 713:1120–33
Krumholz MR, Dekel A, McKee CF. 2012. *Ap. J.* 745:69
Krumholz MR, Klein RI, McKee CF, Offner SSR, Cunningham AJ. 2009. *Science* 323:754–57
Krumholz MR, McKee CF. 2005. *Ap. J.* 630:250–68
Krumholz MR, McKee CF. 2008. *Nature* 451:1082–84
Krumholz MR, McKee CF, Tumlinson J. 2009. *Ap. J.* 699:850–56
Krumholz MR, Thompson TA. 2007. *Ap. J.* 669:289–98
Kuiper R, Klahr H, Beuther H, Henning T. 2011. *Ap. J.* 732:20
Kulkarni SR, Heiles C. 1988. In *Galactic and Extragalactic Radio Astronomy*, ed. GL Verschuur, KI Kellerman, pp. 95–153. New York: Springer-Verlag
Lada CJ, Forbrich J, Lombardi M, Alves JF. 2012. *Ap. J.* 745:190
Lada CJ, Lada EA. 2003. *Annu. Rev. Astron. Astrophys.* 41:57–115
Lada CJ, Lombardi M, Alves JF. 2010. *Ap. J.* 724:687–93
Lada CJ, Muench AA, Rathborne J, Alves JF, Lombardi M. 2008. *Ap. J.* 672:410–22
Lada CJ, Wilking BA. 1984. *Ap. J.* 287:610–21
Lada EA. 1992. *Ap. J. Lett.* 393:L25–28

Larson RB. 1969. *MNRAS* 145:271
Larson RB. 1982. *MNRAS* 200:159–74
Larson RB. 1987. In *Starbursts and Galaxy Evolution*, ed. TX Thuan, T Montmerle, J Tran Thanh Van, p. 467. Paris: Ed. Frontieres Gif sur Yvette
Laurent O, Mirabel IF, Charmandaris V, Gallais P, Madden SC, et al. 2000. *Astron. Astrophys.* 359:887–99
Lee JC, Gil de Paz A, Kennicutt RC Jr, Bothwell M, Dalcanton J, et al. 2011. *Ap. J. Suppl.* 192:6
Lee JC, Gil de Paz A, Tremonti C, Kennicutt RC Jr, Salim S, et al. 2009a. *Ap. J.* 706:599–613
Lee JC, Kennicutt RC, Funes SJJG, Sakai S, Akiyama S. 2007. *Ap. J. Lett.* 671:L113–16
Lee JC, Kennicutt RC Jr, Funes SJJG, Sakai S, Akiyama S. 2009b. *Ap. J.* 692:1305–20
Lee JE, Evans NJ II, Shirley YL, Tatematsu K. 2003. *Ap. J.* 583:789–808
Le Floc'h E, Papovich C, Dole H, Bell EF, Lagache G, et al. 2005. *Ap. J.* 632:169–90
Lehmer BD, Alexander DM, Bauer FE, Brandt WN, Goulding AD, et al. 2010. *Ap. J.* 724:559–71
Leitherer C, Schaerer D, Goldader JD, González Delgado RM, Robert C, et al. 1999. *Ap. J. Suppl.* 123:3–40
Leroy AK, Bolatto A, Gordon K, Sandstrom K, Gratier P, et al. 2011. *Ap. J.* 737:12
Leroy AK, Walter F, Bigiel F, Usero A, Weiss A, et al. 2009. *Astron. J.* 137:4670–96
Leroy AK, Walter F, Brinks E, Bigiel F, de Blok WJG, et al. 2008. *Astron. J.* 136:2782–45
Li W, Evans NJ II, Lada EA. 1997. *Ap. J.* 488:277
Li ZY, Nakamura F. 2006. *Ap. J. Lett.* 640:L187–90
Liszt HS, Pety J, Lucas R. 2010. *Astron. Astrophys.* 518:A45
Liu G, Koda J, Calzetti D, Fukuhara M, Momose R. 2011. *Ap. J.* 735:63
Lockman FJ. 1989. *Ap. J. Suppl.* 71:469–79
Lombardi M, Lada CJ, Alves J. 2010. *Astron. Astrophys.* 512:A67
Longmore SN, Pillai T, Keto E, Zhang Q, Qiu K. 2011. *Ap. J.* 726:97
Longmore SN, Rathborne J, Bastian N, Alves J, Ascenso J, et al. 2012. *Ap. J.* 746:A117
Luna A, Bronfman L, Carrasco L, May J. 2006. *Ap. J.* 641:938–48
Lynds BT. 1962. *Ap. J. Suppl.* 7:1
Madden SC. 2000. *New Astron. Rev.* 44:249–56
Malhotra S, Helou G, Stacey G, Hollenbach D, Lord S, et al. 1997. *Ap. J. Lett.* 491:L27
Maloney P, Black JH. 1988. *Ap. J.* 325:389–401
Mamajek EE. 2009. In *Exoplanets and Disks: Their Formation and Diversity: Proc. Int. Conf., AIP Conf. Ser.* ed. T Usuda, M Tamura, M Ishii, 1158:3–10. Mellville, NY: Am. Inst. Phys.
Marcum PM, O'Connell RW, Fanelli MN, Cornett RH, Waller WH, et al. 2001. *Ap. J. Suppl.* 132:129–98
Martel H, Evans NJ II, Shapiro PR. 2006. *Ap. J. Suppl.* 163:122–44
Martin CL, Kennicutt RC Jr. 2001. *Ap. J.* 555:301–21
Martin DC, Fanson J, Schiminovich D, Morrissey P, Friedman PG, et al. 2005a. *Ap. J. Lett.* 619:L1–6
Martin DC, Seibert M, Buat V, Iglesias-Páramo J, Barlow TA, et al. 2005b. *Ap. J. Lett.* 619:L59–62
Mason KO, Breeveld A, Much R, Carter M, Cordova FA, et al. 2001. *Astron. Astrophys.* 365:L36–44
McClure-Griffiths NM, Dickey JM, Gaensler BM, Green AJ, Haverkorn M, Strasser S. 2005. *Ap. J. Suppl.* 158:178–87
McKee CF. 1989. *Ap. J.* 345:782–801
McKee CF, Ostriker EC. 2007. *Annu. Rev. Astron. Astrophys.* 45:565–687
McKee CF, Ostriker JP. 1977. *Ap. J.* 218:148–69
McKee CF, Williams JP. 1997. *Ap. J.* 476:144
Meier DS, Turner JL. 2004. *Astron. J.* 127:2069–84
Meier DS, Turner JL, Hurt RL. 2008. *Ap. J.* 675:281–302
Men'shchikov A, André P, Didelon P, Knyves V, Schneider N, et al. 2010. *Astron. Astrophys.* 518:L103
Menten KM, Reid MJ, Forbrich J, Brunthaler A. 2007. *Astron. Astrophys.* 474:515–20
Meurer GR, Hanish DJ, Ferguson HC, Knezek PM, Kilborn VA, et al. 2006. *Ap. J. Suppl.* 165:307–37
Meurer GR, Heckman TM, Calzetti D. 1999. *Ap. J.* 521:64–80
Meurer GR, Wong OI, Kim JH, Hanish DJ, Heckman TM, et al. 2009. *Ap. J.* 695:765–80
Mezger PG. 1987. In *Starbursts and Galaxy Evolution*, ed. TX Thuan, T Montmerle, J Tran Thanh Van, p. 3. Paris: Ed. Frontieres Gif sur Yvette
Miller GE, Scalo JM. 1979. *Ap. J. Suppl.* 41:513–47

Misiriotis A, Xilouris EM, Papamastorakis J, Boumis P, Goudis CD. 2006. *Astron. Astrophys.* 459:113–23
Molinari S, Swinyard B, Bally J, Barlow M, Bernard JP, et al. 2010. *Astron. Astrophys.* 518:L100
Momose R. 2012. *The resolved Kennicutt-Schmidt law in nearby galaxies.* PhD thesis, Univ. Tokyo. 165 pp.
Motte F, Andre P, Neri R. 1998. *Astron. Astrophys.* 336:150–72
Mouschovias TCh. 1991. In *The Physics of Star Formation and Early Stellar Evolution*, NATO ASIC Proc. 342, ed. CJ Lada, ND Kylafis, p. 449. Dordrecht: Kluwer
Mouschovias TC, Spitzer L Jr. 1976. *Ap. J.* 210:326
Moustakas J, Kennicutt RC Jr, Tremonti CA. 2006. *Ap. J.* 642:775–96
Mueller KE, Shirley YL, Evans NJ II, Jacobson HR. 2002. *Ap. J. Suppl.* 143:469–97
Murakami H, Baba H, Barthel P, Clements D, Cohen M, et al. 2007. *Publ. Astron. Soc. Jpn.* 59:S369–76
Murphy EJ, Condon JJ, Schinnerer E, Kennicutt RC, Calzetti D, et al. 2011. *Ap. J.* 737:67
Murray N. 2011. *Ap. J.* 729:133
Murray N, Rahman M. 2010. *Ap. J.* 709:424–35
Myers PC. 2009. *Ap. J.* 706:1341–52
Myers PC. 2011. *Ap. J.* 743:98
Nakanishi H, Sofue Y. 2006. *Publ. Astron. Soc. Jpn.* 58:847–60
Narayanan D, Cox TJ, Shirley Y, Davé R, Hernquist L, Walker CK. 2008. *Ap. J.* 684:996–1008
Narayanan D, Krumholz MR, Ostriker EC, Hernquist L. *MNRAS* 421:3127–46
Nguyen Luong Q, Motte F, Schuller F, Schneider N, Bontemps S, et al. 2011. *Astron. Astrophys.* 529:A41
Niklas S, Klein U, Wielebinski R. 1997. *Astron. Astrophys.* 322:19–28
Noeske KG, Faber SM, Weiner BJ, Koo DC, Primack JR, et al. 2007. *Ap. J. Lett.* 660:L47–50
Oey MS, Meurer GR, Yelda S, Furst EJ, Caballero-Nieves SM, et al. 2007. *Ap. J.* 661:801–14
Oka T, Hasegawa T, Hayashi M, Handa T, Sakamoto S. 1998. *Ap. J.* 493:730
Omukai K. 2007. *Publ. Astron. Soc. Jpn.* 59:589–606
Onishi T, Mizuno A, Kawamura A, Ogawa H, Fukui Y. 1998. *Ap. J.* 502:296
Onodera S, Kuno N, Tosaki T, Kohno K, Nakanishi K, et al. 2010. *Ap. J. Lett.* 722:L127–31
Ostriker EC, McKee CF, Leroy AK. 2010. *Ap. J.* 721:975–94
Ostriker EC, Shetty R. 2011. *Ap. J.* 731:41
Ouchi M, Ono Y, Egami E, Saito T, Oguri M, et al. 2009. *Ap. J.* 696:1164–75
Ouchi M, Shimasaku K, Furusawa H, Saito T, Yoshida M, et al. 2010. *Ap. J.* 723:869–94
Overzier RA, Heckman TM, Wang J, Armus L, Buat V, et al. 2011. *Ap. J. Lett.* 726:L7
Pak S, Jaffe DT, van Dishoeck EF, Johansson LEB, Booth RS. 1998. *Ap. J.* 498:735
Palla F, Stahler SW. 1992. *Ap. J.* 392:667–77
Peeters E, Spoon HWW, Tielens AGGM. 2004. *Ap. J.* 613:986–1003
Perault M, Omont A, Simon G, Seguin P, Ojha D, et al. 1996. *Astron. Astrophys.* 315:L165–68
Peretto N, Fuller GA. 2009. *Astron. Astrophys.* 505:405–15
Pérez-González PG, Zamorano J, Gallego J, Aragón-Salamanca A, Gil de Paz A. 2003. *Ap. J.* 591:827–42
Persic M, Rephaeli Y, Braito V, Cappi M, Della Ceca R, et al. 2004. *Astron. Astrophys.* 419:849–62
Pestalozzi MR, Minier V, Booth RS. 2005. *Astron. Astrophys.* 432:737–42
Peterson DE, Caratti o Garatti A, Bourke TL, Forbrich J, Gutermuth RA, et al. 2011. *Ap. J. Suppl.* 194:43
Pflamm-Altenburg J, Weidner C, Kroupa P. 2007. *Ap. J.* 671:1550–58
Pflamm-Altenburg J, Weidner C, Kroupa P. 2009. *MNRAS* 395:394–400
Pierce-Price D, Richer JS, Greaves JS, Holland WS, Jenness T, et al. 2000. *Ap. J. Lett.* 545:L121–25
Pilbratt GL, Riedinger JR, Passvogel T, Crone G, Doyle D, et al. 2010. *Astron. Astrophys.* 518:L1
Pineda JE, Goodman AA, Arce HG, Caselli P, Foster JB, et al. 2010a. *Ap. J. Lett.* 712:L116–21
Pineda JL, Goldsmith PF, Chapman N, Snell RL, Li D, et al. 2010b. *Ap. J.* 721:686–708
Planck Collab.: Ade PAR, Aghanim N, Arnaud M, Ashdown M, et al. 2011a. *Astron. Astrophys.* 536:A1
Planck Collab.: Ade PAR, Aghanim N, Arnaud M, Ashdown M, et al. 2011b. *Astron. Astrophys.* 536:A19
Planck Collab.: Ade PAR, Aghanim N, Arnaud M, Ashdown M, et al. 2011c. *Astron. Astrophys.* 536:A23
Plume R, Jaffe DT, Evans NJ II. 1992. *Ap. J. Suppl.* 78:505–15
Plume R, Jaffe DT, Evans NJ II, Martin-Pintado J, Gomez-Gonzalez J. 1997. *Ap. J.* 476:730
Pogge RW, Eskridge PB. 1993. *Astron. J.* 106:1405–19
Poglitsch A, Waelkens C, Geis N, Feuchtgruber H, Vandenbussche B, et al. 2010. *Astron. Astrophys.* 518:L2

Pontoppidan KM, Boogert ACA, Fraser HJ, van Dishoeck EF, Blake GA, et al. 2008. *Ap. J.* 678:1005–31
Porras A, Christopher M, Allen L, Di Francesco J, Megeath ST, Myers PC. 2003. *Astron. J.* 126:1916–24
Portegies Zwart SF, McMillan SLW, Gieles M. 2010. *Annu. Rev. Astron. Astrophys.* 48:431–93
Prescott MKM, Kennicutt RC Jr, Bendo GJ, Buckalew BA, Calzetti D, et al. 2007. *Ap. J.* 668:182–202
Pudritz RE, Ouyed R, Fendt C, Brandenburg A. 2007. See Reipurth, Jewitt & Keil 2007, pp. 277–94
Purcell CR, Balasubramanyam R, Burton MG, Walsh AJ, Minier V, et al. 2006. *MNRAS* 367:553–76
Quirk WJ, Tinsley BM. 1973. *Ap. J.* 179:69–84
Rahman N, Bolatto AD, Wong T, Leroy AK, Walter F, et al. 2011. *Ap. J.* 730:72
Rahman N, Bolatto AD, Xue R, Wong T, Leroy AK, et al. 2012. *Ap. J.* 745:A183
Raiter A, Schaerer D, Fosbury RAE. 2010. *Astron. Astrophys.* 523:A64
Ranalli P, Comastri A, Setti G. 2003. *Astron. Astrophys.* 399:39–50
Rathborne JM, Johnson AM, Jackson JM, Shah RY, Simon R. 2009. *Ap. J. Suppl.* 182:131–42
Rebull LM, Stapelfeldt KR, Evans NJ II, Jørgensen JK, Harvey PM, et al. 2007. *Ap. J. Suppl.* 171:447–77
Reddy N, Dickinson M, Elbaz D, Morrison G, Giavalisco M, et al. 2012. *Ap. J.* 744:A154
Reid MA, Wadsley J, Petitclerc N, Sills A. 2010. *Ap. J.* 719:561–75
Reid MA, Wilson CD. 2005. *Ap. J.* 625:891–905
Reid MJ, Menten KM, Zheng XW, Brunthaler A, Moscadelli L, et al. 2009. *Ap. J.* 700:137–48
Reipurth B, Jewitt D, Keil K, eds. 2007. *Protostars Planets V*. Tucson: Univ. Ariz. Press
Reiter M, Shirley YL, Wu J, Brogan C, Wootten A, Tatematsu K. 2011a. *Ap. J.* 740:40
Reiter M, Shirley YL, Wu J, Brogan C, Wootten A, Tatematsu K. 2011b. *Ap. J. Suppl.* 195:1
Relaño M, Lisenfeld U, Pérez-González PG, Vílchez JM, Battaner E. 2007. *Ap. J. Lett.* 667:L141–44
Rieke GH, Alonso-Herrero A, Weiner BJ, Pérez-González PG, Blaylock M, et al. 2009. *Ap. J.* 692:556–73
Roberts MS. 1975. In *Galaxies and the Universe*, ed. A Sandage, M Sandage, J Kristian, pp. 309–57. Chicago: Univ. Chicago Press
Robertson BE, Kravtsov AV. 2008. *Ap. J.* 680:1083–111
Robitaille TP, Whitney BA. 2010. *Ap. J. Lett.* 710:L11–15
Robitaille TP, Whitney BA, Indebetouw R, Wood K, Denzmore P. 2006. *Ap. J. Suppl.* 167:256–85
Rochau B, Brandner W, Stolte A, Gennaro M, Gouliermis D, et al. 2010. *Ap. J. Lett.* 716:L90–94
Rodriguez-Fernandez NJ, Braine J, Brouillet N, Combes F. 2006. *Astron. Astrophys.* 453:77–82
Roman-Duval J, Jackson JM, Heyer M, Rathborne J, Simon R. 2010. *Ap. J.* 723:492–507
Roming PWA, Kennedy TE, Mason KO, Nousek JA, Ahr L, et al. 2005. *Space Sci. Rev.* 120:95–142
Rosolowsky E. 2005. *Publ. Astron. Soc. Pac.* 117:1403–10
Rosolowsky E, Dunham MK, Ginsburg A, Bradley ET, Aguirre J, et al. 2010. *Ap. J. Suppl.* 188:123–38
Rosolowsky E, Pineda JE, Gao Y. 2011. *MNRAS* 415:1977–84
Roussel H, Helou G, Hollenbach DJ, Draine BT, Smith JD, et al. 2007. *Ap. J.* 669:959–81
Roussel H, Sauvage M, Vigroux L, Bosma A. 2001. *Astron. Astrophys.* 372:427–37
Ruphy S, Robin AC, Epchtein N, Copet E, Bertin E, et al. 1996. *Astron. Astrophys.* 313:L21–24
Russeil D, Pestalozzi M, Mottram JC, Bontemps S, Anderson LD, et al. 2011. *Astron. Astrophys.* 526:A151
Ryan-Weber EV, Meurer GR, Freeman KC, Putman ME, Webster RL, et al. 2004. *Astron. J.* 127:1431–40
Sadavoy SI, Di Francesco J, Bontemps S, Megeath ST, Rebull LM, et al. 2010. *Ap. J.* 710:1247–70
Salim S, Rich RM. 2010. *Ap. J. Lett.* 714:L290–94
Salim S, Rich RM, Charlot S, Brinchmann J, Johnson BD, et al. 2007. *Ap. J. Suppl.* 173:267–92
Salpeter EE. 1955. *Ap. J.* 121:161
Sana H, Evans CJ. 2010. In *Active OB Stars: Structure, Evolution, Mass Loss, and Critical Limits, Proc. IAU Symp. 272*, ed. C Neiner, G Wade, G Meynet, G Peters, pp. 474–85. Cambridge, UK: Cambridge Univ. Press
Sánchez SF, Kennicutt RC, Gil de Paz A, van de Ven G, Vílchez JM, et al. 2012. *Astron. Astrophys.* 538:A8
Sauvage M, Thuan TX. 1992. *Ap. J. Lett.* 396:L69–73
Scalo J. 1990. In *Physical Processes in Fragmentation and Star Formation*, ed. R Capuzzo-Dolcetta, C Chiosi, A di Fazio, *Astrophys. Space Sci. Libr.* 162:151–76. Dordrecht: Kluwer
Scarlata C, Colbert J, Teplitz HI, Panagia N, Hayes M, et al. 2009. *Ap. J. Lett.* 704:L98–102
Schaye J. 2004. *Ap. J.* 609:667–82
Schechter P. 1976. *Ap. J.* 203:297–306

Schiminovich D, Wyder TK, Martin DC, Johnson BD, Salim S, et al. 2007. *Ap. J. Suppl.* 173:315–41
Schlingman WM, Shirley YL, Schenk DE, Rosolowsky E, Bally J, et al. 2011. *Ap. J. Suppl.* 195:14
Schmidt M. 1959. *Ap. J.* 129:243
Schmidt M. 1963. *Ap. J.* 137:758
Schnurr O, Casoli J, Chené AN, Moffat AFJ, St-Louis N. 2008. *MNRAS* 389:L38–42
Schruba A, Leroy AK, Walter F, Bigiel F, Brinks E, et al. 2011. *Astron. J.* 142:37
Schuller F, Menten KM, Contreras Y, Wyrowski F, Schilke P, et al. 2009. *Astron. Astrophys.* 504:415–27
Schuster KF, Kramer C, Hitschfeld M, Garcia-Burillo S, Mookerjea B. 2007. *Astron. Astrophys.* 461:143–51
Scoville NZ, Evans AS, Thompson R, Rieke M, Hines DC, et al. 2000. *Astron. J.* 119:991–1061
Seibert M, Martin DC, Heckman TM, Buat V, Hoopes C, et al. 2005. *Ap. J. Lett.* 619:L55–58
Shang H, Li ZY, Hirano N. 2007. See Reipurth, Jewitt & Keil 2007, pp. 261–76
Shapiro KL, Falcón-Barroso J, van de Ven G, de Zeeuw PT, Sarzi M, et al. 2010. *MNRAS* 402:2140–86
Sheth K, Vogel SN, Wilson CD, Dame TM. 2008. *Ap. J.* 675:330–39
Shetty R, Glover SC, Dullemond CP, Klessen RS. 2011a. *MNRAS* 412:1686–700
Shetty R, Glover SC, Dullemond CP, Ostriker EC, Harris AI, Klessen RS. 2011b. *MNRAS* 415:3253–74
Shi Y, Helou G, Yan L, Armus L, Wu Y, et al. 2011. *Ap. J.* 733:87
Shirley YL, Evans NJ II, Young KE, Knez C, Jaffe DT. 2003. *Ap. J. Suppl.* 149:375–403
Shirley YL, Huard TL, Pontoppidan KM, Wilner DJ, Stutz AM, et al. 2011. *Ap. J.* 728:143
Shu FH, Adams FC, Lizano S. 1987. *Annu. Rev. Astron. Astrophys.* 25:23–81
Silk J. 1997. *Ap. J.* 481:703
Skibba RA, Engelbracht CW, Dale D, Hinz J, Zibetti S, et al. 2011. *Ap. J.* 738:89
Smith JDT, Draine BT, Dale DA, Moustakas J, Kennicutt RC Jr, et al. 2007. *Ap. J.* 656:770–91
Smith LJ, Norris RPF, Crowther PA. 2002. *MNRAS* 337:1309–28
Snell RL, Carpenter JM, Heyer MH. 2002. *Ap. J.* 578:229–44
Sodroski TJ, Odegard N, Arendt RG, Dwek E, Weiland JL, et al. 1997. *Ap. J.* 480:173
Soifer BT, Helou G, Werner M. 2008. *Annu. Rev. Astron. Astrophys.* 46:201–40
Solomon PM, Rivolo AR, Barrett J, Yahil A. 1987. *Ap. J.* 319:730–41
Solomon PM, Sage LJ. 1988. *Ap. J.* 334:613–25
Solomon PM, Vanden Bout PA. 2005. *Annu. Rev. Astron. Astrophys.* 43:677–725
Stahler SW, Palla F. 2005. *The Formation of Stars.* Weinheim: Wiley-VCH
Stecher TP, Cornett RH, Greason MR, Landsman WB, Hill JK, et al. 1997. *Publ. Astron. Soc. Pac.* 109:584–99
Stil JM, Taylor AR, Dickey JM, Kavars DW, Martin PG, et al. 2006. *Astron. J.* 132:1158–76
Stone JM, Ostriker EC, Gammie CF. 1998. *Ap. J. Lett.* 508:L99–102
Stutz AM, Bieging JH, Rieke GH, Shirley YL, Balog Z, et al. 2007. *Ap. J.* 665:466–77
Stutzki J, Bensch F, Heithausen A, Ossenkopf V, Zielinsky M. 1998. *Astron. Astrophys.* 336:697–720
Sullivan M, Treyer MA, Ellis RS, Bridges TJ, Milliard B, Donas J. 2000. *MNRAS* 312:442–64
Swift JJ, Williams JP. 2008. *Ap. J.* 679:552–56
Symeonidis M, Georgakakis A, Seymour N, Auld R, Bock J, et al. 2011. *MNRAS* 417:2239–52
Tacconi LJ, Genzel R, Smail I, Neri R, Chapman SC, et al. 2008. *Ap. J.* 680:246–62
Tasker EJ. 2011. *Ap. J.* 730:11
Tasker EJ, Tan JC. 2009. *Ap. J.* 700:358–75
Taylor AR, Gibson SJ, Peracaula M, Martin PG, Landecker TL, et al. 2003. *Astron. J.* 125:3145–64
Terebey S, Shu FH, Cassen P. 1984. *Ap. J.* 286:529–51
Thilker DA, Bianchi L, Boissier S, Gil de Paz A, Madore BF, et al. 2005. *Ap. J. Lett.* 619:L79–82
Thilker DA, Bianchi L, Meurer G, Gil de Paz A, Boissier S, et al. 2007. *Ap. J. Suppl.* 173:538–71
Treyer M, Schiminovich D, Johnson B, Seibert M, Wyder T, et al. 2007. *Ap. J. Suppl.* 173:256–66
Treyer M, Schiminovich D, Johnson BD, O'Dowd M, Martin CD, et al. 2010. *Ap. J.* 719:1191–211
Urban A, Martel H, Evans NJ II. 2010. *Ap. J.* 710:1343–64
van der Tak FFS, van Dishoeck EF, Evans NJ II, Blake GA. 2000. *Ap. J.* 537:283–303
van Dishoeck EF, Black JH. 1988. *Ap. J.* 334:771–802
van Dokkum PG, Conroy C. 2011. *Ap. J. Lett.* 735:L13
Vázquez-Semadeni E, Banerjee R, Gómez GC, Hennebelle P, Duffin D, Klessen RS. 2011. *MNRAS* 414:2511–27

Verley S, Corbelli E, Giovanardi C, Hunt LK. 2010. *Astron. Astrophys.* 510:A64
Walsh AJ, Breen SL, Britton T, Brooks KJ, Burton MG, et al. 2011. *MNRAS* 416:1764–821
Walsh AJ, Myers PC, Burton MG. 2004. *Ap. J.* 614:194–202
Walter F, Brinks E, de Blok WJG, Bigiel F, Kennicutt RC Jr, et al. 2008. *Astron. J.* 136:2563–647
Walterbos RAM, Greenawalt B. 1996. *Ap. J.* 460:696
Wang B, Heckman TM. 1996. *Ap. J.* 457:645
Ward-Thompson D, André P, Crutcher R, Johnstone D, Onishi T, Wilson C. 2007a. See Reipurth, Jewitt & Keil 2007, pp. 33–46
Ward-Thompson D, Di Francesco J, Hatchell J, Hogerheijde MR, Nutter D, et al. 2007b. *Publ. Astron. Soc. Pac.* 119:855–70
Ward-Thompson D, Motte F, Andre P. 1999. *MNRAS* 305:143–50
Watson C, Povich MS, Churchwell EB, Babler BL, Chunev G, et al. 2008. *Ap. J.* 681:1341–55
Weedman DW, Feldman FR, Balzano VA, Ramsey LW, Sramek RA, Wuu CC. 1981. *Ap. J.* 248:105–12
Weidner C, Kroupa P. 2006. *MNRAS* 365:1333–47
Weingartner JC, Draine BT. 2001. *Ap. J.* 548:296–30
Weisz DR, Johnson BD, Johnson LC, Skillman ED, Lee JC, et al. 2012. *Ap. J.* 744:44
Weisz DR, Skillman ED, Cannon JM, Dolphin AE, Kennicutt RC Jr, et al. 2008. *Ap. J.* 689:160–83
Werner MW, Roellig TL, Low FJ, Rieke GH, Rieke M, et al. 2004. *Ap. J. Suppl.* 154:1–9
Whittet DCB, Shenoy SS, Bergin EA, Chiar JE, Gerakines PA, et al. 2007. *Ap. J.* 655:332–41
Williams BF, Dalcanton JJ, Johnson LC, Weisz DR, Seth AC, et al. 2011. *Ap. J. Lett.* 734:L22
Williams JP, Blitz L, McKee CF. 2000. In *Protostars and Planets IV*, ed. V Mannings, AP Boss, SS Russell, pp. 97–120. Tucson: Univ. Ariz. Press
Williams JP, McKee CF. 1997. *Ap. J.* 476:166
Wilson CD, Warren BE, Israel FP, Serjeant S, Bendo G, et al. 2009. *Ap. J.* 693:1736–48
Wilson TL, Rood R. 1994. *Annu. Rev. Astron. Astrophys.* 32:191–226
Wolfire MG, Hollenbach D, McKee CF. 2010. *Ap. J.* 716:1191–207
Wong T, Blitz L. 2002. *Ap. J.* 569:157–83
Wong T, Hughes A, Ott J, Muller E, Pineda JL, et al. 2011. *Ap. J. Suppl.* 197:A16
Wouterloot JGA, Brand J. 1989. *Astron. Astrophys. Suppl.* 80:149–87
Wright E, Eisenhardt P, Mainzer A, Ressler M, Cutri R. et al. 2010. *Astron. J.* 140:1868–81
Wu H, Cao C, Hao CN, Liu FS, Wang JL, et al. 2005. *Ap. J. Lett.* 632:L79–82
Wu J, Evans NJ II. 2003. *Ap. J. Lett.* 592:L79–82
Wu J, Evans NJ II, Gao Y, Solomon PM, Shirley YL, Vanden Bout PA. 2005. *Ap. J. Lett.* 635:L173–76
Wu J, Evans NJ II, Shirley YL, Knez C. 2010a. *Ap. J. Suppl.* 188:313–57
Wu J, Vanden Bout PA, Evans NJ II, Dunham MM. 2009. *Ap. J.* 707:988–99
Wu Y, Helou G, Armus L, Cormier D, Shi Y, et al. 2010b. *Ap. J.* 723:895–914
Wu Y, Shi Y, Helou G, Armus L, Dale DA, et al. 2011. *Ap. J.* 734:40
Wu Y, Wei Y, Zhao M, Shi Y, Yu W, et al. 2004. *Astron. Astrophys.* 426:503–15
Wuyts S, Förster Schreiber NM, Lutz D, Nordon R, Berta S, et al. 2011. *Ap. J.* 738:106
Wyder TK, Martin DC, Barlow TA, Foster K, Friedman PG, et al. 2009. *Ap. J.* 696:1834–53
Yan L, Sajina A, Fadda D, Choi P, Armus L, et al. 2007. *Ap. J.* 658:778–93
Yorke HW, Sonnhalter C. 2002. *Ap. J.* 569:846–62
Yun MS, Reddy NA, Condon JJ. 2001. *Ap. J.* 554:803–22
Yusef-Zadeh F, Hewitt JW, Arendt RG, Whitney B, Rieke G, et al. 2009. *Ap. J.* 702:178–225
Zaritsky D, Christlein D. 2007. *Astron. J.* 134:135–41
Zasov AV, Stmakov SG. 1988. *Astrofizika* 29:190
Zhang Q, Fall SM. 1999. *Ap. J. Lett.* 527:L81–84
Zhu YN, Wu H, Cao C, Li HN. 2008. *Ap. J.* 686:155–71
Zinnecker H, Yorke HW. 2007. *Annu. Rev. Astron. Astrophys.* 45:481–563
Zuckerman B, Evans NJ II. 1974. *Ap. J. Lett.* 192:L149–52
Zuckerman B, Palmer P. 1974. *Annu. Rev. Astron. Astrophys.* 12:279–313

Annual Review of Astronomy and Astrophysics

Volume 50, 2012

Contents

Indexes

Errata

An online log of corrections to *Annual Review of Astronomy and Astrophysics* articles may be found at http://astro.annualreviews.org/errata.shtml